A DISCONTINUOUS LEAST-SQUARES SPATIAL DISCRETIZATION FOR THE S_N EQUATIONS

A Thesis

by

LEI ZHU

Submitted to the Office of Graduate Studies of
Texas A&M University
in partial fulfillment of the requirements for the degree of

MASTER OF SCIENCE

August 2008

Major Subject: Nuclear Engineering

A DISCONTINUOUS LEAST-SQUARES SPATIAL DISCRETIZATION FOR THE S_N EQUATIONS

A Thesis

by

LEI ZHU

Submitted to the Office of Graduate Studies of
Texas A&M University
in partial fulfillment of the requirements for the degree of

MASTER OF SCIENCE

Approved by:

Chair of Committee,	Jim E. Morel
Committee Members,	Marvin L. Adams
	Raytcho Lazarov
	Jean C. Ragusa
Head of Department,	Raymond Juzaitis

August 2008

Major Subject: Nuclear Engineering

ABSTRACT

A Discontinuous Least-squares Spatial Discretization for the S_N Equations.

(August 2008)

Lei Zhu, B. Eng., Tsinghua University

Chair of Advisory Committee: Dr. Jim E. Morel

In this thesis, we develop and test a fundamentally new linear-discontinuous least-squares (LDLS) method for spatial discretization of the one-dimensional (1-D) discrete-ordinates (S_N) equations. This new scheme is based upon a least-squares method with a discontinuous trial space. We implement our new method, as well as the linear-discontinuous Galerkin (LDG) method and the lumped linear-discontinuous Galerkin (LLDG) method. The implementation is in FORTRAN.

We run a series of numerical tests to study the robustness, L_2 accuracy, and the thick diffusion limit performance of the new LDLS method. By robustness we mean the resistance to negativities and rapid damping of oscillations. Computational results indicate that the LDLS method yields a uniform second-order error. It is more robust than the LDG method and more accurate than the LLDG method. However, it fails to preserve the thick diffusion limit. Consequently, it is viable for neutronics but not for radiative transfer since radiative transfer problems can be highly diffusive.

ACKNOWLEDGEMENTS

I would first like to thank my committee chair, Dr. Morel, for his guidance and support throughout this research. He first introduced me to the computational research field and has always been an excellent and kind advisor. I thank Dr. Lazarov for his valuable advice on finite element theory. I also thank the other two members of my committee, Dr. Adams and Dr. Ragusa, who made many suggestions which were invaluable contributions to my research.

I would also like to thank my friends for their encouragement, and the faculty and staff in the Department of Nuclear Engineering for their support. Finally, I thank my mother, my father, and my girl friend, Shanshan Gong, for their love.

TABLE OF CONTENTS

CHAPTER Page

LIST OF FIGURES

FIGURE Page

FIGURE Page

LIST OF TABLES

CHAPTER I

INTRODUCTION

Description of the problem

One of the most important innovations in transport spatial discretization over the last 30 years was the introduction of discontinuous Galerkin (DG) methods[1]. Such methods are known to be highly accurate and far more robust than continuous finite-element methods. Nonetheless, DG methods must still be lumped to achieve adequate robustness for demanding applications such as thermal radiation transport in the high energy density regime. Lumping can be very difficult on unstructured meshes[2]. In addition, DG methods give non-uniform errors. For instance, the average and outflow fluxes obtained with the linear-discontinuous Galerkin (LDG) method in 1-D are third-order accurate while the interior inflow value is only second-order accurate. If the error is measured with the L_2 norm, the LDG method gives second-order accuracy in both 1-D and multidimensional calculations.

Least-squares methods are generally highly accurate and have certain advantages over other methods for a posteriori error estimation[3]. However, the standard least-squares methods are generally not conservative and conservation is important for spatial discretization techniques in the nuclear engineering community.

Thus, a method that would be inherently more robust than the DG method and yield second-order accuracy in both 1-D and multidimensional calculations would be

---

This thesis follows the style of *Nuclear Science and Engineering*.

highly desirable. In this thesis, we propose, implement, and test a new linear-discontinuous least-squares (LDLS) method for spatial discretization of the 1-D discrete-ordinates equations. This new scheme is based upon a least-squares method with a discontinuous trial space. In the following chapters, we show a detailed derivation of the LDLS method and the spatial discretization schemes. The S_N equations are solved iteratively via source iteration. Fourier analysis is performed to study the iterative convergence behavior. We have implemented our new method in FORTRAN, and we have run a series of numerical tests to study accuracy and robustness, iterative convergence properties, and the thick diffusion limit performance of the new LDLS method.

Basic concepts of the transport equation and discrete-ordinates (S_N) equations

We start with the general form of continuous transport equation with both scattering source and inhomogeneous source:

$$\frac{1}{v(E)}\frac{\partial \psi(\vec{r},E,\vec{\Omega},t)}{\partial t}+\vec{\Omega}\cdot\vec{\nabla}\psi(\vec{r},E,\vec{\Omega},t)+\sigma_t(\vec{r},E,t)\psi(\vec{r},E,\vec{\Omega},t)= \int_{4\pi}\int_{0}^{\infty}\sigma_s(\vec{r},E'\to E,\vec{\Omega}'\to\vec{\Omega},t)\psi(\vec{r},E',\vec{\Omega}',t)dE'\,d\vec{\Omega}'+Q(\vec{r},E,\vec{\Omega},t), \tag{1.1}$$

where $\vec{r}$ is the Cartesian coordinates of the particle position, $\vec{\Omega}$ is a unit Cartesian vector representing the direction of particle flow, E is the particle energy, t is the time, $v(E)$ is the particle speed, $\psi(\vec{r},E,\vec{\Omega},t)$ is the angular flux, $Q(\vec{r},E,\vec{\Omega},t)$ is the inhomogeneous source, $\sigma_t(\vec{r},E,t)$ is the total macroscopic cross-section, and

$\sigma_s(\vec{r}, E' \to E, \vec{\Omega}' \to \vec{\Omega}, t)$ is the scattering kernel. The purpose of this work is to investigate methods for the spatial discretization of the S_N equations, so it is sufficient to consider the problem with the following assumptions:

Steady state ($\frac{\partial \psi(\vec{r}, E, \vec{\Omega}, t)}{\partial t} = 0$);

Mono-energetic;

Isotropic scattering and isotropic external sources;

One-dimensional (1-D) slab geometry;

Constant cross sections.

Under these conditions, the transport equation can be written as:

$$\mu \frac{\partial \psi}{\partial x} + \sigma_t \psi(\mu, x) = \frac{\sigma_s}{2} \phi(x) + \frac{Q(x)}{2}, \tag{1.2}$$

where the scalar flux is:

$$\phi(x) = \int_{-1}^{1} \psi(\mu, x) d\mu. \tag{1.3}$$

Eq. (1.2) remains continuous in the angular and spatial variables. We first discretize the angles to get the S_N equations:

$$\mu_m \frac{d\psi_m(x)}{dx} + \sigma_t \psi_m(x) = \frac{\sigma_s}{2} \sum_{m=1}^{N} w_m \psi_m(x) + Q_m(x), \tag{1.4}$$

where $m = 1, ..., N$. In this study, we apply a symmetric Gauss quadrature set of order *N*, where *N* is even. The directions are ordered such that for $m = 1, ..., N/2$, $\mu_m < 0$. For $m = N/2 + 1, ..., N$, $\mu_m > 0$. The quadrature weights are normalized to 2.0,

i.e., $\sum_{m=1}^{N} w_m = 2.0$. The detailed spatial discretization schemes for Eq. (1.4) will be introduced in the next chapter.

Introduction to iterative methods

Source Iteration (SI)

The S_N equations are solved via source iteration. Source iteration is based upon the following facts:

- All coupling between directions occurs on the right side of Eq. (1.4);
- A first-order advection-removal equation exists for each direction on the left side of the equation;
- Each such equation can be solved by performing a "sweep".

By "sweep", the angular flux is first calculated for the first cell on the incoming boundary. Its outflow becomes the incoming boundary for the next spatial cell. The SI algorithm for Eq. (1.4) can be mathematically represented as follows:

$$\mu_m \frac{d\psi_m^{l+1}(x)}{dx} + \sigma_t \psi_m^{l+1}(x) = \frac{\sigma_s}{2} \phi^l(x) + Q_m(x), \quad m = 1,..., N \tag{1.5}$$

where l is the iteration index and the scalar flux is given by:

$$\phi^l(x) = \sum_{m=1}^{N} w_m \psi^l{}_m(x). \tag{1.6}$$

Assuming an infinite homogeneous medium, Fourier analysis[4] for the spatially continuous form of the S_N equations shows that the spectral radius of SI is equivalent to the scattering ratio c:

$$\rho_{SI} = c = \frac{\sigma_s}{\sigma_t}. \tag{1.7}$$

The spectral radius is the magnitude of the largest iteration eigenvalue. Thus, it is the asymptotic rate of error reduction after many iterations when only the slowest converging mode remains in the error. For optically thin or highly absorbing systems in which particles scatter just a few times on the average before being absorbed or escaping the system, the SI process will converge quickly. While for optically thick diffusive systems in which particles can scatter an arbitrary number of times on the average before being absorbed or escaping the system, the SI process will converge slowly and will be quite costly. In the latter case, SI is not a practical iterative scheme.

Diffusion Synthetic Acceleration (DSA)

In optically thick diffusive systems in which particles can scatter many times on the average before being absorbed or escaping the system, the SI process must be accelerated. During the past several decades, much effort has been made in acceleration algorithms. One of the most widely applied methods is Diffusion Synthetic-Acceleration (DSA).

The principle of the DSA is to use a diffusion approximation to estimate the error of the scalar flux obtained from SI so that the accuracy can be improved and the iterative convergence accelerated. We next derive the DSA scheme. The first step is to solve the S_N equations by SI:

$$\mu_m \frac{d\psi_m^{l+1/2}(x)}{dx} + \sigma_t \psi_m^{l+1/2}(x) = \frac{\sigma_s}{2}\phi^l(x) + Q_m(x), \tag{1.8}$$

where $m = 1,..., N$. The errors at this step in the angular and scalar fluxes are respectively given by:

$$\delta\psi_m^{l+1/2}(x) = \psi_m(x) - \psi_m^{l+1/2}(x), \tag{1.9}$$

and

$$\delta\phi^{l+1/2}(x) = \phi(x) - \phi^{l+1/2}(x), \tag{1.10}$$

where $\psi_m(x)$ and $\phi(x)$ are the exact solutions of the angular flux and scalar flux to the S_N equations. We subtract the SI equation from the continuous transport equation to get:

$$\mu_m \frac{\partial \delta\psi_m^{l+1/2}(x)}{\partial x} + \sigma_t \delta\psi_m^{l+1/2}(\mu, x) = \frac{\sigma_s}{2}\delta\phi^l(x). \tag{1.11}$$

Subtract the quantity $\frac{\sigma_s}{2}\delta\phi^{l+1/2}(x)$ from both sides of the above equation to obtain the exact equation for $\delta\psi_m^{l+1/2}$:

$$\mu_m \frac{\partial \delta\psi_m^{l+1/2}(x)}{\partial x} + \sigma_t \delta\psi_m^{l+1/2}(\mu, x) - \frac{\sigma_s}{2}\delta\phi^{l+1/2}(x) = \frac{\sigma_s}{2}(\delta\phi^l(x) - \delta\phi^{l+1/2}(x)). \tag{1.12}$$

Re-expressing the right hand side using Eq. (1.10) gives:

$$\mu_m \frac{\partial \delta\psi_m^{l+1/2}(x)}{\partial x} + \sigma_t \delta\psi_m^{l+1/2}(\mu, x) - \frac{\sigma_s}{2}\delta\phi^{l+1/2}(x) = \frac{\sigma_s}{2}(\phi^{l+1/2}(x) - \phi^l(x)). \tag{1.13}$$

Thus, the error of the angular flux at iteration step $l + 1/2$ satisfies the transport equation with a source equal to:

$$\frac{\sigma_s}{2}(\phi^{l+1/2}(x) - \phi^l(x)). \tag{1.14}$$

However, it is obvious that this equation for $\delta\psi_m^{l+1/2}(x)$ is as difficult to solve as that for $\psi_m(x)$. We need to substitute an approximation to Eq. (1.13) that simple enough to solve but accurate in a certain sense.

The central theme of the DSA scheme is to substitute the diffusion equation for the exact transport equation for the error. The following is the DSA scheme:

$$\mu_m \frac{d\psi_m^{l+1/2}(x)}{dx} + \sigma_t \psi_m^{l+1/2}(x) = \frac{\sigma_s}{2}\phi^l(x) + Q_m(x), \tag{1.15}$$

$$\phi^l(x) = \sum_{m=1}^{N} w_m \psi^l{}_m(x), \tag{1.16}$$

$$-\frac{\partial}{\partial x}\frac{1}{3\sigma_t}\frac{\partial \Delta\phi^{l+1/2}(x)}{\partial x} + \sigma_a \Delta\phi^{l+1/2}(x) = \sigma_s(\phi^{l+1/2}(x) - \phi^l(x)), \tag{1.17}$$

$$\phi^{l+1}(x) = \phi^{l+1/2}(x) + \Delta\phi^{l+1/2}(x), \tag{1.18}$$

where $\Delta\phi(x)$ denotes the estimated scalar flux error from the diffusion equation as opposed to $\delta\phi(x)$, the true error.

An infinite-medium Fourier analysis[4] shows that DSA attenuates the errors of the low frequency modes which are most poorly attenuated by the SI. At the same time, DSA also underestimates the high frequency modes which are strongly attenuated by the SI. Thus, DSA can decrease the spectral radius and efficiently accelerate the iteration process. Fourier analysis gives the spectral radius of DSA as:

$$\rho_{DSA} \le 0.2247c, \tag{1.19}$$

where *c* is the scattering ratio.

S_2 synthetic acceleration (S2SA)

In this study, S_2 synthetic acceleration is applied instead of DSA. This means that the S_2 equations are substituted for the diffusion equation. In 1-D slab geometry, the S_2 equations are analytically equivalent to the diffusion equation. The reason we choose the S2SA scheme in the code is that we can use the same spatial discretization scheme for the acceleration as for the SI itself. Consistency of the spatial discretization for the acceleration equation with that of the transport equation is essential for unconditional stability and effectiveness[5]. The S2SA scheme is:

$$\mu_m \frac{d\psi_m^{l+1/2}(x)}{dx} + \sigma_t \psi_m^{l+1/2}(x) = \frac{\sigma_s}{2}\phi^l(x) + Q_m(x), \tag{1.20}$$

$$\phi^l(x) = \sum_{m=1}^{N} w_m \psi^l{}_m(x), \tag{1.21}$$

$$\pm\frac{1}{\sqrt{3}}\frac{df_\pm^{l+1/2}(x)}{dx} + \sigma_t f_\pm^{l+1/2}(x) - \frac{\sigma_s}{2}(f_+^{l+1/2}(x) + f_-^{l+1/2}(x)) = \frac{\sigma_s}{2}(\phi^{l+1/2}(x) - \phi^l(x)), \tag{1.22}$$

$$\phi^{l+1}(x) = \phi^{l+1/2}(x) + f^{l+1/2}(x), \tag{1.23}$$

where

$$f^{l+1/2}(x) = f_+^{l+1/2}(x) + f_-^{l+1/2}(x), \tag{1.24}$$

where $f_\pm(x)$ are the flux of particles traveling in the positive and negative directions. We subtract Eq. (1.23) from the trivial equation, $\phi(x) = \phi(x)$, to obtain:

$$\delta\phi^{l+1}(x) = \delta\phi^{l+1/2}(x) - f^{l+1/2}(x), \tag{1.25}$$

The scalar flux error at step $l+1$ is equal to the scalar flux error at step $l+1/2$ minus the scalar flux error estimate from the S_2 equations.

Overview of chapters

In this chapter, we briefly described several spatial discretization methods for the S_N equations. We gave the 1-D S_N equations with some assumptions. The iteration techniques including SI, DSA and S2SA were introduced.

In Chapter II, we propose the new LDLS method and show the detailed spatial discretization of the S_N equations with the LDLS, LDG and LLDG methods. The spatial discretization of the S2SA scheme is also presented. The robustness and accuracy of the LDLS method is investigated through a simplified pure absorber transport equation.

Chapter III presents a single mode Fourier analysis for the spectral radius from both the LDG and LLDG methods in order to make a comparison with that for the LDLS method. Both SI and S2SA iteration techniques are analyzed and implemented in MATLAB.

Chapter IV gives a detailed asymptotic analysis for the LDLS method to study its performance in the thick diffusion limit.

Chapter V presents the computational results for the new LDLS method and is divided into three parts. The first part gives the computational results for the accuracy measurements of the LDLS method compared with the other two methods. The second part shows the computational results for the spectral radii in some problems. The result is compared with the spectral radius obtained from the Fourier analysis. The third part is a study of the performance of the LDLS method in thick diffusion limit.

Chapter VI summarizes the conclusions from the previous chapters and gives some suggestions for future work.

CHAPTER II

SPATIAL DISCRETIZATION FOR S_N EQUATIONS

In this chapter, we first review the spatial discretization of the linear-discontinuous Galerkin (LDG) methods for the S_N equations. Then we propose the new linear-discontinuous least-squares (LDLS) method. The accuracy of the method is investigated for a simple pure absorber problem and compared with analogous results for the LDG and LLDG methods. Algorithms for S2SA acceleration are derived.

Linear-discontinuous Galerkin (LDG) methods

We begin the derivation of the LDG method by introducing the weighted residual method. We firstly give the indexing for the spatial discretization in Fig. 2.1. In this study, we focus on 1-D slab geometry problems with uniform spatial meshes. Note from the figure that half-integral indices imply the cell-edge quantities, i.e.,

$$\begin{aligned} \psi_{m,i-1/2} &= \psi_{m,R,i-1} \quad \text{for } \mu_m > 0 \\ &= \psi_{m,L,i} \quad \text{for } \mu_m < 0. \end{aligned} \tag{2.1}$$

Integral indices imply the cell-average quantities, i.e.,

$$\psi_{m,i} = \frac{1}{2}(\psi_{m,L,i} + \psi_{m,R,i}). \tag{2.2}$$

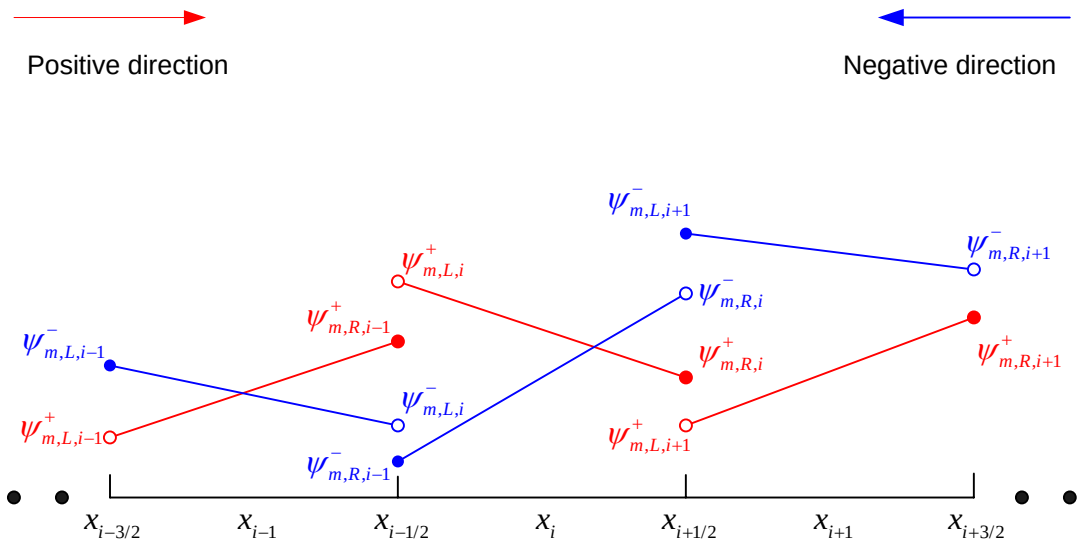

Fig. 2.1. Spatial discretization and the spatial shape of the angular flux.

Here we consider the following 1-D form:

$$A\psi(\vec{x}) = Q(\vec{x}), \tag{2.3}$$

where A is a linear operator, $\psi(\vec{x})$ is the solution and $Q(\vec{x})$ is the source function. The set of the trial space basis function for representing the solution is $\{B_i(\vec{x})\}_{i=1}^{L}$. Assuming the trial-space functions are chosen so that $\psi(\vec{x})$ naturally meets the boundary conditions, the approximate trial-space expansion for $\psi(\vec{x})$ is:

$$\tilde{\psi}(\vec{x}) = \sum_{i=1}^{L} \psi_i B_i(\vec{x}). \tag{2.4}$$

Define the residual as follows:

$$R(\vec{x}) = Q(\vec{x}) - A\tilde{\psi}(\vec{x}). \tag{2.5}$$

The error in the solution is proportional to the size of the residual. We want to choose the expansion coefficients $\{\psi_i\}_{i=1}^{L}$ so that the residual is small. There are several typical approaches. The weighted Residual method is defined by choosing the expansion coefficients $\{\psi_i\}_{i=1}^{L}$ so that the residual is orthogonal over the problem domain to the weighting functions $\{W_i(\vec{x})\}_{i=1}^{L}$, that is:

$$\int_{\vec{x}} R(\vec{x}) W_i(\vec{x}) d\vec{x} = 0, \tag{2.6}$$

where $i = 1,...,L$ .The set of N linearly-independent functions $\{W_i(\vec{x})\}_{i=1}^{L}$ form an L-dimensional space of functions called the weighting space. If the trial space is identical to the weighting space, i.e.,

$$B_i(\vec{x}) = W_i(\vec{x}), \tag{2.7}$$

the weighted residual method is named the Galerkin method. The linear-discontinuous Galerkin method is widely applied in the spatial discretization for the transport equation because of its characteristics of robustness and accuracy. We start the Galerkin method by choosing cardinal weight and basis functions which are unity at a given support point and zero at other support points. For the 1-D LDG problem, the weight and basis functions vary linearly from one to zero across the cell, $x \in [x_{i-1/2}, x_{i+1/2}]$:

$$B_{L,i}(x) = W_{L,i}(x) = \frac{x_{i+1/2} - x}{h_i}, \tag{2.8}$$

$$B_{R,i}(x) = W_{R,i}(x) = \frac{x - x_{i-1/2}}{h_i}. \tag{2.9}$$

To solve Eq. (1.4), we define the angular flux as follows on cell *i*:

For $\mu_m > 0$,

$$\begin{aligned} &\psi_{m,i}(x) = \psi_{m,R,i-1} \quad \text{for } x = x_{i-1/2}, \\ &\psi_{m,i}(x) = \psi_{m,L,i} B_{L,i}(x) + \psi_{m,R,i} B_{R,i}(x) \quad \text{otherwise.} \end{aligned} \tag{2.10}$$

For $\mu_m < 0$,

$$\begin{aligned} &\psi_{m,i}(x) = \psi_{m,L,i+1} \quad \text{for } x = x_{i+1/2}, \\ &\psi_{m,i}(x) = \psi_{m,L,i} B_{L,i}(x) + \psi_{m,R,i} B_{R,i}(x) \quad \text{otherwise.} \end{aligned} \tag{2.11}$$

An analogous spatial representation is assumed for the inhomogeneous source, except that there is no need to uniquely define Q on the cell interfaces. Thus,

$$Q_{m,i}(x) = Q_{m,L,i} B_{L,i}(x) + Q_{m,R,i} B_{R,i}(x) \quad \text{for } x \in [x_{i-1/2}, x_{i+1/2}]. \tag{2.12}$$

Multiplying Eq. (1.4) by the weight functions and integrating over the volume of the *i*th cell, we can obtain the standard LDG scheme:

For $\mu_m > 0$,

$$\begin{aligned} &\mu_m[\frac{1}{2}(\psi_{m,L,i} + \psi_{m,R,i}) - \psi_{m,R,i-1}] + \frac{\sigma_{t,i} h_i}{2}[(\frac{1+\beta}{2})\psi_{m,L,i} + (\frac{1-\beta}{2})\psi_{m,R,i}] = \\ &\frac{\sigma_{s,i} h_i}{4}[(\frac{1+\beta}{2})\phi_{L,i} + (\frac{1-\beta}{2})\phi_{R,i}] + \frac{h_i}{2}[(\frac{1+\beta}{2})Q_{m,L,i} + (\frac{1-\beta}{2})Q_{m,R,i}], \end{aligned} \tag{2.13}$$

$$\begin{aligned} &\mu_m[\psi_{m,R,i} - \frac{1}{2}(\psi_{m,L,i} + \psi_{m,R,i})] + \frac{\sigma_{t,i} h_i}{2}[(\frac{1-\beta}{2})\psi_{m,L,i} + (\frac{1+\beta}{2})\psi_{m,R,i}] = \\ &\frac{\sigma_{s,i} h_i}{4}[(\frac{1-\beta}{2})\phi_{L,i} + (\frac{1+\beta}{2})\phi_{R,i}] + \frac{h_i}{2}[(\frac{1-\beta}{2})Q_{m,L,i} + (\frac{1+\beta}{2})Q_{m,R,i}]. \end{aligned} \tag{2.14}$$

For $\mu_m < 0$,

$$\begin{aligned} &\mu_m[\frac{1}{2}(\psi_{m,L,i} + \psi_{m,R,i}) - \psi_{m,L,i}] + \frac{\sigma_{t,i} h_i}{2}[(\frac{1+\beta}{2})\psi_{m,L,i} + (\frac{1-\beta}{2})\psi_{m,R,i}] = \\ &\frac{\sigma_{s,i} h_i}{4}[(\frac{1+\beta}{2})\phi_{L,i} + (\frac{1-\beta}{2})\phi_{R,i}] + \frac{h_i}{2}[(\frac{1+\beta}{2})Q_{m,L,i} + (\frac{1-\beta}{2})Q_{m,R,i}], \end{aligned} \tag{2.15}$$

$$\mu_m[\psi_{m,L,i+1} - \frac{1}{2}(\psi_{m,L,i} + \psi_{m,R,i})] + \frac{\sigma_{t,i}h_i}{2}[(\frac{1-\beta}{2})\psi_{m,L,i} + (\frac{1+\beta}{2})\psi_{m,R,i}] = \frac{\sigma_{s,i}h_i}{4}[(\frac{1-\beta}{2})\phi_{L,i} + (\frac{1+\beta}{2})\phi_{R,i}] + \frac{h_i}{2}[(\frac{1-\beta}{2})Q_{m,L,i} + (\frac{1+\beta}{2})Q_{m,R,i}], \tag{2.16}$$

where

$$\phi_{L,i} = \sum_{m=1}^{N} w_m \psi_{m,L,i}, \tag{2.17}$$

$$\phi_{R,i} = \sum_{m=1}^{N} w_m \psi_{m,R,i}, \tag{2.18}$$

and $\beta = 1/3$. For each direction, there are two unknowns and two equations, so the system is closed. The parameter β is the mass lumping parameter. If β=1.0, we obtain the lumped linear-discontinuous Galerkin (LLDG) equations. By lumping, the robustness in the thick diffusion limit is improved, but it also reduces the accuracy.

Incompatibility of traditional least-squares methods with a discontinuous trial space

The traditional least-squares method is based upon choosing the expansion coefficients to minimize the functional, Γ, the integral of the square of the residual:

$$\Gamma = \int_{\vec{x}} R^2(\vec{x}) d\vec{x}. \tag{2.19}$$

However, these kinds of schemes are not compatible with a discontinuous trial space. This is due to the fact that the derivative of a discontinuous function takes the form of a delta-function at the point of discontinuity. If the residual contains a delta-function, the

integrand will contain the square of a delta-function, the integral of which is undefined. These concepts can be demonstrated mathematically as follows.

The trial space is the same for both the LDG method and LDLS method on the domain of $x \in [x_{i-1/2}, x_{i+1/2}]$ as in Eqs. (2.8) and (2.9). The definitions of the angular flux and the inhomogeneous source for the LDLS method are the same as those of the LDG method in Eqs. (2.10)-(2.12). The derivative of the angular flux is given by:

For $\mu_m > 0$,

$$\frac{d\psi_{m,i}(x)}{dx} = (\psi_{m,L,i} - \psi_{m,R,i-1})\delta(x - x_{i-1/2}) + \frac{1}{h_i}(\psi_{m,R,i} - \psi_{m,L,i}). \tag{2.20}$$

For $\mu_m < 0$,

$$\frac{d\psi_{m,i}(x)}{dx} = (\psi_{m,L+1,i} - \psi_{m,R,i})\delta(x - x_{i+1/2}) + \frac{1}{h_i}(\psi_{m,R,i} - \psi_{m,L,i}), \tag{2.21}$$

Thus, the residual is given by:

For $\mu_m > 0$,

$$\begin{aligned} R_{+,i}(x) &= S_{m,L,i}B_{L,i}(x) + S_{m,R,i}B_{R,i}(x) - \sigma_{t,i}(\psi_{m,L,i}B_{L,i} + \psi_{m,R,i}B_{R,i}) \\ &- \frac{\mu_m}{h_i}(\psi_{m,R,i} - \psi_{m,L,i}) - \mu_m(\psi_{m,L,i} - \psi_{m,R,i-1})\delta(x - x_{i-1/2}). \end{aligned} \tag{2.22}$$

For $\mu_m < 0$,

$$\begin{aligned} R_{-,i}(x) &= S_{m,L,i}B_{L,i}(x) + S_{m,R,i}B_{R,i}(x) - \sigma_{t,i}(\psi_{m,L,i}B_{L,i} + \psi_{m,R,i}B_{R,i}) \\ &- \frac{\mu_m}{h_i}(\psi_{m,R,i} - \psi_{m,L,i}) - \mu_m(\psi_{m,L,i+1} - \psi_{m,R,i})\delta(x - x_{i+1/2}), \end{aligned} \tag{2.23}$$

where the source term $S_m(x)$ includes both the isotropic external source $Q(x)$ and the isotropic scattering source,

$$S_{m,i}(x) = \frac{\sigma_{s,i}}{2} \sum_{m=1}^{N} w_m \psi_{m,i}(x) + Q_{m,i}(x). \tag{2.24}$$

Based on the traditional least-squares method, the integral of the square of the residual Γ need to be minimized over the interval $[x_{i-1/2}, x_{i+1/2}]$, where

$$\tilde{\Gamma}_{\pm,i} = \int_{x_{i-1/2}}^{x_{i+1/2}} R_{\pm,i}{}^2(x)dx. \tag{2.25}$$

If substitute Eqs. (2.22) and (2.23) into Eq. (2.25), it is clear that the integrand contains the square of a delta-function, and this kind of integral is undefined.

The new linear-discontinuous least-squares (LDLS) method

We want to find a method that would be inherently more robust than the DG method and yield a uniform level of second-order accuracy in both 1-D and multidimensional calculations. The incompatibility of the traditional least squares method with a discontinuous trial space is that the integrand contains the square of a delta-function, and the integral of the square of a delta-function does not exist. However, one can avoid the delta-function problem by minimizing the residual over the semi-open interval $(x_{i-1/2}, x_{i+1/2}]$ for $\mu_m > 0$ and $[x_{i-1/2}, x_{i+1/2})$ for $\mu_m < 0$. But in this case, the equations have no knowledge of the boundary value of the angular flux and the trivial solution ($\psi = 0$) is obtained. The central theme of our approach is to first avoid the delta-function difficulty by minimizing the square of the residual over the semi-open interval, and then imparting both conservation and knowledge of the boundary value to

the equations by constraining the solution to satisfy the balance equation. The scheme is demonstrated mathematically as following:

We use the same definition of the residual and the same Cardinal basis functions. However, we define:

$$\Gamma_{+,i}(\psi_{m,L,i},\psi_{m,R,i},\lambda_i)=\int_{x^{+}_{i-1/2}}^{x_{i+1/2}} {R_{+,i}}^2(x)dx-\lambda_i\int_{x_{i-1/2}}^{x_{i+1/2}} R_{+,i}(x)dx \quad \text{for } \mu_m>0, \tag{2.26}$$

$$\Gamma_{-,i}(\psi_{m,L,i},\psi_{m,R,i},\lambda_i)=\int_{x_{i-1/2}}^{x^{-}_{i+1/2}} {R_{-,i}}^2(x)dx-\lambda_i\int_{x_{i-1/2}}^{x_{i+1/2}} R_{-,i}(x)dx \quad \text{for } \mu_m<0, \tag{2.27}$$

where λ_i is a Lagrange multiplier and in which the balance equation for the closed domain $[x_{i-1/2},x_{i+1/2}]$ is:

$$\int_{x_{i-1/2}}^{x_{i+1/2}} R_{+,i}(x)dx=0 \quad \text{for } \mu_m>0, \tag{2.28}$$

$$\int_{x_{i-1/2}}^{x_{i+1/2}} R_{-,i}(x)dx=0 \quad \text{for } \mu_m<0. \tag{2.29}$$

Expanding Eqs. (2.28) and (2.29), we get:

$$\mu_m(\psi_{m,R,i}-\psi_{m,R,i-1})+\sigma_{t,i}h_i\frac{\psi_{m,L,i}+\psi_{m,R,i}}{2}=h_i\frac{S_{m,L,i}+S_{m,R,i}}{2} \quad \text{for } \mu_m>0, \tag{2.30}$$

$$\mu_m(\psi_{m,L,i+1}-\psi_{m,L,i})+\sigma_{t,i}h_i\frac{\psi_{m,L,i}+\psi_{m,R,i}}{2}=h_i\frac{S_{m,L,i}+S_{m,R,i}}{2} \quad \text{for } \mu_m<0, \tag{2.31}$$

where the total source term contains the scattering source and the inhomogeneous source:

$$S_{m,L,i}=\frac{\sigma_s}{2}\phi_{L,i}+Q_{m,L,i}, \tag{2.32}$$

$$S_{m,R,i} = \frac{\sigma_s}{2}\phi_{R,i} + Q_{m,R,i}. \tag{2.33}$$

Equivalently, we solve the following three equations for $\psi_{m,L,i}$, $\psi_{m,R,i}$ and λ_i, respectively:

For $\mu_m > 0$,

$$\frac{\partial \Gamma_{+,i}(\psi_{m,L,i}, \psi_{m,R,i}, \lambda_i)}{\partial \psi_{m,L,i}} = 0, \tag{2.34}$$

$$\frac{\partial \Gamma_{+,i}(\psi_{m,L,i}, \psi_{m,R,i}, \lambda_i)}{\partial \psi_{m,R,i}} = 0, \tag{2.35}$$

$$\frac{\partial \Gamma_{+,i}(\psi_{m,L,i}, \psi_{m,R,i}, \lambda_i)}{\partial \lambda_i} = 0. \tag{2.36}$$

For $\mu_m < 0$,

$$\frac{\partial \Gamma_{-,i}(\psi_{m,L,i}, \psi_{m,R,i}, \lambda_i)}{\partial \psi_{m,L,i}} = 0, \tag{2.37}$$

$$\frac{\partial \Gamma_{-,i}(\psi_{m,L,i}, \psi_{m,R,i}, \lambda_i)}{\partial \psi_{m,R,i}} = 0, \tag{2.38}$$

$$\frac{\partial \Gamma_{-,i}(\psi_{m,L,i}, \psi_{m,R,i}, \lambda_i)}{\partial \lambda_i} = 0. \tag{2.39}$$

Writing these equations in more detail, for $\mu_m > 0$, we get:

$$\int_{x^+_{i-1/2}}^{x_{i+1/2}} 2R_{+,i}(x)\frac{\partial R_{+,i}(x)}{\partial \psi_{m,L,i}}dx - \lambda_i \frac{\partial[\int_{x_{i-1/2}}^{x_{i+1/2}} R_{+,i}(x)dx]}{\partial \psi_{m,L,i}} = 0, \tag{2.40}$$

$$\int_{x^+_{i-1/2}}^{x_{i+1/2}} 2R_{+,i}(x)\frac{\partial R_{+,i}(x)}{\partial \psi_{m,R,i}}dx - \lambda_i \frac{\partial[\int_{x_{i-1/2}}^{x_{i+1/2}} R_{+,i}(x)dx]}{\partial \psi_{m,R,i}} = 0, \tag{2.41}$$

$$\int_{x_{i-1/2}}^{x_{i+1/2}} R_{+,i}(x)dx = 0. \tag{2.42}$$

For $\mu_m < 0$ we get:

$$\int_{x_{i-1/2}}^{\bar{x}_{i+1/2}} 2R_{-,i}(x)\frac{\partial R_{-,i}(x)}{\partial \psi_{m,L,i}}dx - \lambda_i \frac{\partial[\int_{x_{i-1/2}}^{x_{i+1/2}} R_{-,i}(x)dx]}{\partial \psi_{m,L,i}} = 0, \tag{2.43}$$

$$\int_{x_{i-1/2}}^{\bar{x}_{i+1/2}} 2R_{-,i}(x)\frac{\partial R_{-,i}(x)}{\partial \psi_{m,R,i}}dx - \lambda_i \frac{\partial[\int_{x_{i-1/2}}^{x_{i+1/2}} R_{-,i}(x)dx]}{\partial \psi_{m,R,i}} = 0, \tag{2.44}$$

$$\int_{x_{i-1/2}}^{x_{i+1/2}} R_{-,i}(x)dx = 0. \tag{2.45}$$

Substituting the expression for the residual in Eqs. (2.22) and (2.23) into Eqs. (2.40)-(2.45), we obtain:

For $\mu_m > 0$,

$$\int_{x^+_{i-1/2}}^{x_{i+1/2}} \{2[S_{m,L,i}B_{L,i}(x) + S_{m,R,i}B_{R,i}(x) - \sigma_{t,i}(\psi_{m,L,i}B_{L,i} + \psi_{m,R,i}B_{R,i}) - \frac{\mu_m}{h_i}(\psi_{m,R,i} - \psi_{m,L,i})](\frac{\mu_m}{h_i} - \sigma_{t,i}B_{L,i})\}dx + \lambda_i(\frac{\sigma_{t,i}h_i}{2}) = 0, \tag{2.46}$$

$$\int_{x^+_{i-1/2}}^{x_{i+1/2}} \{2[S_{m,L,i}B_{L,i}(x) + S_{m,R,i}B_{R,i}(x) - \sigma_{t,i}(\psi_{m,L,i}B_{L,i} + \psi_{m,R,i}B_{R,i}) - \frac{\mu_m}{h_i}(\psi_{m,R,i} - \psi_{m,L,i})](-\frac{\mu_m}{h_i} - \sigma_{t,i}B_{R,i})\}dx + \lambda_i(\frac{\sigma_{t,i}h_i}{2} + \mu_m) = 0, \tag{2.47}$$

$$\mu_m(\psi_{m,R,i}-\psi_{m,R,i-1})+\sigma_{t,i}h_i\frac{\psi_{m,L,i}+\psi_{m,R,i}}{2}=h_i\frac{S_{m,L,i}+S_{m,R,i}}{2}. \tag{2.48}$$

For $\mu_m<0$,

$$\int_{x_{i-1/2}}^{\bar{x}_{i+1/2}}\{2[S_{m,L,i}B_{L,i}(x)+S_{m,R,i}B_{R,i}(x)-\sigma_{t,i}(\psi_{m,L,i}B_{L,i} +\psi_{m,R,i}B_{R,i})-\frac{\mu_m}{h_i}(\psi_{m,R,i}-\psi_{m,L,i})](\frac{\mu_m}{h_i}-\sigma_{t,i}B_{L,i})\}dx+\lambda_i(\frac{\sigma_{t,i}h_i}{2}-\mu_m)=0, \tag{2.49}$$

$$\int_{x_{i-1/2}}^{\bar{x}_{i+1/2}}\{2[S_{m,L,i}B_{L,i}(x)+S_{m,R,i}B_{R,i}(x)-\sigma_{t,i}(\psi_{m,L,i}B_{L,i} +\psi_{m,R,i}B_{R,i})-\frac{\mu_m}{h_i}(\psi_{m,R,i}-\psi_{m,L,i})](-\frac{\mu_m}{h_i}-\sigma_{t,i}B_{R,i})\}dx+\lambda_i(\frac{\sigma_{t,i}h_i}{2})=0, \tag{2.50}$$

$$\mu_m(\psi_{m,L,i+1}-\psi_{m,L,i})+\sigma_{t,i}h_i\frac{\psi_{m,L,i}+\psi_{m,R,i}}{2}=h_i\frac{S_{m,L,i}+S_{m,R,i}}{2}. \tag{2.51}$$

We have three equations and three unknowns for each direction, so the system is closed and we are able to obtain $\psi_{m,L,i}$, $\psi_{m,R,i}$ and λ_i (although λ_i is not physically significant) for each spatial cell. This completes our description of the LDLS method for the 1-D slab-geometry S_N equations.

Robustness and accuracy analysis for different methods with a simplified pure absorber problem

To demonstrate the concepts and derive results for the basic methods with a minimum of complexity, here we first consider the following simplified transport equation:

$$\frac{\partial\psi}{\partial x}+\sigma\psi=0, \tag{2.52}$$

which is defined over the interval $[0, x_0]$, with the left boundary condition, $\psi_L^{exact}(0) = 1$.

The exact solution for $\psi(x_0)$ (the outflow) is:

$$\psi_R^{exact}(x_0) = \exp(-\sigma x_0). \tag{2.53}$$

The Taylor-series expansion about $\tau = 0$ is:

$$\psi_R^{exact}(\tau) = 1 - \tau + \frac{1}{2}\tau^2 - \frac{1}{6}\tau^3 + \frac{1}{24}\tau^4 + O(\tau^5), \tag{2.54}$$

where $\tau = \sigma x_0$ is the total mean-free-paths of the cell given.

The solution of the average flux is:

$$\psi_{avg}^{exact}(x) = \frac{1}{x_0}\int_0^{x_0} \exp(-\sigma x)dx = \frac{1-\exp(-\tau)}{\tau}. \tag{2.55}$$

The Taylor-series expansion about $\tau = 0$ is:

$$\psi_{avg}^{exact}(\tau) = 1 - \frac{1}{2}\tau + \frac{1}{6}\tau^2 - \frac{1}{24}\tau^3 + \frac{1}{120}\tau^4 + O(\tau^5). \tag{2.56}$$

Solving this simplified pure absorber problem with LDG method and LLDG method from Eqs. (2.13)-(2.16), and with LDLS method from Eqs. (2.46)-(2.51), we can get the following solutions in Table 2.1:

Table 2.1

Single-cell solutions from different schemes.

	Interior inflow	Outflow	Average flux
Exact	1	$\exp(-\tau)$	$\frac{1-\exp(-\tau)}{\tau}$
LDLS	$\frac{\tau^3+4\tau^2+12\tau+12}{\tau^4+2\tau^3+4\tau^2+12\tau+12}$	$\frac{\tau^3-2\tau^2+12}{\tau^4+2\tau^3+4\tau^2+12\tau+12}$	$\frac{\tau^3+\tau^2+6\tau+12}{\tau^4+2\tau^3+4\tau^2+12\tau+12}$
LDG	$\frac{6+4\tau}{6+4\tau+\tau^2}$	$\frac{6-2\tau}{6+4\tau+\tau^2}$	$\frac{6+\tau}{6+4\tau+\tau^2}$
LLDG	$\frac{1+\tau}{1+\tau+\frac{1}{2}\tau^2}$	$\frac{1}{1+\tau+\frac{1}{2}\tau^2}$	$\frac{1+\frac{1}{2}\tau}{1+\tau+\frac{1}{2}\tau^2}$

From Table 2.1, the outflow from LDG becomes negative after three (3) mean-free-paths, while that from both the LLDG and LDLS methods remains positive over the whole domain. In order to investigate the accuracy of each method, the Taylor-series expansion about $\tau = 0$ is applied to the expressions in Table 2.1 and the results are shown in Table 2.2.

Table 2.2

Taylor-series expansion for the solutions about $\tau = 0$.

	Interior inflow	Outflow	Average flux
Exact	1	$1-\tau+\frac{1}{2}\tau^2-\frac{1}{6}\tau^3+\frac{1}{24}\tau^4+O(\tau^5)$	$1-\frac{1}{2}\tau+\frac{1}{6}\tau^2-\frac{1}{24}\tau^3+\frac{1}{120}\tau^4+O(\tau^5)$
LDLS	$1-\frac{1}{12}\tau^3+O(\tau^5)$	$1-\tau+\frac{1}{2}\tau^2-\frac{1}{4}\tau^3+\frac{1}{6}\tau^4+O(\tau^5)$	$1-\frac{1}{2}\tau+\frac{1}{4}\tau^2-\frac{1}{6}\tau^3+\frac{1}{12}\tau^4+O(\tau^5)$
LDG	$1-\frac{1}{6}\tau^2+\frac{1}{9}\tau^3-\frac{5}{108}\tau^4+O(\tau^5)$	$1-\tau+\frac{1}{2}\tau^2-\frac{1}{6}\tau^3+\frac{1}{36}\tau^4+O(\tau^5)$	$1-\frac{1}{2}\tau+\frac{1}{6}\tau^2-\frac{1}{36}\tau^3-\frac{1}{108}\tau^4+O(\tau^5)$
LLDG	$1-\frac{1}{2}\tau^2+\frac{1}{2}\tau^3-\frac{1}{4}\tau^4+O(\tau^5)$	$1-\tau+\frac{1}{2}\tau^2-\frac{1}{4}\tau^4+O(\tau^5)$	$1-\frac{1}{2}\tau+\frac{1}{4}\tau^3-\frac{1}{4}\tau^4+O(\tau^5)$

The error obtained from a single step is called the local error. The local error is computed assuming the inflow is exact. The error obtained in a cell that is sufficiently far from an outer boundary is called the global error. In general, the global error is one order lower than the local error because of the error build up as outflow errors become inflow errors for adjacent cells. The local error for the fluxes is given in Table 2.3 based on the result in Table 2.2. Also, the global error for the fluxes is given in Table 2.4.

From Table 2.4, we can see that both the LDLS and the LLDG methods yield a uniform second order global error.

Table 2.3

Local error for the fluxes.

	Interior inflow	Outflow	Average Flux
LDLS	3^{rd}	3^{rd}	2^{nd}
LDG	2^{nd}	4^{th}	3^{rd}
LLDG	2^{nd}	3^{rd}	2^{nd}

Table 2.4

Global error for the fluxes.

	Interior inflow	Outflow	Average Flux
LDLS	2^{nd}	2^{nd}	2^{nd}
LDG	2^{nd}	3^{rd}	3^{rd}
LLDG	2^{nd}	2^{nd}	2^{nd}

The outflow with different methods is plotted in the Fig. 2.2. It can be observed that the LDG method yields a negative solution for thicknesses greater than 3 mean-free-paths. Both the LLDG and LDLS solutions are positive and monotone. Therefore, both the LLDG and LDLS methods are more robust than the LDG method. The LDLS solution is more accurate than the LLDG solution for small τ, while for large τ the

LLDG method varies as τ^{-2} whereas the LDG method and the LDLS method vary as τ^{-1}, so the LLDG method is the most accurate for large τ .

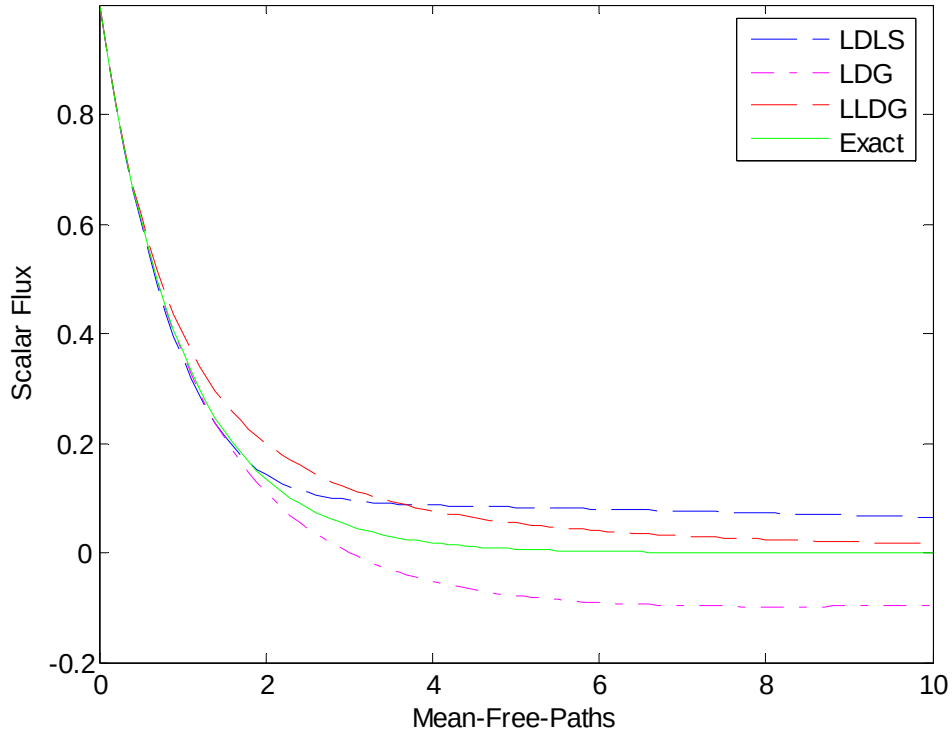

Fig. 2.2. Comparison of pure absorber solutions.

S2SA spatial discretization for the LDG method

The basic concept and scheme of S2SA acceleration has been introduced in the last chapter. In this section, we give three detailed spatial discretizations for the S2SA scheme applied with the LDG, LLDG, and LDLS schemes, respectively. As mentioned before, the advantage of S2SA is that we can use the same spatial discretization scheme for both the low-order S_2 transport equations and the high-order S_N equations thereby

ensuring consistancy. Recall that SI with S2SA in the continuous spatial scheme is described in Eqs. (1.20)-(1.23).

We first show the spatial discretization of the S2SA scheme for both the LDG and LLDG methods. Based on Eqs. (2.13)-(2.18), the high-order stage (SI) can be written as:

For $\mu_m > 0$,

$$\mu_m[\frac{1}{2}(\psi_{m,L,i}^{l+1/2}+\psi_{m,R,i}^{l+1/2})-\psi_{m,R,i-1}^{l+1/2}]+\frac{\sigma_{t,i}h_i}{2}[(\frac{1+\beta}{2})\psi_{m,L,i}^{l+1/2}+(\frac{1-\beta}{2})\psi_{m,R,i}^{l+1/2}]= \frac{\sigma_{s,i}h_i}{4}[(\frac{1+\beta}{2})\phi_{L,i}^{l}+(\frac{1-\beta}{2})\phi_{R,i}^{l}]+\frac{h_i}{2}[(\frac{1+\beta}{2})Q_{m,L,i}+(\frac{1-\beta}{2})Q_{m,R,i}], \tag{2.57}$$

$$\mu_m[\psi_{m,R,i}^{l+1/2}-\frac{1}{2}(\psi_{m,L,i}^{l+1/2}+\psi_{m,R,i}^{l+1/2})]+\frac{\sigma_{t,i}h_i}{2}[(\frac{1-\beta}{2})\psi_{m,L,i}^{l+1/2}+(\frac{1+\beta}{2})\psi_{m,R,i}^{l+1/2}]= \frac{\sigma_{s,i}h_i}{4}[(\frac{1-\beta}{2})\phi_{L,i}^{l}+(\frac{1+\beta}{2})\phi_{R,i}^{l}]+\frac{h_i}{2}[(\frac{1-\beta}{2})Q_{m,L,i}+(\frac{1+\beta}{2})Q_{m,R,i}]. \tag{2.58}$$

For $\mu_m < 0$,

$$\mu_m[\frac{1}{2}(\psi_{m,L,i}^{l+1/2}+\psi_{m,R,i}^{l+1/2})-\psi_{m,L,i}^{l+1/2}]+\frac{\sigma_{t,i}h_i}{2}[(\frac{1+\beta}{2})\psi_{m,L,i}^{l+1/2}+(\frac{1-\beta}{2})\psi_{m,R,i}^{l+1/2}]= \frac{\sigma_{s,i}h_i}{4}[(\frac{1+\beta}{2})\phi_{L,i}^{l}+(\frac{1-\beta}{2})\phi_{R,i}^{l}]+\frac{h_i}{2}[(\frac{1+\beta}{2})Q_{m,L,i}+(\frac{1-\beta}{2})Q_{m,R,i}], \tag{2.59}$$

$$\mu_m[\psi_{m,L,i+1}^{l+1/2}-\frac{1}{2}(\psi_{m,L,i}^{l+1/2}+\psi_{m,R,i}^{l+1/2})]+\frac{\sigma_{t,i}h_i}{2}[(\frac{1-\beta}{2})\psi_{m,L,i}^{l+1/2}+(\frac{1+\beta}{2})\psi_{m,R,i}^{l+1/2}]= \frac{\sigma_{s,i}h_i}{4}[(\frac{1-\beta}{2})\phi_{L,i}^{l}+(\frac{1+\beta}{2})\phi_{R,i}^{l}]+\frac{h_i}{2}[(\frac{1-\beta}{2})Q_{m,L,i}+(\frac{1+\beta}{2})Q_{m,R,i}], \tag{2.60}$$

where

$$\phi_{L,i}^{l}=\sum_{m=1}^{N}w_m\psi_{m,L,i}^{l}, \tag{2.61}$$

$$\phi_{R,i}^{l}=\sum_{m=1}^{N}w_m\psi_{m,R,i}^{l}, \tag{2.62}$$

and where the parameter β is the mass lumping parameter with $\beta = 1/3$ corresponding to LDG and $\beta = 1$ corresponding to LLDG. For the low-order (S_2) equations, the spatial discretization and the trial space are the same as those for the SI equation with S_2 quadrature. The flux of particles traveling in the positive $(\mu_m = 1/\sqrt{3})$ and negative $(\mu_m = -1/\sqrt{3})$ direction in the trial space on the domain of $x \in [x_{i-1/2}, x_{i+1/2}]$ can be written as:

For the positive direction,

$$\begin{aligned} f_{+,i}(x) &= f_{+,R,i-1} \quad \text{for } x = x_{i-1/2}, \\ f_{+,i}(x) &= f_{+,L,i}B_{L,i}(x) + f_{+,R,i}B_{R,i}(x) \quad \text{otherwise.} \end{aligned} \tag{2.63}$$

For the negative direction,

$$\begin{aligned} f_{-,i}(x) &= f_{-,L,i+1} \quad \text{for } x = x_{i+1/2}, \\ f_{-,i}(x) &= f_{-,L,i}B_{L,i}(x) + f_{-,R,i}B_{R,i}(x) \quad \text{otherwise.} \end{aligned} \tag{2.64}$$

The following is the scheme for the low-order (S_2) equations:

For the positive direction,

$$\begin{aligned} &\frac{1}{\sqrt{3}}[\frac{1}{2}(f_{+,L,i}^{l+1/2} + f_{+,R,i}^{l+1/2}) - f_{+,R,i-1}^{l+1/2}] + \frac{\sigma_{t,i}h_i}{2}[(\frac{1+\beta}{2})f_{+,L,i}^{l+1/2} + (\frac{1-\beta}{2})f_{+,R,i}^{l+1/2}] = \\ &\frac{\sigma_{s,i}h_i}{4}[(\frac{1+\beta}{2})(f_{+,L,i}^{l+1/2} + f_{-,L,i}^{l+1/2}) + (\frac{1-\beta}{2})(f_{+,R,i}^{l+1/2} + f_{-,R,i}^{l+1/2})] \\ &+ \frac{\sigma_{s,i}h_i}{4}[(\frac{1+\beta}{2})(\phi_{L,i}^{l+1/2} - \phi_{L,i}^{l}) + (\frac{1-\beta}{2})(\phi_{R,i}^{l+1/2} - \phi_{R,i}^{l})], \end{aligned} \tag{2.65}$$

$$\begin{aligned} &\frac{1}{\sqrt{3}}[f_{+,R,i}^{l+1/2} - \frac{1}{2}(f_{+,L,i}^{l+1/2} + f_{+,R,i}^{l+1/2})] + \frac{\sigma_{t,i}h_i}{2}[(\frac{1-\beta}{2})f_{+,L,i}^{l+1/2} + (\frac{1+\beta}{2})f_{+,R,i}^{l+1/2}] = \\ &\frac{\sigma_{s,i}h_i}{4}[(\frac{1-\beta}{2})(f_{+,L,i}^{l+1/2} + f_{-,L,i}^{l+1/2}) + (\frac{1+\beta}{2})(f_{+,R,i}^{l+1/2} + f_{-,R,i}^{l+1/2})] \\ &+ \frac{\sigma_{s,i}h_i}{4}[(\frac{1-\beta}{2})(\phi_{L,i}^{l+1/2} - \phi_{L,i}^{l}) + (\frac{1+\beta}{2})(\phi_{R,i}^{l+1/2} - \phi_{R,i}^{l})]. \end{aligned} \tag{2.66}$$

For the negative direction,

$$-\frac{1}{\sqrt{3}}[\frac{1}{2}(f_{-,L,i}^{l+1/2}+f_{-,R,i}^{l+1/2})-f_{-,L,i}^{l+1/2}]+\frac{\sigma_{t,i}h_i}{2}[(\frac{1+\beta}{2})f_{-,L,i}^{l+1/2}+(\frac{1-\beta}{2})f_{-,R,i}^{l+1/2}]=$$
$$\frac{\sigma_{s,i}h_i}{4}[(\frac{1+\beta}{2})(f_{+,L,i}^{l+1/2}+f_{-,L,i}^{l+1/2})+(\frac{1-\beta}{2})(f_{+,R,i}^{l+1/2}+f_{-,R,i}^{l+1/2})] \quad (2.67)$$
$$+\frac{\sigma_{s,i}h_i}{4}[(\frac{1+\beta}{2})(\phi_{L,i}^{l+1/2}-\phi_{L,i}^{l})+(\frac{1-\beta}{2})(\phi_{R,i}^{l+1/2}-\phi_{R,i}^{l})],$$

$$-\frac{1}{\sqrt{3}}[f_{-,L,i+1}^{l+1/2}-\frac{1}{2}(f_{-,L,i}^{l+1/2}+f_{-,R,i}^{l+1/2})]+\frac{\sigma_{t,i}h_i}{2}[(\frac{1-\beta}{2})f_{-,L,i}^{l+1/2}+(\frac{1+\beta}{2})f_{-,R,i}^{l+1/2}]=$$
$$\frac{\sigma_{s,i}h_i}{4}[(\frac{1-\beta}{2})(f_{+,L,i}^{l+1/2}+f_{-,L,i}^{l+1/2})+(\frac{1+\beta}{2})(f_{+,R,i}^{l+1/2}+f_{-,R,i}^{l+1/2})] \quad (2.68)$$
$$+\frac{\sigma_{s,i}h_i}{4}[(\frac{1-\beta}{2})(\phi_{L,i}^{l+1/2}-\phi_{L,i}^{l})+(\frac{1+\beta}{2})(\phi_{R,i}^{l+1/2}-\phi_{R,i}^{l})],$$

where $\phi_{L,i}=\sum_{m=1}^{N}w_m\psi_{m,L,i}$, and $\phi_{R,i}=\sum_{m=1}^{N}w_m\psi_{m,R,i}$. The parameter β is the mass lumping parameter. If $\beta=\frac{1}{3}$, we obtain the S2SA scheme for the standard LDG equations. If β=1.0, we obtain the S2SA scheme for the lumped linear-discontinuous Galerkin (LLDG) equations.

For the positive direction, there are two equations and two unknowns $f_{+,L,i}^{l+1/2}$ and $f_{+,R,i}^{l+1/2}$ per cell. The boundary flux $f_{+,R,i-1}^{l+1/2}$ can be eliminated via upwinding, i.e., Eq. (2.63). For the negative direction, there are two equations and two unknowns $f_{-,L,i}^{l+1/2}$ and $f_{-,R,i}^{l+1/2}$ per cell. The boundary flux $f_{-,L,i+1}^{l+1/2}$ can be eliminated via upwinding, i.e., Eq. (2.64). If we consider the entire slab which contains *I* spatial cells, there are 4*I* equations and 4*I* unknowns (the left and right boundary fluxes can be obtained from the boundary

conditions). Therefore, the system is closed. We can solve the $4I$ coupled equations through the following matrix:

$$A_{4I\times 4I}\vec{F}_{4I} = \delta\vec{\varphi}_{4I}, \tag{2.69}$$

where $\vec{F}_{4I}$ is the solution we desire, i.e.,

$$\begin{aligned}\vec{F}_{4I} = [\, & f_{+,L,1}^{l+1/2}, f_{-,L,1}^{l+1/2}, f_{+,R,1}^{l+1/2}, f_{-,R,1}^{l+1/2}, ..., f_{+,L,i}^{l+1/2}, f_{-,L,i}^{l+1/2}, f_{+,R,i}^{l+1/2}, f_{-,R,i}^{l+1/2}, \\ & ..., f_{+,L,I}^{l+1/2}, f_{-,L,I}^{l+1/2}, f_{+,R,I}^{l+1/2}, f_{-,R,I}^{l+1/2}]^T.\end{aligned} \tag{2.70}$$

The coefficient matrix $A_{4I\times 4I}$ is a 7-diagonal $4I\times 4I$ matrix, and the source term $\delta\vec{\phi}_{4I}$ is obtained from the solution of SI iterate. After solving the above equations, the accelerated scalar flux can be obtained as:

$$\phi_{L,i}^{l+1} = \phi_{L,i}^{l+1/2} + f_{+,L,i}^{l+1/2} + f_{-,L,i}^{l+1/2}, \tag{2.71}$$

$$\phi_{R,i}^{l+1} = \phi_{R,i}^{l+1/2} + f_{+,R,i}^{l+1/2} + f_{-,R,i}^{l+1/2}. \tag{2.72}$$

S2SA spatial discretization for the LDLS method

For the LDLS method, the definition of the flux representation for the S_2 equations is the same as that for LDG on the domain of $x\in[x_{i-1/2}, x_{i+1/2}]$ as in Eqs. (2.63) and (2.64). Based on Eqs. (2.46)-(2.51), the high-order stage (SI) can be written as:

For $\mu_m > 0$,

$$\begin{aligned}\int_{x^+_{i-1/2}}^{x_{i+1/2}} & \{2[S_{m,L,i}^{l}B_{L,i}(x) + S_{m,R,i}^{l}B_{R,i}(x) - \sigma_{t,i}(\psi_{m,L,i}^{l+1/2}B_{L,i} \\ & + \psi_{m,R,i}^{l+1/2}B_{R,i}) - \frac{\mu_m}{h_i}(\psi_{m,R,i}^{l+1/2} - \psi_{m,L,i}^{l+1/2})](\frac{\mu_m}{h_i} - \sigma_{t,i}B_{L,i})\}dx + \lambda_i(\frac{\sigma_{t,i}h_i}{2}) = 0,\end{aligned} \tag{2.73}$$

$$\int_{x^{+}_{i-1/2}}^{x_{i+1/2}} \{2[S^{l}_{m,L,i}B_{L,i}(x)+S^{l}_{m,R,i}B_{R,i}(x)-\sigma_{t,i}(\psi^{l+1/2}_{m,L,i}B_{L,i} +\psi^{l+1/2}_{m,R,i}B_{R,i})-\frac{\mu_m}{h_i}(\psi^{l+1/2}_{m,R,i}-\psi^{l+1/2}_{m,L,i})](-\frac{\mu_m}{h_i}-\sigma_{t,i}B_{R,i})\}dx+\lambda_i(\frac{\sigma_{t,i}h_i}{2}+\mu_m)=0, \quad (2.74)$$

$$\mu_m(\psi^{l+1/2}_{m,R,i}-\psi^{l+1/2}_{m,R,i-1})+\sigma_{t,i}h_i\frac{\psi^{l+1/2}_{m,L,i}+\psi^{l+1/2}_{m,R,i}}{2}=h_i\frac{S^{l}_{m,L,i}+S^{l}_{m,R,i}}{2}. \quad (2.75)$$

For $\mu_m<0$,

$$\int_{x_{i-1/2}}^{x^{-}_{i+1/2}} \{2[S^{l}_{m,L,i}B_{L,i}(x)+S^{l}_{m,R,i}B_{R,i}(x)-\sigma_{t,i}(\psi^{l+1/2}_{m,L,i}B_{L,i} +\psi^{l+1/2}_{m,R,i}B_{R,i})-\frac{\mu_m}{h_i}(\psi^{l+1/2}_{m,R,i}-\psi^{l+1/2}_{m,L,i})](\frac{\mu_m}{h_i}-\sigma_{t,i}B_{L,i})\}dx+\lambda_i(\frac{\sigma_{t,i}h_i}{2}-\mu_m)=0, \quad (2.76)$$

$$\int_{x_{i-1/2}}^{x^{-}_{i+1/2}} \{2[S^{l}_{m,L,i}B_{L,i}(x)+S^{l}_{m,R,i}B_{R,i}(x)-\sigma_{t,i}(\psi^{l+1/2}_{m,L,i}B_{L,i} +\psi^{l+1/2}_{m,R,i}B_{R,i})-\frac{\mu_m}{h_i}(\psi^{l+1/2}_{m,R,i}-\psi^{l+1/2}_{m,L,i})](-\frac{\mu_m}{h_i}-\sigma_{t,i}B_{R,i})\}dx+\lambda_i(\frac{\sigma_{t,i}h_i}{2})=0, \quad (2.77)$$

$$\mu_m(\psi^{l+1/2}_{m,L,i+1}-\psi^{l+1/2}_{m,L,i})+\sigma_{t,i}h_i\frac{\psi^{l+1/2}_{m,L,i}+\psi^{l+1/2}_{m,R,i}}{2}=h_i\frac{S^{l}_{m,L,i}+S^{l}_{m,R,i}}{2}, \quad (2.78)$$

where

$$S^{l}_{m,L,i}=\frac{\sigma_{s,i}}{2}\sum_{m=1}^{N}w_m\psi^{l}_{m,L,i}+Q_{m,L,i}, \quad (2.79)$$

$$S^{l}_{m,R,i}=\frac{\sigma_{s,i}}{2}\sum_{m=1}^{N}w_m\psi^{l}_{m,R,i}+Q_{m,R,i}. \quad (2.80)$$

Based on these SI equations, the residual for S_2 acceleration can be written as:

For the positive direction,

$$
\begin{aligned}
r_{+,i}(x) &= \frac{\sigma_{s,i}}{2}[(\phi_{L,i}^{l+1/2} - \phi_{L,i}^{l})B_{L,i}(x) + (\phi_{L,i}^{l+1/2} - \phi_{L,i}^{l})B_{R,i}(x)] \\
&+ \frac{\sigma_{s,i}}{2}[(f_{+,L,i}^{l+1/2} + f_{-,L,i}^{l+1/2})B_{L,i}(x) + (f_{+,R,i}^{l+1/2} + f_{-,R,i}^{l+1/2})B_{R,i}(x)] \\
&- \sigma_{t,i}[f_{+,L,i}^{l+1/2}B_{L,i}(x) + f_{+,R,i}^{l+1/2}B_{R,i}(x)] - \frac{1}{\sqrt{3}h_i}(f_{+,R,i}^{l+1/2} - f_{+,L,i}^{l+1/2}) \\
&- \frac{1}{\sqrt{3}}(f_{+,L,i}^{l+1/2} - f_{+,R,i-1}^{l+1/2})\delta(x - x_{i-1/2}).
\end{aligned}
\tag{2.81}
$$

For the negative direction,

$$
\begin{aligned}
r_{-,i}(x) &= \frac{\sigma_{s,i}}{2}[(\phi_{L,i}^{l+1/2} - \phi_{L,i}^{l})B_{L,i}(x) + (\phi_{L,i}^{l+1/2} - \phi_{L,i}^{l})B_{R,i}(x)] \\
&+ \frac{\sigma_{s,i}}{2}[(f_{+,L,i}^{l+1/2} + f_{-,L,i}^{l+1/2})B_{L,i}(x) + (f_{+,R,i}^{l+1/2} + f_{-,R,i}^{l+1/2})B_{R,i}(x)] \\
&- \sigma_{t,i}[f_{-,L,i}^{l+1/2}B_{L,i}(x) + f_{-,R,i}^{l+1/2}B_{R,i}(x)] + \frac{1}{\sqrt{3}h_i}(f_{-,R,i}^{l+1/2} - f_{-,L,i}^{l+1/2}) \\
&+ \frac{1}{\sqrt{3}}(f_{+,L,i+1}^{l+1/2} - f_{+,R,i}^{l+1/2})\delta(x - x_{i+1/2}).
\end{aligned}
\tag{2.82}
$$

The least-squares functionals for the S_2 equations take the following form:

$$
\gamma_{+,i}(f_{+,L,i}^{l+1/2}, f_{+,R,i}^{l+1/2}, \lambda_i) = \int_{x^{+}_{i-1/2}}^{x_{i+1/2}} r_{+,i}{}^{2}(x)dx - \lambda_i \int_{x_{i-1/2}}^{x_{i+1/2}} r_{+,i}(x)dx, \tag{2.83}
$$

$$
\gamma_{-,i}(f_{-,L,i}^{l+1/2}, f_{-,R,i}^{l+1/2}, \lambda_i) = \int_{x_{i-1/2}}^{x^{-}_{i+1/2}} r_{-,i}{}^{2}(x)dx - \lambda_i \int_{x_{i-1/2}}^{x_{i+1/2}} r_{-,i}(x)dx, \tag{2.84}
$$

where λ_i is a Lagrange multiplier. The balance equation in the closed domain $[x_{i-1/2}, x_{i+1/2}]$ is:

For the positive direction,

$$
\int_{x_{i-1/2}}^{x_{i+1/2}} r_{+,i}(x)dx = 0. \tag{2.85}
$$

For the negative direction,

$$\int_{x_{i-1/2}}^{x_{i+1/2}} r_{-,i}(x)dx = 0. \tag{2.86}$$

Substituting Eqs. (2.81) and (2.82) into Eqs. (2.85) and (2.86), we obtain the balance equations as follows:

For the positive direction,

$$\begin{aligned} &\frac{1}{\sqrt{3}}(f_{+,R,i}^{l+1/2} - f_{+,R,i-1}^{l+1/2}) + \sigma_{t,i}h_i \frac{f_{+,L,i}^{l+1/2} + f_{+,R,i}^{l+1/2}}{2} \\ &= \frac{\sigma_{s,i}h_i}{2} \frac{(f_{+,L,i}^{l+1/2} + f_{-,L,i}^{l+1/2}) + (f_{+,R,i}^{l+1/2} + f_{-,R,i}^{l+1/2})}{2} \\ &+ \frac{\sigma_{s,i}h_i}{2} \frac{(\phi_{L,i}^{l+1/2} - \phi_{L,i}^{l}) + (\phi_{R,i}^{l+1/2} - \phi_{R,i}^{l})}{2}. \end{aligned} \tag{2.87}$$

For the negative direction,

$$\begin{aligned} &-\frac{1}{\sqrt{3}}(f_{-,L,i+1}^{l+1/2} - f_{-,L,i}^{l+1/2}) + \sigma_{t,i}h_i \frac{f_{-,L,i}^{l+1/2} + f_{-,R,i}^{l+1/2}}{2} \\ &= \frac{\sigma_{s,i}h_i}{2} \frac{(f_{+,L,i}^{l+1/2} + f_{-,L,i}^{l+1/2}) + (f_{+,R,i}^{l+1/2} + f_{-,R,i}^{l+1/2})}{2} \\ &+ \frac{\sigma_{s,i}h_i}{2} \frac{(\phi_{L,i}^{l+1/2} - \phi_{L,i}^{l}) + (\phi_{R,i}^{l+1/2} - \phi_{R,i}^{l})}{2}. \end{aligned} \tag{2.88}$$

Now we solve the following three equations for each direction, respectively:

For the positive direction,

$$\frac{\partial \gamma_{+,i}(f_{+,L,i}^{l+1/2}, f_{+,R,i}^{l+1/2}, \lambda_i)}{\partial f_{+,L,i}^{l+1/2}} = 0, \tag{2.89}$$

$$\frac{\partial \gamma_{+,i}(f_{+,L,i}^{l+1/2}, f_{+,R,i}^{l+1/2}, \lambda_i)}{\partial f_{+,R,i}^{l+1/2}} = 0, \tag{2.90}$$

$$\frac{\partial \gamma_{+,i}(f_{+,L,i}^{l+1/2}, f_{+,R,i}^{l+1/2}, \lambda_i)}{\partial \lambda} = 0. \tag{2.91}$$

For the negative direction,

$$\frac{\partial \gamma_{-,i}(f_{-,L,i}^{l+1/2}, f_{-,R,i}^{l+1/2}, \lambda_i)}{\partial f_{-,L,i}^{l+1/2}} = 0, \tag{2.92}$$

$$\frac{\partial \gamma_{-,i}(f_{-,L,i}^{l+1/2}, f_{-,R,i}^{l+1/2}, \lambda_i)}{\partial f_{-,R,i}^{l+1/2}} = 0, \tag{2.93}$$

$$\frac{\partial \gamma_{-,i}(f_{-,L,i}^{l+1/2}, f_{-,R,i}^{l+1/2}, \lambda_i)}{\partial \lambda} = 0. \tag{2.94}$$

For the positive direction, there are three equations and three unknowns per cell, i.e., $f_{+,L,i}^{l+1/2}$, $f_{+,R,i}^{l+1/2}$ and the Lagrange multiplier λ_i. λ_i is not physically significant and can be eliminated. Thus, now we have two equations and two unknowns per cell, so the system is close. The boundary flux $f_{+,R,i-1}^{l+1/2}$ can be eliminated via upwinding, i.e., Eq. (2.63). For the negative direction, there are three equations and three unknowns $f_{-,L,i}^{l+1/2}$, $f_{-,R,i}^{l+1/2}$ and λ_i per cell. After eliminating λ_i, we have two equations and two unknowns, so the system is close. The boundary flux $f_{-,L,i+1}^{l+1/2}$ can be eliminated via upwinding, i.e., Eq. (2.64).

If we consider the entire slab which contains *I* spatial cells, there are 4*I* equations and 4*I* unknowns (the left and right boundary fluxes can be obtained from the boundary conditions). Therefore, the system is closed. We solve the 4*I* coupled equations also through Eq. (2.69). The coefficient matrix $A_{4I\times 4I}$ is a 7-diagonal $4I \times 4I$ matrix, and the

source term $\delta\vec{\phi}_{4I}$ is obtained from the solution of SI iterate. After solving the above equations, the scalar flux with the corrected error can be obtained as:

$$\phi_{L,i}^{l+1} = \phi_{L,i}^{l+1/2} + f_{+,L,i}^{l+1/2} + f_{-,L,i}^{l+1/2}, \tag{2.95}$$

$$\phi_{R,i}^{l+1} = \phi_{R,i}^{l+1/2} + f_{+,R,i}^{l+1/2} + f_{-,R,i}^{l+1/2}. \tag{2.96}$$

Summary

In this chapter, we briefly described the most commonly applied spatial discretization method: linear-discontinuous Galerkin (LDG) method. We proposed our new LDLS method. We also presented the spatially discretized form of the S2SA scheme. The equations obtained were implemented in a FORTRAN code and the numerical results will be presented in Chapter V.

We explored the robustness of the LDLS method through a simplified pure absorber transport equation and compared the robustness of the solutions from LDG and LLDG. We found that the LDLS method is more robust than the LDG method and more accurate than the LLDG method in the 1-D slab geometry.

CHAPTER III

FOURIER ANALYSIS FOR SPECTRAL RADIUS

In this chapter, we perform a Fourier analysis for the LDG, LLDG, and LDLS methods to investigate the iterative convergence behavior of both the source iteration and S2SA process. We consider an infinite, homogenous medium and uniform mesh problem. All the calculations are implemented by MATLAB.

Derivation of Fourier analysis for the LDG method

The continuous form of the S2SA scheme is given in Eqs. (1.20)-(1.23). In this section we want to perform the Fourier analysis for the LDG method. Our first task is to obtain the scalar flux error at step $l+1/2$ in terms of the scalar flux error at step l. The exact LDG scheme is given in Eqs. (2.13)-(2.18), and its SI scheme is given in Eqs. (2.57)-(2.62) in the previous chapter. Based on these equations, we obtain the exact equations for the error:

For $\mu_m > 0$,

$$\mu_m[\frac{1}{2}(\delta\psi_{m,L,i}^{l+1/2}+\delta\psi_{m,R,i}^{l+1/2})-\delta\psi_{m,R,i-1}^{l+1/2}]+\frac{\sigma_{t,i}h_i}{2}[(\frac{1+\beta}{2})\delta\psi_{m,L,i}^{l+1/2}+(\frac{1-\beta}{2})\delta\psi_{m,R,i}^{l+1/2}] = \frac{\sigma_{s,i}h_i}{4}[(\frac{1+\beta}{2})\delta\phi_{L,i}^{l}+(\frac{1-\beta}{2})\delta\phi_{R,i}^{l}], \tag{3.1}$$

$$\mu_m[\delta\psi_{m,R,i}^{l+1/2}-\frac{1}{2}(\delta\psi_{m,L,i}^{l+1/2}+\delta\psi_{m,R,i}^{l+1/2})]+\frac{\sigma_{t,i}h_i}{2}[(\frac{1-\beta}{2})\delta\psi_{m,L,i}^{l+1/2}+(\frac{1+\beta}{2})\delta\psi_{m,R,i}^{l+1/2}] = \frac{\sigma_{s,i}h_i}{4}[(\frac{1-\beta}{2})\delta\phi_{L,i}^{l}+(\frac{1+\beta}{2})\delta\phi_{R,i}^{l}]. \tag{3.2}$$

For $\mu_m < 0$,

$$\mu_m[\frac{1}{2}(\delta\psi_{m,L,i}^{l+1/2} + \delta\psi_{m,R,i}^{l+1/2}) - \delta\psi_{m,L,i}^{l+1/2}] + \frac{\sigma_{t,i}h_i}{2}[(\frac{1+\beta}{2})\delta\psi_{m,L,i}^{l+1/2} + (\frac{1-\beta}{2})\delta\psi_{m,R,i}^{l+1/2}] = \frac{\sigma_{s,i}h_i}{4}[(\frac{1+\beta}{2})\delta\phi_{L,i}^{l} + (\frac{1-\beta}{2})\delta\phi_{R,i}^{l}], \tag{3.3}$$

$$\mu_m[\delta\psi_{m,L,i+1}^{l+1/2} - \frac{1}{2}(\delta\psi_{m,L,i}^{l+1/2} + \delta\psi_{m,R,i}^{l+1/2})] + \frac{\sigma_{t,i}h_i}{2}[(\frac{1-\beta}{2})\delta\psi_{m,L,i}^{l+1/2} + (\frac{1+\beta}{2})\delta\psi_{m,R,i}^{l+1/2}] = \frac{\sigma_{s,i}h_i}{4}[(\frac{1-\beta}{2})\delta\phi_{L,i}^{l} + (\frac{1+\beta}{2})\delta\phi_{R,i}^{l}], \tag{3.4}$$

where the error of the flux is given as:

$$\delta\psi_{m,L,i}^{l+1/2} = \psi_{m,L,i} - \psi_{m,L,i}^{l+1/2}, \tag{3.5}$$

$$\delta\psi_{m,R,i}^{l+1/2} = \psi_{m,R,i} - \psi_{m,R,i}^{l+1/2}, \tag{3.6}$$

$$\delta\phi_{L,i}^{l} = \phi_{L,i} - \phi_{L,i}^{l}, \tag{3.7}$$

$$\delta\phi_{R,i}^{l} = \phi_{R,i} - \phi_{R,i}^{l}, \tag{3.8}$$

and where the parameter β is the mass lumping parameter with $\beta = 1/3$ corresponding to LDG and $\beta = 1$ corresponding to LLDG.

We assume an infinite homogeneous, uniform mesh $(h_i = h)$. The spatial dependence of the discrete flux error is defined by a single Fourier mode, i.e.,

$$\delta\psi_{m,L,i}^{l+1/2} = \delta\Psi_{m,L}^{l+1/2}\exp(j\Lambda x_{i-1/2}), \tag{3.9}$$

$$\delta\psi_{m,R,i}^{l+1/2} = \delta\Psi_{m,R}^{l+1/2}\exp(j\Lambda x_{i+1/2}), \tag{3.10}$$

$$\delta\phi_{L,i}^{l} = \delta\Phi_{L}^{l}\exp(j\Lambda x_{i-1/2}), \tag{3.11}$$

$$\delta\phi_{R,i}^{l} = \delta\Phi_{R}^{l}\exp(j\Lambda x_{i+1/2}), \tag{3.12}$$

where $j=\sqrt{-1}$ and $-\infty<\Lambda<\infty$. We set a parameter $\theta=\Lambda h$ where h is the cell width. Substituting Eqs. (3.9)-(3.12) into the exact SI equations for the error, i.e., Eqs. (3.1)-(3.4), and dividing by $\exp(j\Lambda x_{i-1/2})$, we obtain the follows:

For $\mu_m>0$,

$$\mu_m[\frac{1}{2}(\delta\Psi_{m,L}^{l+1/2}+e^{j\theta}\delta\Psi_{m,R}^{l+1/2})-\delta\Psi_{m,R}^{l+1/2}]+\frac{\sigma_{t,i}h_i}{2}[(\frac{1+\beta}{2})\delta\Psi_{m,L}^{l+1/2} +(\frac{1-\beta}{2})e^{j\theta}\delta\Psi_{m,R}^{l+1/2}]=\frac{\sigma_{s,i}h_i}{4}[(\frac{1+\beta}{2})\delta\Phi_L^l+(\frac{1-\beta}{2})e^{j\theta}\delta\Phi_R^l], \tag{3.13}$$

$$\mu_m[e^{j\theta}\delta\Psi_{m,R}^{l+1/2}-\frac{1}{2}(\delta\Psi_{m,L}^{l+1/2}+e^{j\theta}\delta\Psi_{m,R}^{l+1/2})]+\frac{\sigma_{t,i}h_i}{2}[(\frac{1-\beta}{2})\delta\Psi_{m,L}^{l+1/2} +(\frac{1+\beta}{2})e^{j\theta}\delta\Psi_{m,R}^{l+1/2}]=\frac{\sigma_{s,i}h_i}{4}[(\frac{1-\beta}{2})\delta\Phi_L^l+(\frac{1+\beta}{2})e^{j\theta}\delta\Phi_R^l]. \tag{3.14}$$

For $\mu_m<0$,

$$\mu_m[\frac{1}{2}(\delta\Psi_{m,L}^{l+1/2}+e^{j\theta}\delta\Psi_{m,R}^{l+1/2})-\delta\Psi_{m,L}^{l+1/2}]+\frac{\sigma_{t,i}h_i}{2}[(\frac{1+\beta}{2})\delta\Psi_{m,L}^{l+1/2} +(\frac{1-\beta}{2})e^{j\theta}\delta\Psi_{m,R}^{l+1/2}]=\frac{\sigma_{s,i}h_i}{4}[(\frac{1+\beta}{2})\delta\Phi_L^l+(\frac{1-\beta}{2})e^{j\theta}\delta\Phi_R^l], \tag{3.15}$$

$$\mu_m[e^{j\theta}\delta\Psi_{m,L}^{l+1/2}-\frac{1}{2}(\delta\Psi_{m,L}^{l+1/2}+e^{j\theta}\delta\Psi_{m,R}^{l+1/2})]+\frac{\sigma_{t,i}h_i}{2}[(\frac{1-\beta}{2})\delta\Psi_{m,L}^{l+1/2}+ (\frac{1+\beta}{2})e^{j\theta}\delta\Psi_{m,R}^{l+1/2}]=\frac{\sigma_{s,i}h_i}{4}[(\frac{1-\beta}{2})\delta\Phi_L^l+(\frac{1+\beta}{2})e^{j\theta}\delta\Phi_R^l], \tag{3.16}$$

From Eqs. (3.13) and (3.14) for $\mu_m>0$, and from Eqs. (3.15) and (3.16) for $\mu_m<0$, respectively, we obtain the following equation for any given direction μ_m:

$$\begin{pmatrix}\delta\Psi_{m,L}^{l+1/2}\\ \delta\Psi_{m,R}^{l+1/2}\end{pmatrix}=M_m\begin{pmatrix}\delta\Phi_L^l\\ \delta\Phi_R^l\end{pmatrix}, \tag{3.17}$$

where M_m is the coefficient matrix solved from Eqs. (3.13) and (3.14) for $\mu_m > 0$, and from Eqs. (3.15) and (3.16) for $\mu_m < 0$. We write M_m as:

$$M_m = \begin{pmatrix} m_{11} & m_{12} \\ m_{21} & m_{22} \end{pmatrix}. \tag{3.18}$$

Multiplying Eq. (3.17) by w_m and summing over $m = 1,...,N$, we obtain the equation we desired, i.e., the scalar flux error at step $l+1/2$ in terms of the scalar flux error at step l:

$$\begin{pmatrix} \delta\Phi_L^{l+1/2} \\ \delta\Phi_R^{l+1/2} \end{pmatrix} = H_{SI} \begin{pmatrix} \delta\Phi_L^{l} \\ \delta\Phi_R^{l} \end{pmatrix}, \tag{3.19}$$

where

$$\delta\Phi_L^{l+1/2} = \sum_{m=1}^{N} \delta\Psi_{m,L}^{l+1/2} w_m, \tag{3.20}$$

$$\delta\Phi_R^{l+1/2} = \sum_{m=1}^{N} \delta\Psi_{m,R}^{l+1/2} w_m, \tag{3.21}$$

and where H_{SI} represents the source iteration eigenfunction matrix:

$$H_{SI} = \begin{pmatrix} h_{11} & h_{12} \\ h_{21} & h_{22} \end{pmatrix}, \tag{3.22}$$

$$h_{ij} = \sum_{m=1}^{N} m_{ij} w_m \text{ for } i = 1,2 \text{ and } j = 1,2. \tag{3.23}$$

Let $\alpha_{H_{SI},\max}(\theta)$ be the larger of the two eigenvalues of H_{SI} for a given value of θ. Then the "global" spectral radius that relates the scalar flux error at step $l+1/2$ to the scalar flux error at step l after sufficiently many iterations is given by:

$$\rho_{SI} = \max_{\text{all } \theta} \alpha_{H_{SI},\max}(\theta) \tag{3.24}$$

We refer to $\alpha_{H_{HSI},\max}(\theta)$ as the "local" spectral radius since it is the effective spectral radius for the single Fourier mode associated with a given value of θ.

Now let's move on to the low order S_2 equations. Our next task is to obtain the S_2 scalar flux error estimate in terms of the scalar flux error at step l. The discrete form of the low order S_2 scheme for the LDG method is given in Eqs. (2.65)-(2.68) . The spatial dependence of the S_2 flux error is defined by a single Fourier mode, i.e.,

$$f_{\pm,L,i}^{l+1/2} = F_{\pm,L}^{l+1/2}\exp(j\Lambda x_{i-1/2}), \tag{3.25}$$

$$f_{\pm,R,i}^{l+1/2} = F_{\pm,R}^{l+1/2}\exp(j\Lambda x_{i+1/2}), \tag{3.26}$$

Substituting Eqs. (3.11)-(3.12), Eqs. (3.20)-(3.21), and Eqs. (3.25)-(3.26) into the low-order S_2 scheme in Eqs. (2.65)-(2.68), and dividing by $\exp(j\Lambda x_{i-1/2})$, we get:

For the positive direction,

$$\begin{aligned}
&\frac{1}{\sqrt{3}}[\frac{1}{2}(F_{+,L}^{l+1/2}+e^{j\theta}F_{+,R}^{l+1/2})-F_{+,R}^{l+1/2}]+\frac{\sigma_{t,i}h_i}{2}[(\frac{1+\beta}{2})F_{+,L}^{l+1/2}+(\frac{1-\beta}{2})e^{j\theta}F_{+,R}^{l+1/2}]=\\
&\frac{\sigma_{s,i}h_i}{4}[(\frac{1+\beta}{2})(F_{+,L}^{l+1/2}+F_{-,L}^{l+1/2})+(\frac{1-\beta}{2})e^{j\theta}(F_{+,R}^{l+1/2}+F_{-,R}^{l+1/2})]\\
&+\frac{\sigma_{s,i}h_i}{4}[(\frac{1+\beta}{2})(\Phi_L^{l+1/2}-\Phi_L^{l})+(\frac{1-\beta}{2})e^{j\theta}(\Phi_R^{l+1/2}-\Phi_R^{l})],
\end{aligned} \tag{3.27}$$

$$\begin{aligned}
&\frac{1}{\sqrt{3}}[e^{j\theta}F_{+,R}^{l+1/2}-\frac{1}{2}(F_{+,L}^{l+1/2}+e^{j\theta}F_{+,R}^{l+1/2})]+\frac{\sigma_{t,i}h_i}{2}[(\frac{1-\beta}{2})F_{+,L}^{l+1/2}+(\frac{1+\beta}{2})e^{j\theta}F_{+,R}^{l+1/2}]=\\
&\frac{\sigma_{s,i}h_i}{4}[(\frac{1-\beta}{2})(F_{+,L}^{l+1/2}+F_{-,L}^{l+1/2})+(\frac{1+\beta}{2})e^{j\theta}(F_{+,R}^{l+1/2}+F_{-,R}^{l+1/2})]\\
&+\frac{\sigma_{s,i}h_i}{4}[(\frac{1-\beta}{2})(\Phi_L^{l+1/2}-\Phi_L^{l})+(\frac{1+\beta}{2})e^{j\theta}(\Phi_R^{l+1/2}-\Phi_R^{l})].
\end{aligned} \tag{3.28}$$

For the negative direction,

$$-\frac{1}{\sqrt{3}}[\frac{1}{2}(F_{-,L}^{l+1/2}+e^{j\theta}F_{-,R}^{l+1/2})-F_{-,L}^{l+1/2}]+\frac{\sigma_{t,i}h_i}{2}[(\frac{1+\beta}{2})F_{-,L}^{l+1/2}+(\frac{1-\beta}{2})e^{j\theta}F_{-,R}^{l+1/2}]=$$
$$\frac{\sigma_{s,i}h_i}{4}[(\frac{1+\beta}{2})(F_{+,L}^{l+1/2}+F_{-,L}^{l+1/2})+(\frac{1-\beta}{2})e^{j\theta}(F_{+,R}^{l+1/2}+F_{-,R}^{l+1/2})] \quad (3.29)$$
$$+\frac{\sigma_{s,i}h_i}{4}[(\frac{1+\beta}{2})(\Phi_L^{l+1/2}-\Phi_L^{l})+(\frac{1-\beta}{2})e^{j\theta}(\Phi_R^{l+1/2}-\Phi_R^{l})],$$

$$-\frac{1}{\sqrt{3}}[e^{j\theta}F_{-,L}^{l+1/2}-\frac{1}{2}(F_{-,L}^{l+1/2}+e^{j\theta}F_{-,R}^{l+1/2})]+\frac{\sigma_{t,i}h_i}{2}[(\frac{1-\beta}{2})F_{-,L}^{l+1/2}+(\frac{1+\beta}{2})e^{j\theta}F_{-,R}^{l+1/2}]=$$
$$\frac{\sigma_{s,i}h_i}{4}[(\frac{1-\beta}{2})(F_{+,L}^{l+1/2}+F_{-,L}^{l+1/2})+(\frac{1+\beta}{2})e^{j\theta}(F_{+,R}^{l+1/2}+F_{-,R}^{l+1/2})] \quad (3.30)$$
$$+\frac{\sigma_{s,i}h_i}{4}[(\frac{1-\beta}{2})(\Phi_L^{l+1/2}-\Phi_L^{l})+(\frac{1+\beta}{2})e^{j\theta}(\Phi_R^{l+1/2}-\Phi_R^{l})].$$

Substituting Eq. (3.19) into Eqs. (3.27)-(3.30), followed by considerable manipulation, we obtain the equation we desired, i.e., the S_2 scalar flux error estimate in terms of the scalar flux error at step l :

$$\begin{pmatrix} F_L^{l+1/2} \\ F_R^{l+1/2} \end{pmatrix} = H_{S2}\begin{pmatrix} \delta\Phi_L^{l} \\ \delta\Phi_R^{l} \end{pmatrix}, \quad (3.31)$$

where the S_2 scalar flux error:

$$F_L^{l+1/2} = F_{+,L}^{l+1/2}+F_{-,L}^{l+1/2}, \quad (3.32)$$

$$F_R^{l+1/2} = F_{+,R}^{l+1/2}+F_{-,R}^{l+1/2}. \quad (3.33)$$

and where H_{S2} represents the S_2 error eigenfunction matrix.

Until now we have expressed the scalar flux error at step $l+1/2$ in terms of the scalar flux error at step l in Eq. (3.19), and the eigenfunction matrix H_{SI}. We have also expressed the S_2 scalar flux error estimate in terms of the scalar flux error at step l in Eq. (3.31), and the eigenfunction matrix H_{S2}. Our final task is to find out the eigenfunction

matrix H_{S2SA} that relates the scalar flux error at step $l+1$ to the scalar flux error at step l.

Based on Eq.(1.25), the scalar flux error at step $l+1$ is equal to the scalar flux error at step $l+1/2$ minus the scalar flux error estimate from the S_2 equations. Thus, we subtract Eq. (3.31) from Eq. (3.19) to obtain:

$$\begin{pmatrix} \delta\Phi_L^{l+1/2} - F_L^{l+1/2} \\ \delta\Phi_R^{l+1/2} - F_R^{l+1/2} \end{pmatrix} = (H_{SI} - H_{S2}) \begin{pmatrix} \delta\Phi_L^{l} \\ \delta\Phi_R^{l} \end{pmatrix}, \tag{3.34}$$

Thus,

$$\begin{pmatrix} \delta\Phi_L^{l+1} \\ \delta\Phi_R^{l+1} \end{pmatrix} = H_{S2SA} \begin{pmatrix} \delta\Phi_L^{l} \\ \delta\Phi_R^{l} \end{pmatrix}, \tag{3.35}$$

where H_{S2SA} represents the S2SA eigenfunction matrix:

$$H_{S2SA} = H_{SI} - H_{S2}. \tag{3.36}$$

Let $\alpha_{H_{S2SA},\max}(\theta)$ be the larger of the two eigenvalues of H_{S2SA} for a given value of θ. Then the global spectral radius that relates the scalar flux error at step $l+1$ to the scalar flux error at step l for sufficiently many iterations is given by:

$$\rho_{S2SA} = \max_{\text{all } \theta} \alpha_{H_{S2SA},\max}(\theta) \tag{3.37}$$

We refer to $\alpha_{H_{H_{S2SA}},\max}(\theta)$ as the "local" spectral radius since it is the effective spectral radius for the single Fourier mode associated with a given value of θ.

At this point, we have derived an expression for the spectral radius of the SI scheme ρ_{SI}. We have also obtained an expression for the desired spectral radius ρ_{S2SA}, that relates the scalar flux error at step $l+1$ to the scalar flux error at step l. Thus, we

have completed the description of the Fourier analysis for the LDG (and LLDG) method. We can now compute the eigenvalues for the infinite, homogenous medium and uniform mesh problem. The quadrature set is chosen to be S_8 Gauss quadrature. The scattering ratio is chosen to be either $c = 1.0$ (pure scattering) or $c = 0.98$. The total cross sections is chosen to be $\sigma_t = 1.0$.

Results for the LDG method ($\beta = 1/3$) are given in Figs. 3.1-3.4. It can be observed from Figs. 3.1 and 3.2 which show the global spectral radius of SI $\sigma_t h = 0.01$ is equal to the scattering ratio *c*, and the spectral radius of S2SA is at roughly $0.222c$. We can also observe that the local spectral radius has a periodic dependence upon θ ($\theta = \Lambda h$).

From Figs. 3.3 and 3.4, which show the global spectral radius as a function of $\sigma_t h$, it can be seen that the S2SA scheme remains effective for all optical cell thicknesses, i.e. $\rho_{S2SA} < 0.222c$. The S2SA in the problems with absorption gives a spectral radius of 0 in the limit as $\sigma_t h \to \infty$, while it converges to 0.12 in a pure scattering ($c = 1$) problem.

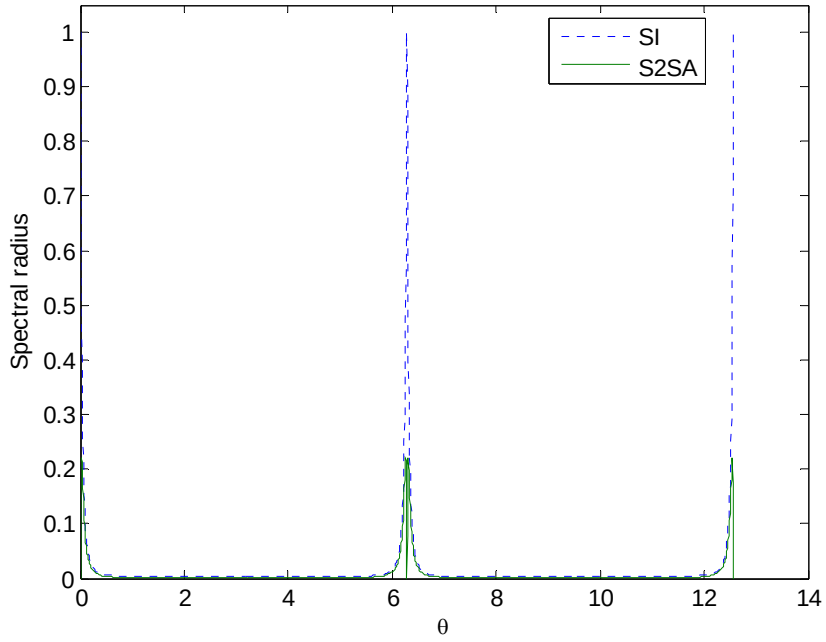

Fig. 3.1. Local spectral radii from LDG with $c = 1.0$ and $\sigma_t h = 0.01$.

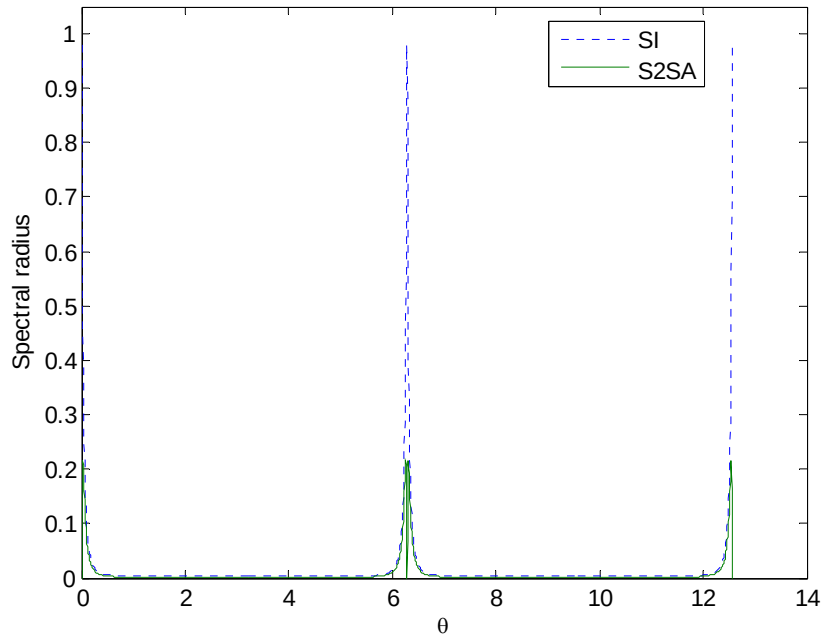

Fig. 3.2. Local spectral radii from LDG with $c = 0.98$ and $\sigma_t h = 0.01$.

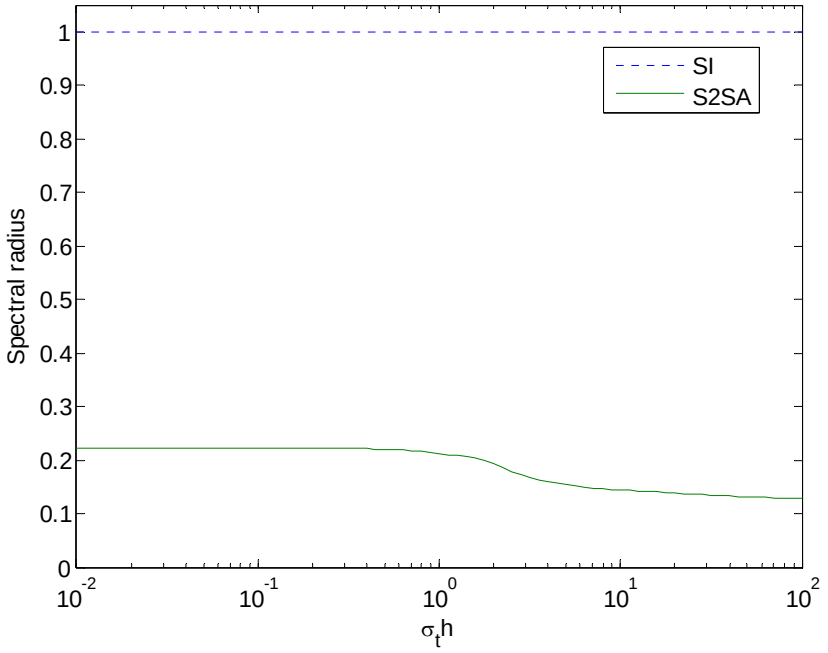

Fig. 3.3. Global spectral radii from LDG with $c = 1.0$.

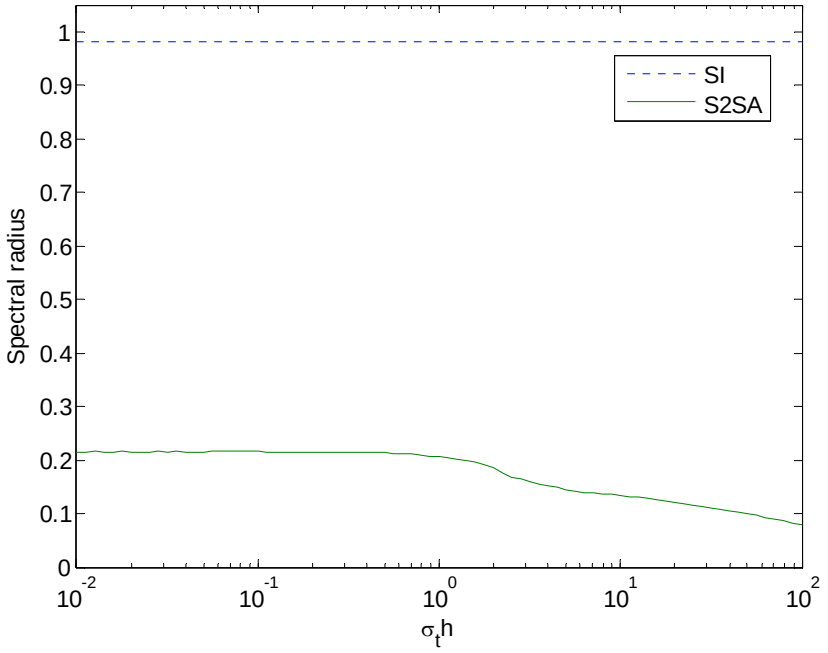

Fig. 3.4. Global spectral radii from LDG with $c = 0.98$.

Results for the LLDG method ($\beta = 1$) are given in Figs. 3.5-3.8 and they are quite similar to the results for the LDG method. It can be observed from Figs. 3.5 and 3.6 that for $\sigma_t h = 0.01$ the global spectral radius of SI is equal to the scattering ratio *c*, and the global spectral radius of S2SA is at roughly $0.222c$. We can also observe that the local spectral radius has a periodic dependence upon θ ($\theta = \Lambda h$).

From Figs. 3.7 and 3.8, which show the global spectral radius as a function of $\sigma_t h$, it can be seen that the S2SA scheme remains effective for all optical cell thicknesses, i.e. $\rho_{S2SA} < 0.222c$. The S2SA in the problems with absorption gives a spectral radius of 0 in the limit as $\sigma_t h \to \infty$, while it converges to 0.12 in a pure scattering ($c = 1$) problem, which gives the same results as the LDG method.

Derivation of Fourier analysis for the LDLS method

In this section, we perform a Fourier analysis for the LDLS method to determine the iterative convergence rate of both the SI and S2SA process. The analysis process is similar to that of the LDG method.

Our first task is to obtain the scalar flux error at step $l + 1/2$ in terms of the scalar flux error at step l. The exact LDLS solution is given by Eqs. (2.46)-(2.51) and the SI scheme is given by Eqs. (2.73)-(2.80). Based on these equations, eliminating the Lagrange multiplier λ_i and after some manipulation using Maple, we obtain the exact solution for the error:

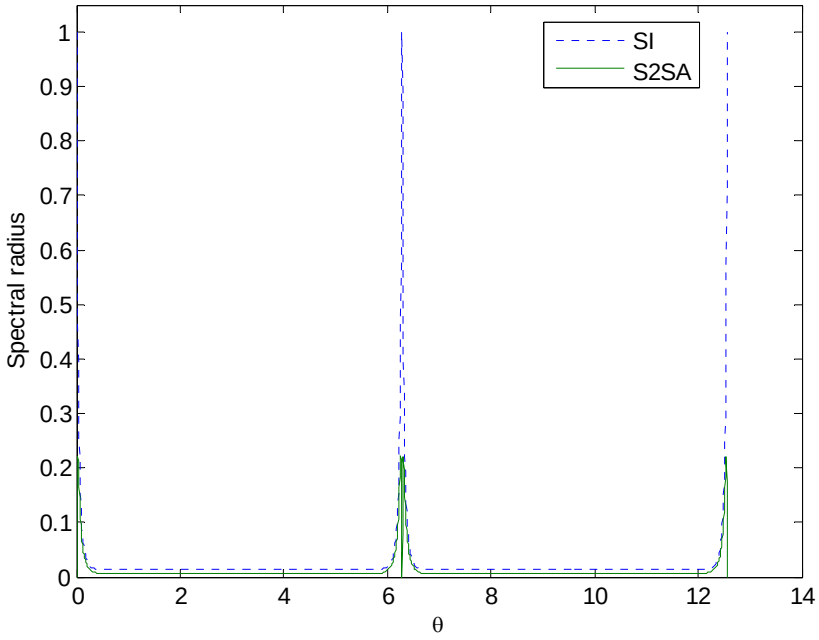

Fig. 3.5. Local spectral radii from LLDG with $c = 1.0$ and $\sigma_t h = 0.01$.

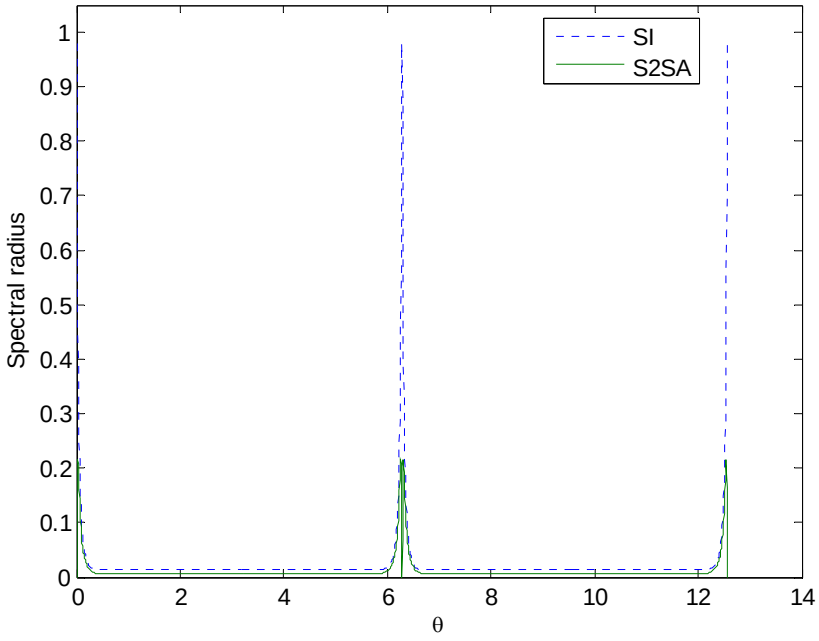

Fig. 3.6. Local spectral radii from LLDG with $c = 0.98$ and $\sigma_t h = 0.01$.

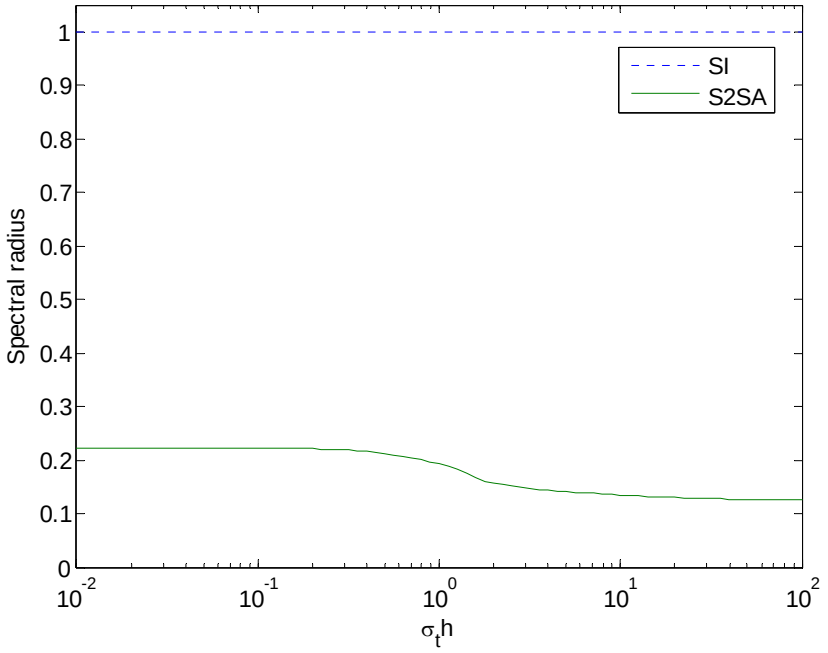

Fig. 3.7. Global spectral radii from LLDG with $c = 1.0$.

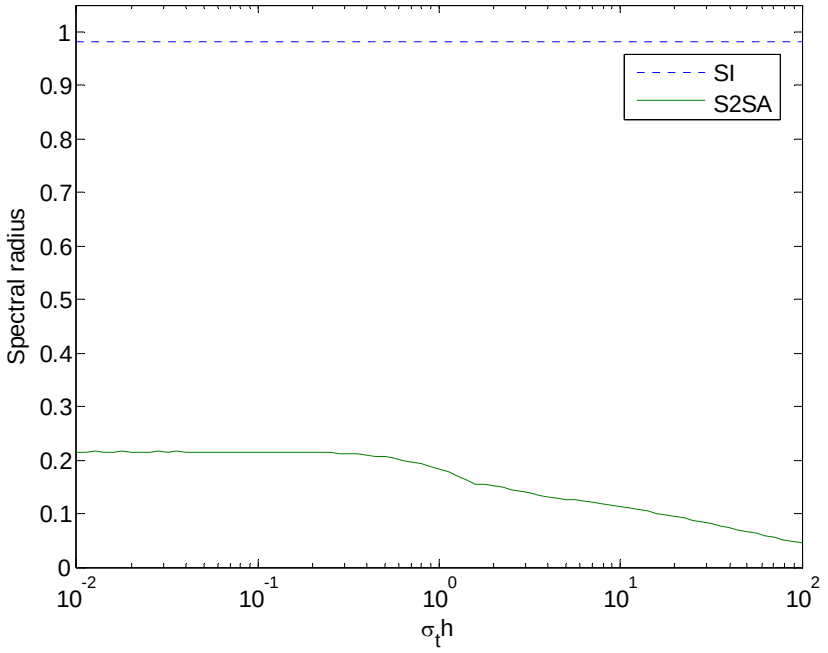

Fig. 3.8. Global spectral radii from LLDG with $c = 0.98$.

For $\mu_m > 0$,

$$A_1 \delta\psi_{m,L,i}^{l+1/2} + B_1 \delta\psi_{m,R,i}^{l+1/2} + C_1 \delta\phi_{L,i}^{l} + D_1 \delta\phi_{R,i}^{l} = 0, \tag{3.38}$$

$$\mu_m (\delta\psi_{m,R,i}^{l+1/2} - \delta\psi_{m,R,i-1}^{l+1/2}) + \sigma_{t,i} h_i \frac{\delta\psi_{m,L,i}^{l+1/2} + \delta\psi_{m,R,i}^{l+1/2}}{2} = \frac{\sigma_{s,i} h_i}{2} \frac{\delta\phi_{L,i}^{l} + \delta\phi_{R,i}^{l}}{2}. \tag{3.39}$$

For $\mu_m < 0$,

$$A_2 \delta\psi_{m,L,i}^{l+1/2} + B_2 \delta\psi_{m,R,i}^{l+1/2} + C_2 \delta\phi_{L,i}^{l} + D_2 \delta\phi_{R,i}^{l} = 0, \tag{3.40}$$

$$\mu_m (\delta\psi_{m,L,i+1}^{l+1/2} - \delta\psi_{m,L,i}^{l+1/2}) + \sigma_{t,i} h_i \frac{\delta\psi_{m,L,i}^{l+1/2} + \delta\psi_{m,R,i}^{l+1/2}}{2} = \frac{\sigma_{s,i} h_i}{2} \frac{\delta\phi_{L,i}^{l} + \delta\phi_{R,i}^{l}}{2}, \tag{3.41}$$

where the coefficients $A_i, B_i, C_i, D_i,\ i = 1,2$ are polynomial coefficients. They are all functions of $\mu_m, h_i, \sigma_{t,i}$ and $\sigma_{s,i}$. Substituting the single Fourier mode of the flux error in Eqs. (3.9)-(3.12) into Eqs. (3.38)-(3.41), and dividing by $\exp(j\Lambda x_{i-1/2})$, we obtain:

For $\mu_m > 0$,

$$A_1 \delta\Psi_{m,L}^{l+1/2} + B_1 e^{j\theta} \delta\Psi_{m,R}^{l+1/2} + C_1 \delta\Phi_{L}^{l} + D_1 e^{j\theta} \delta\Phi_{R}^{l} = 0, \tag{3.42}$$

$$\mu_m (e^{j\theta} \delta\Psi_{m,R}^{l+1/2} - \delta\Psi_{m,R}^{l+1/2}) + \sigma_{t,i} h_i \frac{\delta\Psi_{m,L}^{l+1/2} + e^{j\theta} \delta\Psi_{m,R}^{l+1/2}}{2} = \frac{\sigma_{s,i} h_i}{2} \frac{\delta\Phi_{L}^{l} + e^{j\theta} \delta\Phi_{R}^{l}}{2}. \tag{3.43}$$

For $\mu_m < 0$,

$$A_2 \delta\Psi_{m,L}^{l+1/2} + B_2 e^{j\theta} \delta\Psi_{m,R}^{l+1/2} + C_2 \delta\Phi_{L}^{l} + D_2 e^{j\theta} \delta\Phi_{R}^{l} = 0, \tag{3.44}$$

$$\mu_m (e^{j\theta} \delta\Psi_{m,L}^{l+1/2} - \delta\Psi_{m,L}^{l+1/2}) + \sigma_{t,i} h_i \frac{\delta\Psi_{m,L}^{l+1/2} + e^{j\theta} \delta\Psi_{m,R}^{l+1/2}}{2} = \frac{\sigma_{s,i} h_i}{2} \frac{\delta\Phi_{L}^{l} + e^{j\theta} \delta\Phi_{R}^{l}}{2}. \tag{3.45}$$

Similarly to the LDG method, we adopt the same procedure as from Eq. (3.17) to Eq. (3.24) to obtain the local and global spectral radii of SI scheme for the LDLS method.

Our next task is to obtain the S_2 scalar flux error estimate in terms of the scalar flux error at step l, and to obtain the desired spectral radius that relates the scalar flux error at step $l+1$ to the scalar flux error at step l. The discrete form of the low order S_2 scheme for the LDLS method is given in Eqs. (2.89)-(2.94). The spatial dependence of the S_2 flux error is defined by the single Fourier mode given in Eqs. (3.25)-(3.26). Substituting Eqs. (3.11)-(3.12) and Eqs. (3.25)-(3.26) into the low-order S_2 scheme in Eqs. (2.89)-(2.94), and dividing by $\exp(j\Lambda x_{i-1/2})$, we get:

For the positive direction,

$$\begin{aligned} &A_3F_{+,L}^{l+1/2} + B_3e^{j\theta}F_{+,R}^{l+1/2} + C_3F_L^{l+1/2} + D_3e^{j\theta}F_R^{l+1/2} \\ &+E_3(\Phi_L^{l+1/2} - \Phi_L^l) + F_3e^{j\theta}(\Phi_R^{l+1/2} - \Phi_R^l) = 0, \end{aligned} \tag{3.46}$$

$$\begin{aligned} &\frac{1}{\sqrt{3}}(e^{j\theta}F_{+,R}^{l+1/2} - F_{+,R}^{l+1/2}) + \sigma_{t,i}h_i\frac{F_{+,L}^{l+1/2} + e^{j\theta}F_{+,R}^{l+1/2}}{2} = \frac{\sigma_{s,i}h_i}{4}(F_L^{l+1/2} + e^{j\theta}F_R^{l+1/2}) \\ &+\frac{\sigma_{s,i}h_i}{4}[(\Phi_L^{l+1/2} - \Phi_L^l) + e^{j\theta}(\Phi_R^{l+1/2} - \Phi_R^l)]. \end{aligned} \tag{3.47}$$

For the negative direction,

$$\begin{aligned} &A_4F_{-,L}^{l+1/2} + B_4e^{j\theta}F_{-,R}^{l+1/2} + C_4F_L^{l+1/2} + D_4e^{j\theta}F_R^{l+1/2} \\ &+E_4(\Phi_L^{l+1/2} - \Phi_L^l) + F_4e^{j\theta}(\Phi_R^{l+1/2} - \Phi_R^l) = 0, \end{aligned} \tag{3.48}$$

$$\begin{aligned} &-\frac{1}{\sqrt{3}}(e^{j\theta}F_{-,L}^{l+1/2} - F_{-,L}^{l+1/2}) + \sigma_{t,i}h_i\frac{F_{-,L}^{l+1/2} + e^{j\theta}F_{-,R}^{l+1/2}}{2} = \frac{\sigma_{s,i}h_i}{4}(F_L^{l+1/2} + e^{j\theta}F_R^{l+1/2}) \\ &+\frac{\sigma_{s,i}h_i}{4}[(\Phi_L^{l+1/2} - \Phi_L^l) + e^{j\theta}(\Phi_R^{l+1/2} - \Phi_R^l)]. \end{aligned} \tag{3.49}$$

where the coefficients $A_i, B_i, C_i, D_i,\ i = 3,4$ are polynomial coefficients. They are all functions of $\mu_m, h_i, \sigma_{t,i}$ and $\sigma_{s,i}$.

Similarly to the LDG method, we adopt the same procedure as from Eq. (3.31) to Eq. (3.37) to obtain the local and global spectral radii of the S2SA scheme for the LDLS method.

At this point, we have derived an expression for the spectral radius of the SI scheme ρ_{SI}. We have also obtained an expression for the desired spectral radius ρ_{S2SA}, that relates the scalar flux error at step $l+1$ to the scalar flux error at step l. Thus, we have completed the description of the Fourier analysis for the LDLS method. We can now compute the eigenvalues for the infinite, homogenous medium and uniform mesh problem. The quadrature set is chosen to be S_8 Gauss quadrature. The scattering ratio is chosen to be either $c = 1.0$ (pure scattering) or $c = 0.98$. The total cross sections is chosen to be $\sigma_t = 1.0$.

Results for the LDLS method are given in Figs. 3.9-3.12. It can be observed from Figs. 3.9 and 3.10 that for $\sigma_t h = 0.01$, the global spectral radius of SI is equal to the scattering ratio *c*, and the spectral radius of S2SA is at roughly $0.222c$. We can also observe that the local spectral radius has a periodic dependence upon θ ($\theta = \Lambda h$).

From Figs. 3.11 and 3.12 which show the global spectral radius as a function of $\sigma_t h$, it can be observed that the S2SA scheme remains effective for all cell thicknesses. For small mean-free-paths ($\sigma_t h < 0.1$), the spectral radius remains at $\sigma_{S2SA} = 0.222c$, while there is a peak at roughly $\sigma_t h = 0.8$. The S2SA scheme in the problems with

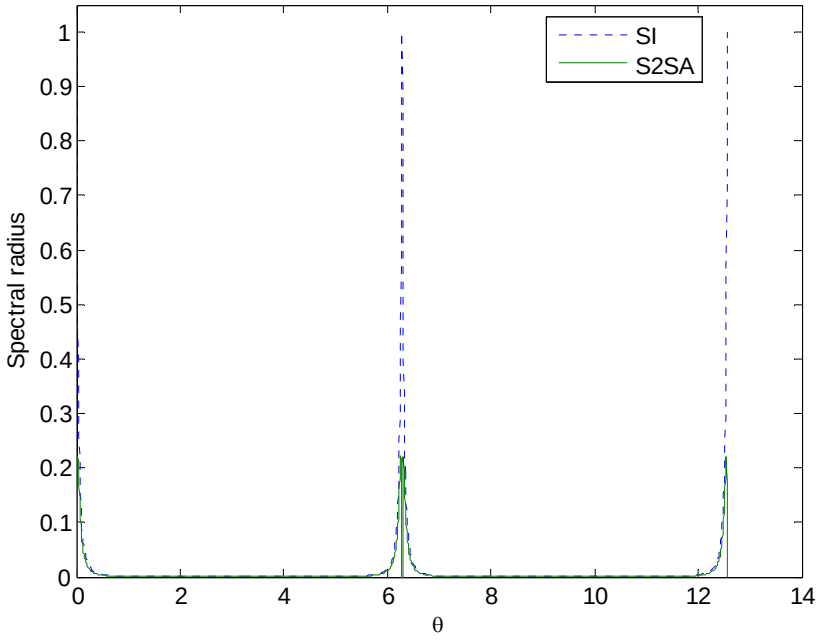

Fig. 3.9. Local spectral radii from LDLS with $c = 1.0$ and $\sigma_t h = 0.01$.

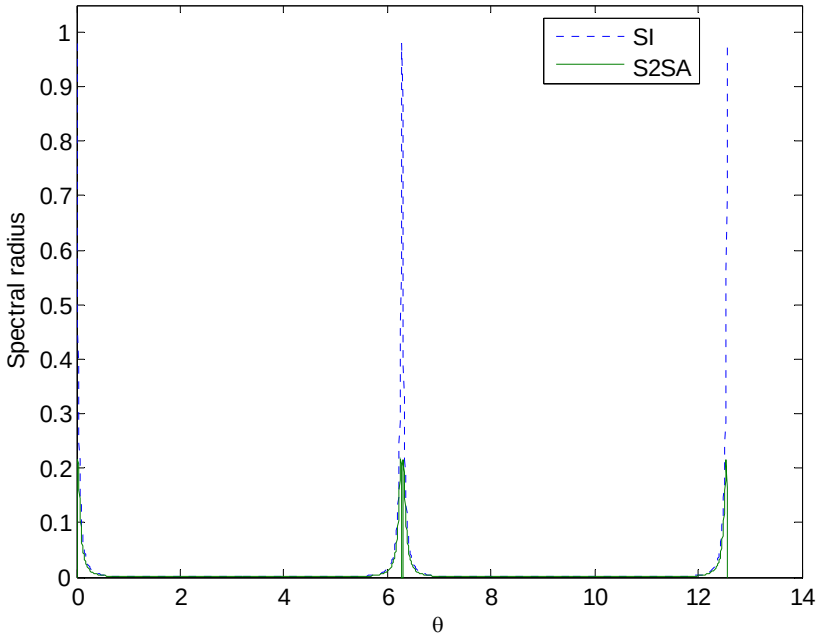

Fig. 3.10. Local spectral radii from LDLS with $c = 0.98$ and $\sigma_t h = 0.01$.

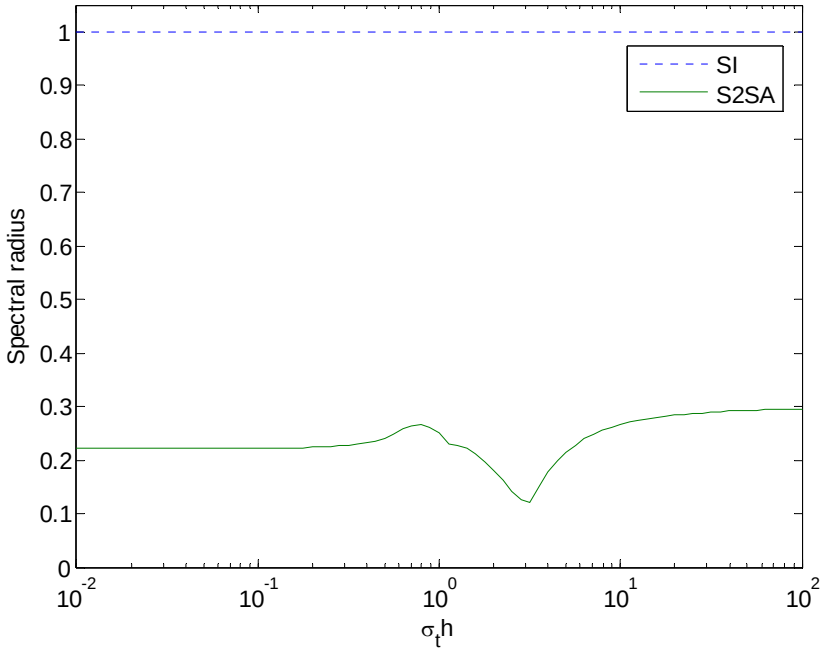

Fig. 3.11. Global spectral radii from LDLS with $c = 1.0$.

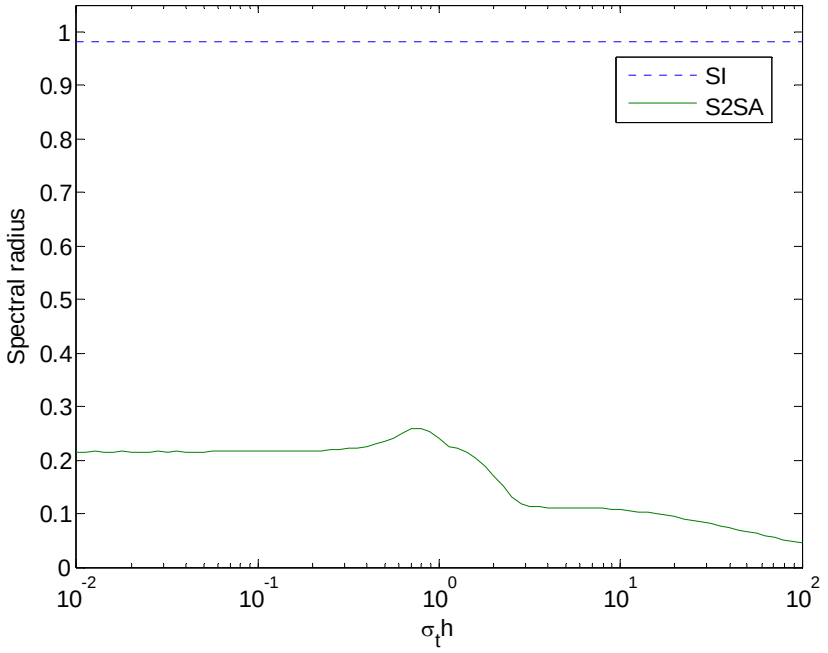

Fig. 3.12. Global spectral radii from LDLS with $c = 0.98$.

absorption gives a spectral radius of 0 in the limit as $\sigma_t h \to \infty$, while it converges to 0.3 in a pure scattering ($c = 1$) problem.

Summary

To investigate the iterative convergence behavior of the LDLS method, we presented a detailed discrete Fourier analysis for the LDG, LLDG, and LDLS methods. Our analysis suggests that the S_2 synthetic acceleration of LDG remains effective for all cell thicknesses and $\sigma_{S2SA} < 0.222c$. For LDLS, although the S_2 synthetic acceleration remains effective for all cell thicknesses, there is a peak of the spectral radius at roughly $\sigma_t h = 0.8$. The S2SA in the problems with absorption gives a spectral radius of 0 in the limit as $\sigma_t h \to \infty$, while it converges to 0.3 in a pure scattering ($c = 1$) problem. Computational results for the spectral radii will be presented in Chapter V to make a comparison with theory.

CHAPTER IV

ASYMPTOTIC ANALYSIS

In this chapter, we study the optically thick diffusive problem by performing a detailed asymptotic analysis[6] for the new LDLS method for the 1-D one-group steady-state transport equation with isotropic source and scattering. We focus on optically thick diffusive problems to find out whether the thick diffusion limit is preserved with the LDLS spatial discretization scheme.

Introduction

Neutron transport problems are rarely highly diffusive and generally exhibit a spatial scale length of a few mean-free-paths $(\lambda_{mfp} = 1/\sigma_t)$ or less. However, thermal radiation transport problems often include highly diffusive regions which exhibit a spatial scale length of a diffusion-length $(\lambda_D = 1/\sqrt{3\sigma_a\sigma_t})$, which can be equal to an arbitrary number of mean-free-paths. The 1-D diffusion equation with Mark boundary conditions is:

$$-\frac{d}{dx}\frac{1}{3\sigma_t(x)}\frac{d\phi(x)}{dx}+\sigma_a(x)\phi(x)=Q(x), \tag{4.1}$$

$$(\phi-\sqrt{3}D\frac{\partial\phi}{\partial x})\Big|_{x=0}=4j_L^+, \tag{4.2}$$

$$(\phi+\sqrt{3}D\frac{\partial\phi}{\partial x})\Big|_{x=X}=4j_R^-, \tag{4.3}$$

where j_L^+ and j_R^- are the boundary incident currents.

To define the asymptotic diffusion limit, we now introduce a small parameter ε, and make the following scalings:

$$\sigma_t \to \frac{\sigma_t}{\varepsilon}, \tag{4.4}$$

$$\sigma_a \to \varepsilon\sigma_a, \tag{4.5}$$

$$\sigma_s \to \frac{\sigma_t}{\varepsilon} - \varepsilon\sigma_a, \tag{4.6}$$

$$Q \to \varepsilon Q. \tag{4.7}$$

These scalings will be applied to the transport equation, but before doing so it is useful to apply them to the diffusion equation. Substituting Eqs. (4.4)-(4.7) into Eqs. (4.1)-(4.3),

$$-\frac{d}{dx}\frac{\varepsilon}{3\sigma_t(x)}\frac{d\phi(x)}{dx} + \varepsilon\sigma_a(x)\phi(x) = \varepsilon Q(x). \tag{4.8}$$

$$(\phi - \sqrt{3}\varepsilon D\frac{\partial\phi}{\partial x})\Big|_{x=0} = 4j_L^+, \tag{4.9}$$

$$(\phi + \sqrt{3}\varepsilon D\frac{\partial\phi}{\partial x})\Big|_{x=X} = 4j_R^+. \tag{4.10}$$

It can be easily observed that the diffusion equation is invariant to the scaling. When $\varepsilon \to 0$, the boundary conditions become the Dirichlet boundary condition. The mean-free-path and the diffusion length become:

$$\lambda_{mfp} = \varepsilon / \sigma_t, \tag{4.11}$$

$$\lambda_D = 1/\sqrt{3\sigma_a\sigma_t}. \tag{4.12}$$

λ_D is the scale length for diffusive problems, not λ_{mfp}. Intuitively, one would expect to obtain accurate transport solutions for diffusive problems when the spatial cell size is small relative to a diffusion length , i.e., $h / \lambda_D \ll 1$. However, only if a transport scheme preserves the thick diffusion limit will an accurate solution be obtained. Truncation error analysis for the transport equation states that convergence in general requires $h / \lambda_{mfp} \ll 1$. So all consistent discretization schemes will yield an accurate solution if $h / \lambda_{mfp} \ll 1$. However, from Eq. (4.11) and (4.12), it can be seen that λ_{mfp} is $O(\varepsilon)$ and λ_D is $O(1)$. Thus requiring $h / \lambda_{mfp} \ll 1$ can be arbitrarily expensive relative to requiring $h / \lambda_D \ll 1$ since $\lambda_{mfp} / \lambda_D \to 0$ as $\varepsilon \to 0$. Thus, transport meshing efficiency for highly diffusive problems requires the diffusion limit. If a scheme preserves the thick diffusion limit, the required mesh spacing becomes fixed in the limit as $\varepsilon \to 0$. However, if a scheme does not preserve the thick diffusion limit, the required mesh spacing is proportional to ε.

We turn to the 1-D one-group steady-state transport equation with isotropic source and scattering. Applying the scaling, it now becomes:

$$\mu \frac{\partial \psi(\mu, x)}{\partial x} + \frac{\sigma_t(x)}{\varepsilon} \psi(\mu, x) = [\frac{\sigma_t(x)}{\varepsilon} - \varepsilon \sigma_a(x)] \frac{1}{2} \int_{-1}^{1} \psi(\mu, x) d\mu + \frac{\varepsilon Q(x)}{2}. \quad (4.13)$$

The following section describes the spatial discretization of Eq. (4.13) and the results from the asymptotic analysis when $\varepsilon \to 0$.

A summary of the asymptotic analysis for the LLDG method

If discretize Eq. (4.13) by the LLDG method, we have the following scaled equations:

$$\mu_m\left(\frac{\psi_{m,L,i}+\psi_{m,R,i}}{2}-\psi_{m,i-1/2}\right)+\frac{\sigma_{t,i}h_i}{2\varepsilon}\psi_{m,L,i}=\frac{\left(\frac{\sigma_{t,i}}{\varepsilon}-\varepsilon\sigma_{a,i}\right)h_i}{4}\phi_{L,i}+\frac{\varepsilon h_i}{2}Q_{m,L,i}, \quad (4.14)$$

$$\mu_m\left(\psi_{m,i+1/2}-\frac{\psi_{m,L,i}+\psi_{m,R,i}}{2}\right)+\frac{\sigma_{t,i}h_i}{2\varepsilon}\psi_{m,R,i}=\frac{\left(\frac{\sigma_{t,i}}{\varepsilon}-\varepsilon\sigma_{a,i}\right)h_i}{4}\phi_{R,i}+\frac{\varepsilon h_i}{2}Q_{m,R,i}. \quad (4.15)$$

where

$$\phi_{L,i}=\sum_{m=1}^{N}w_m\psi_{m,L,i}, \quad (4.16)$$

$$\phi_{R,i}=\sum_{m=1}^{N}w_m\psi_{m,R,i}. \quad (4.17)$$

We first expand the discrete solution in a power series in ε:

$$\psi_{m,L,i}=\sum_{n=0}^{\infty}\psi_{m,L,i}^{(n)}\varepsilon^n, \quad (4.18)$$

$$\psi_{m,R,i}=\sum_{n=0}^{\infty}\psi_{m,R,i}^{(n)}\varepsilon^n. \quad (4.19)$$

Substituting these expressions into Eqs. (4.14) and (4.15) and equating all terms that multiply each power of ε, we obtain one equation for each power of ε.

The ε^0 equations yield:

$$\psi_{m,L,i}^{(0)}=\frac{1}{2}\phi_{L,i}^{(0)}, \quad (4.20)$$

$$\psi_{m,R,i}^{(0)}=\frac{1}{2}\phi_{R,i}^{(0)}, \quad (4.21)$$

which implies that the leading-order angular flux is isotropic. The current is defined as:

$$J_i = \sum_{m=1}^{N} \psi_{m,i} \mu_m w_m. \tag{4.22}$$

Thus, the isotropy of the leading-order angular flux yields the leading-order current to be zero (0):

$$J^{(0)} = 0. \tag{4.23}$$

The ε^1 equation is:

$$\mu_m [\frac{1}{2}(\psi^{(0)}_{m,L,i} + \psi^{(0)}_{m,R,i}) - \psi^{(0)}_{m,i-1/2}] + \frac{\sigma_{t,i} h_i}{2} \psi^{(1)}_{m,L,i} = \frac{\sigma_{t,i} h_i}{4} \phi^{(1)}_{L,i}, \tag{4.24}$$

$$\mu_m [\psi^{(0)}_{m,i+1/2} - \frac{1}{2}(\psi^{(0)}_{m,L,i} + \psi^{(0)}_{m,R,i})] + \frac{\sigma_{t,i} h_i}{2} \psi^{(1)}_{m,R,i} = \frac{\sigma_{t,i} h_i}{4} \phi^{(1)}_{R,i}, \tag{4.25}$$

Multiplying Eq. (4.24) by w_m and summing over $m = 1, ..., N$, we obtain the continuity of the leading-order angular flux and scalar flux:

$$\psi^{(0)}_{m,L,i} = \psi^{(0)}_{m,R,i-1}, \tag{4.26}$$

$$\phi^{(0)}_{L,i} = \phi^{(0)}_{R,i-1}, \tag{4.27}$$

Adding Eq. (4.24) and (4.25), we obtain:

$$\mu_m (\psi^{(0)}_{m,i+1/2} - \psi^{(0)}_{m,i-1/2}) + \sigma_{t,i} h_i \frac{\psi^{(1)}_{m,L,i} + \psi^{(1)}_{m,R,i}}{2} = \frac{\sigma_{t,i} h_i}{2} \frac{\phi^{(1)}_{L,i} + \phi^{(1)}_{R,i}}{2}. \tag{4.28}$$

Multiplying Eq. (4.28) by $\mu_m w_m$ and summing over $m = 1, ..., N$, after considerable manipulation, we obtain the discretized form of Fick's Law for the first-order current:

$$J^{(1)}_i = -\frac{1}{3\sigma_{t,i} h_i} (\phi^{(0)}_{i+1/2} - \phi^{(0)}_{i-1/2}) \tag{4.29}$$

The ε^2 equation for the *i*th cell is:

$$\mu_m[\frac{1}{2}(\psi^{(1)}_{m,L,i}+\psi^{(1)}_{m,R,i})-\psi^{(1)}_{m,i-1/2}]+\frac{\sigma_{t,i}h_i}{2}\psi^{(2)}_{m,L,i}=\frac{\sigma_{t,i}h_i}{4}\phi^{(2)}_{L,i}-\frac{\sigma_{a,i}h_i}{4}\phi^{(0)}_{L,i}+\frac{h_i}{4}Q_{L,i}, \quad (4.30)$$

$$\mu_m[\psi^{(1)}_{m,i+1/2}-\frac{1}{2}(\psi^{(1)}_{m,L,i}+\psi^{(1)}_{m,R,i})]+\frac{\sigma_{t,i}h_i}{2}\psi^{(2)}_{m,R,i}=\frac{\sigma_{t,i}h_i}{4}\phi^{(2)}_{R,i}-\frac{\sigma_{a,i}h_i}{4}\phi^{(0)}_{R,i}+\frac{h_i}{4}Q_{R,i}. \quad (4.31)$$

Eq. (4.30) for the cell *i+1* is:

$$\begin{aligned}&\mu_m[\frac{1}{2}(\psi^{(1)}_{m,L,i+1}+\psi^{(1)}_{m,R,i+1})-\psi^{(1)}_{m,i+1/2}]+\frac{\sigma_{t,i}h_i}{2}\psi^{(2)}_{m,L,i+1}\\&=\frac{\sigma_{t,i}h_i}{4}\phi^{(2)}_{L,i+1}-\frac{\sigma_{a,i}h_i}{4}\phi^{(0)}_{L,i+1}+\frac{h_i}{4}Q_{L,i+1}.\end{aligned} \quad (4.32)$$

Adding Eq. (4.31) and Eq. (4.32), multiplying by w_m and summing over $m=1,...,N$, we get:

$$J^{(1)}_{i+1}-J^{(1)}_i+\frac{1}{2}(\sigma_{a,i}h_i+\sigma_{a,i+1}h_{i+1})\phi^{(0)}_{i+1/2}=\frac{1}{2}(h_i+h_{i+1})Q_{i+1/2}, \quad (4.33)$$

where

$$J^{(1)}_i=\sum_{m=1}^{N}\psi^{(1)}_{m,i}\mu_m w_m, \quad (4.34)$$

$$Q_{i+1/2}=\frac{h_iQ_{R,i}+h_{i+1}Q_{L,i+1}}{h_i+h_{i+1}}, \quad (4.35)$$

$$\phi^{(0)}_{i+1/2}=\phi^{(0)}_{R,i}=\phi^{(0)}_{L,i+1}. \quad (4.36)$$

Substituting Eq. (4.29) into Eq. (4.33), we get:

$$-\frac{\phi^{(0)}_{i+3/2}-\phi^{(0)}_{i+1/2}}{3\sigma_{t,i+1}h_{i+1}}+\frac{\phi^{(0)}_{i+1/2}-\phi^{(0)}_{i-1/2}}{3\sigma_{t,i}h_i}+\frac{1}{2}(\sigma_{a,i}h_i+\sigma_{a,i+1}h_{i+1})\phi^{(0)}_{i+1/2}=\frac{1}{2}(h_i+h_{i+1})Q_{i+1/2}. \quad (4.37)$$

Eq. (4.37) is a valid discretization of the diffusion equation, i.e., Eq. (4.1). Thus, the leading-order scalar flux satisfies the diffusion equation which implies that the

LLDG method preserves the thick diffusion limit. The LDG method yields a similar result[6] as follows:

$$
\begin{aligned}
&-\frac{\phi^{(0)}_{i+3/2}-\phi^{(0)}_{i+1/2}}{3\sigma_{t,i+1}h_{i+1}}+\frac{\phi^{(0)}_{i+1/2}-\phi^{(0)}_{i-1/2}}{3\sigma_{t,i}h_i}+\frac{1}{2}\sigma_{a,i}h_i\left(\frac{2}{3}\phi^{(0)}_{i+1/2}+\frac{1}{3}\phi^{(0)}_{i-1/2}\right)\\
&+\frac{1}{2}\sigma_{a,i+1}h_{i+1}\left(\frac{2}{3}\phi^{(0)}_{i+1/2}+\frac{1}{3}\phi^{(0)}_{i+3/2}\right)\\
&=\frac{1}{2}h_i\left(\frac{2}{3}Q_{i+1/2}+\frac{1}{3}Q_{i-1/2}\right)+\frac{1}{2}h_{i+1}\left(\frac{2}{3}Q_{i+1/2}+\frac{1}{3}Q_{i+3/2}\right).
\end{aligned}
\tag{4.38}
$$

In the following section, we discuss the behavior of the new LDLS method in the thick diffusion limit.

Asymptotic analysis for the LDLS method

In this section, we give a brief description of the asymptotic analysis for the LDLS method, as well as a summary of the results. Recall from Chapter II that the LDLS method is expressed as:

For $\mu_m > 0$,

$$
\int_{x^+_{i-1/2}}^{x_{i+1/2}} \{2[S_{m,L,i}B_{L,i}(x)+S_{m,R,i}B_{R,i}(x)-\sigma_{t,i}(\psi_{m,L,i}B_{L,i} +\psi_{m,R,i}B_{R,i})-\frac{\mu_m}{h_i}(\psi_{m,R,i}-\psi_{m,L,i})](\frac{\mu_m}{h_i}-\sigma_{t,i}B_{L,i})\}dx+\lambda(\frac{\sigma_{t,i}h_i}{2})=0 \tag{4.39}
$$

$$
\int_{x^+_{i-1/2}}^{x_{i+1/2}} \{2[S_{m,L,i}B_{L,i}(x)+S_{m,R,i}B_{R,i}(x)-\sigma_{t,i}(\psi_{m,L,i}B_{L,i} +\psi_{m,R,i}B_{R,i})-\frac{\mu_m}{h_i}(\psi_{m,R,i}-\psi_{m,L,i})](-\frac{\mu_m}{h_i}-\sigma_{t,i}B_{R,i})\}dx+\lambda(\frac{\sigma_{t,i}h_i}{2}+\mu_m)=0 \tag{4.40}
$$

$$
\mu_m(\psi_{m,R,i}-\psi_{m,R,i-1})+\sigma_{t,i}h_i\frac{\psi_{m,L,i}+\psi_{m,R,i}}{2}=h_i\frac{S_{m,L,i}+S_{m,R,i}}{2} \tag{4.41}
$$

For $\mu_m < 0$,

$$\int_{x_{i-1/2}}^{x^-_{i+1/2}} \{2[S_{m,L,i}B_{L,i}(x)+S_{m,R,i}B_{R,i}(x)-\sigma_{t,i}(\psi_{m,L,i}B_{L,i} +\psi_{m,R,i}B_{R,i})-\frac{\mu_m}{h_i}(\psi_{m,R,i}-\psi_{m,L,i})](\frac{\mu_m}{h_i}-\sigma_{t,i}B_{L,i})\}dx+\lambda(\frac{\sigma_{t,i}h_i}{2}-\mu_m)=0 \quad (4.42)$$

$$\int_{x_{i-1/2}}^{x^-_{i+1/2}} \{2[S_{m,L,i}B_{L,i}(x)+S_{m,R,i}B_{R,i}(x)-\sigma_{t,i}(\psi_{m,L,i}B_{L,i} +\psi_{m,R,i}B_{R,i})-\frac{\mu_m}{h_i}(\psi_{m,R,i}-\psi_{m,L,i})](-\frac{\mu_m}{h_i}-\sigma_{t,i}B_{R,i})\}dx+\lambda(\frac{\sigma_{t,i}h_i}{2})=0 \quad (4.43)$$

$$\mu_m(\psi_{m,L,i+1}-\psi_{m,L,i})+\sigma_{t,i}h_i\frac{\psi_{m,L,i}+\psi_{m,R,i}}{2}=h_i\frac{S_{m,L,i}+S_{m,R,i}}{2} \quad (4.44)$$

where

$$S_{m,L,i}=\frac{\sigma_{s,i}}{2}\sum_{m=1}^{N}w_m\psi_{m,L,i}+\frac{1}{2}Q_{m,L,i} \quad (4.45)$$

$$S_{m,R,i}=\frac{\sigma_{s,i}}{2}\sum_{m=1}^{N}w_m\psi_{m,R,i}+\frac{1}{2}Q_{m,R,i} \quad (4.46)$$

Eq. (4.41) and Eq. (4.44) are the balance equations for positive and negative directions. They can be combined for all directions as:

$$\mu_m(\psi_{m,i+1/2}-\psi_{m,i-1/2})+\sigma_{t,i}h_i\frac{\psi_{m,L,i}+\psi_{m,R,i}}{2}=\frac{\sigma_{s,i}h_i}{2}\frac{(\phi_{L,i}+\phi_{R,i})}{2}+\frac{h_i}{2}\frac{Q_{L,i}+Q_{R,i}}{2} \quad (4.47)$$

If we eliminate the variable λ from Eq. (4.39) and (4.40) and perform considerable manipulation, we can obtain Eq. (4.48) for $\mu_m > 0$:

$$\begin{aligned}&(2\sigma_{t,i}^2h_i^2\mu_m-\sigma_{t,i}^3h_i^3-12\mu_m^3)\psi_{m,L,i}\\&+(12\sigma_{t,i}h_i\mu_m^2+4\sigma_{t,i}^2h_i^2\mu_m+\sigma_{t,i}^3h_i^3+12\mu_m^3)\psi_{m,R,i}\\&=(-\sigma_{t,i}^2h_i^3+2\sigma_{t,i}h_i^2\mu_m+6h_i\mu_m^2)S_{m,L,i}+(\sigma_{t,i}^2h_i^3+4\sigma_{t,i}h_i^2\mu_m+6h_i\mu_m^2)S_{m,R,i}\end{aligned} \quad (4.48)$$

Eliminating λ from Eq. (4.42) and (4.43) and performing considerable manipulation, we obtain Eq. (4.49) for $\mu_m < 0$:

$$
\begin{aligned}
&(-12\sigma_{t,i}h_i\mu_m^2+4\sigma_{t,i}^2h_i^2\mu_m-\sigma_{t,i}^3h_i^3+12\mu_m^3)\psi_{m,L,i}\\
&+(2\sigma_{t,i}^2h_i^2\mu_m+\sigma_{t,i}^3h_i^3-12\mu_m^3)\psi_{m,R,i}\\
&=(-\sigma_{t,i}^2h_i^3+4\sigma_{t,i}h_i^2\mu_m-6h_i\mu_m^2)S_{m,L,i}+(\sigma_{t,i}^2h_i^3+2\sigma_{t,i}h_i^2\mu_m-6h_i\mu_m^2)S_{m,R,i}
\end{aligned}
\tag{4.49}
$$

Introducing the small parameter ε and making the variable changes in Eqs. (4.4)-(4.7), from Eq. (4.47) we get:

$$
\begin{aligned}
&\mu_m(\psi_{m,i+1/2}-\psi_{m,i-1/2})+\frac{\sigma_{t,i}}{\varepsilon}h_i\frac{\psi_{m,L,i}+\psi_{m,R,i}}{2}\\
&=\frac{(\frac{\sigma_{t,i}}{\varepsilon}-\varepsilon\sigma_{a,i})h_i}{2}\frac{(\phi_{L,i}+\phi_{R,i})}{2}+\frac{h_i\varepsilon}{2}\frac{Q_{L,i}+Q_{R,i}}{2}
\end{aligned}
\tag{4.50}
$$

From Eq. (4.48) we obtain the least-squares equation for $\mu_m>0$ as:

$$
\begin{aligned}
&(2\varepsilon\sigma_{t,i}^2h_i^2\mu_m-\sigma_{t,i}^3h_i^3-12\varepsilon^3\mu_m^3)\psi_{m,L,i}\\
&+(12\varepsilon^2\sigma_{t,i}h_i\mu_m^2+4\varepsilon\sigma_{t,i}^2h_i^2\mu_m+\sigma_{t,i}^3h_i^3+12\varepsilon^3\mu_m^3)\psi_{m,R,i}\\
&=(-\varepsilon\sigma_{t,i}^2h_i^3+2\varepsilon^2\sigma_{t,i}h_i^2\mu_m+6\varepsilon^3h_i\mu_m^2)[(\frac{\sigma_{t,i}}{\varepsilon}-\varepsilon\sigma_{a,i})\frac{\phi_{L,i}}{2}+\frac{Q_{L,i}}{2}]\\
&+(\varepsilon\sigma_{t,i}^2h_i^3+4\varepsilon^2\sigma_{t,i}h_i^2\mu_m+6\varepsilon^3h_i\mu_m^2)[(\frac{\sigma_{t,i}}{\varepsilon}-\varepsilon\sigma_{a,i})\frac{\phi_{R,i}}{2}+\frac{Q_{R,i}}{2}]
\end{aligned}
\tag{4.51}
$$

and from Eq. (4.49) for $\mu_m<0$:

$$
\begin{aligned}
&(-12\varepsilon^2\sigma_{t,i}h_i\mu_m^2+4\varepsilon\sigma_{t,i}^2h_i^2\mu_m-\sigma_{t,i}^3h_i^3+12\varepsilon^3\mu_m^3)\psi_{m,L,i}\\
&+(2\varepsilon\sigma_{t,i}^2h_i^2\mu_m+\sigma_{t,i}^3h_i^3-12\varepsilon^3\mu_m^3)\psi_{m,R,i}\\
&=(-\varepsilon\sigma_{t,i}^2h_i^3+4\varepsilon^2\sigma_{t,i}h_i^2\mu_m-6\varepsilon^3h_i\mu_m^2)[(\frac{\sigma_{t,i}}{\varepsilon}-\varepsilon\sigma_{a,i})\frac{\phi_{L,i}}{2}+\frac{Q_{L,i}}{2}]\\
&+(\varepsilon\sigma_{t,i}^2h_i^3+2\varepsilon^2\sigma_{t,i}h_i^2\mu_m-6\varepsilon^3h_i\mu_m^2)[(\frac{\sigma_{t,i}}{\varepsilon}-\varepsilon\sigma_{a,i})\frac{\phi_{R,i}}{2}+\frac{Q_{R,i}}{2}]
\end{aligned}
\tag{4.52}
$$

Expanding the discrete solution in a power series in ε as in Eqs. (4.18)-(4.19), the ε^0 equations from Eqs. (4.50)-(4.52) yield:

$$\psi_{m,L,i}^{(0)} + \psi_{m,R,i}^{(0)} = \frac{1}{2}(\phi_{L,i}^{(0)} + \phi_{R,i}^{(0)}) \tag{4.53}$$

$$\sigma_{t,i}^3 h_i^3 (\psi_{m,R,i}^{(0)} - \psi_{m,L,i}^{(0)}) = \sigma_{t,i}^3 h_i^3 \frac{1}{2}(\phi_{R,i}^{(0)} - \phi_{L,i}^{(0)}) \text{ for } \mu_m > 0, \tag{4.54}$$

$$\sigma_{t,i}^3 h_i^3 (\psi_{m,R,i}^{(0)} - \psi_{m,L,i}^{(0)}) = \sigma_{t,i}^3 h_i^3 \frac{1}{2}(\phi_{R,i}^{(0)} - \phi_{L,i}^{(0)}) \text{ for } \mu_m < 0. \tag{4.55}$$

Solving Eqs. (4.53)-(4.55), we obtain isotropy of the leading-order angular flux:

$$\psi_{m,L,i}^{(0)} = \frac{1}{2}\phi_{L,i}^{(0)}, \tag{4.56}$$

$$\psi_{m,R,i}^{(0)} = \frac{1}{2}\phi_{R,i}^{(0)}, \tag{4.57}$$

which further yields the leading-order current to be zero:

$$J^{(0)} = 0. \tag{4.58}$$

The ε^1 equations are as follows:

$$\mu_m(\psi_{m,i+1/2}^{(0)} - \psi_{m,i-1/2}^{(0)}) + \sigma_{t,i} h_i \frac{\psi_{m,L,i}^{(1)} + \psi_{m,R,i}^{(1)}}{2} = \frac{\sigma_{t,i} h_i}{2} \frac{\phi_{L,i}^{(1)} + \phi_{R,i}^{(1)}}{2}, \tag{4.59}$$

$$\begin{aligned} &\sigma_{t,i}^3 h_i^3 (\psi_{m,R,i}^{(1)} - \psi_{m,L,i}^{(1)}) + 2\sigma_{t,i}^2 h_i^2 \mu_m (\psi_{m,L,i}^{(0)} + 2\psi_{m,R,i}^{(0)}) \\ &= \sigma_{t,i}^3 h_i^3 \frac{1}{2}(\phi_{R,i}^{(1)} - \phi_{L,i}^{(1)}) + 2\sigma_{t,i}^2 h_i^2 \mu_m \frac{1}{2}(\phi_{L,i}^{(0)} + 2\phi_{R,i}^{(0)}) \quad \text{for } \mu_m > 0, \end{aligned} \tag{4.60}$$

$$\begin{aligned} &\sigma_{t,i}^3 h_i^3 (\psi_{m,R,i}^{(1)} - \psi_{m,L,i}^{(1)}) + 2\sigma_{t,i}^2 h_i^2 \mu_m (2\psi_{m,L,i}^{(0)} + \psi_{m,R,i}^{(0)}) \\ &= \sigma_{t,i}^3 h_i^3 \frac{1}{2}(\phi_{R,i}^{(1)} - \phi_{L,i}^{(1)}) + 2\sigma_{t,i}^2 h_i^2 \mu_m \frac{1}{2}(2\phi_{L,i}^{(0)} + \phi_{R,i}^{(0)}) \quad \text{for } \mu_m < 0. \end{aligned} \tag{4.61}$$

Multiplying Eq. (4.59) by $\mu_m w_m$ and summing over $m = 1, ..., N$, and after considerable manipulation, we obtain the discretize form of Fick's Law for the first-order current:

$$J_i^{(1)} = -\frac{1}{3\sigma_{t,i}h_i}(\phi_{i+1/2}^{(0)} - \phi_{i-1/2}^{(0)}) \tag{4.62}$$

Multiplying Eq. (4.59) by w_m and sum over $m = 1,...,N$, we obtain:

$$\phi_{L,i+1}^{(0)} - \phi_{R,i}^{(0)} = \phi_{L,i}^{(0)} - \phi_{R,i-1}^{(0)}. \tag{4.63}$$

Multiplying Eq. (4.60) by $\mu_m w_m$ and summing over $m = N/2+1,...,N$; and multiplying Eq. (4.61) by $\mu_m w_m$ and summing over $m = 1,...,N/2$, we respectively obtain:

$$J_{+,R,i}^{(1)} - J_{+,L,i}^{(1)} = \frac{1}{4}(\phi_{R,i}^{(1)} - \phi_{L,i}^{(1)}), \tag{4.64}$$

and

$$J_{-,R,i}^{(1)} - J_{-,L,i}^{(1)} = -\frac{1}{4}(\phi_{R,i}^{(1)} - \phi_{L,i}^{(1)}), \tag{4.65}$$

where the half range currents are defined as:

$$J_{+,L,i}^{(1)} = \sum_{m=N/2+1}^{N} \psi_{m,L,i}^{(1)} \mu_m w_m, \tag{4.66}$$

$$J_{+,R,i}^{(1)} = \sum_{m=N/2+1}^{N} \psi_{m,R,i}^{(1)} \mu_m w_m, \tag{4.67}$$

$$J_{-,L,i}^{(1)} = \sum_{m=1}^{N/2} \psi_{m,L,i}^{(1)} \mu_m w_m, \tag{4.68}$$

$$J_{-,R,i}^{(1)} = \sum_{m=1}^{N/2} \psi_{m,R,i}^{(1)} \mu_m w_m. \tag{4.69}$$

Adding Eqs. (4.64) and (4.65), we get:

$$J_{L,i}^{(1)} = J_{R,i}^{(1)} = J_i^{(1)}. \tag{4.70}$$

Eq. (4.70) shows that the first-order current is constant over a particular spatial cell. Subtracting Eq. (4.65) from Eq. (4.64), we get:

$$(J^{(1)}_{+,R,i} - J^{(1)}_{-,R,i}) - (J^{(1)}_{+,L,i} - J^{(1)}_{-,L,i}) = \frac{1}{4}(\phi^{(1)}_{R,i} - \phi^{(1)}_{L,i}). \tag{4.71}$$

Eqs. (4.62), (4.63), (4.70) and (4.71) are all the information we can obtain from the ε^1 equations based on the LDLS method. Eq. (4.62) shows the Fick's law for the first-order current, which is expected. Eq. (4.63) shows that the leading-order scalar flux, and thus angular flux, is not continuous, which is unexpected, and the value of jump is constant between each two cells. Eq. (4.70) gives a constant first-order current over the spatial cell. Eq. (4.71) has no physical meaning, but will be used in the manipulation for the ε^2 equations.

Compared to the LLDG method, the ε^1 equations from LDLS method are not able to yield the continuity of the leading-order angular flux but only give a constant jump between each adjacent pair of spatial cells.

The ε^2 equations are:

$$\mu_m(\psi^{(1)}_{m,i+1/2} - \psi^{(1)}_{m,i-1/2}) + \sigma_{t,i}h_i\psi^{(2)}_{m,i} = \frac{\sigma_{t,i}h_i}{2}\phi^{(2)}_i - \frac{\sigma_{a,i}h_i}{2}\phi^{(0)}_i + \frac{h_i}{2}Q_i, \tag{4.72}$$

$$\begin{aligned}
&-6\sigma_{t,i}h_i\mu_m^2(\psi^{(0)}_{m,R,i} - \psi^{(0)}_{m,L,i}) \\
&-2\sigma_{t,i}^2h_i^2\mu_m(\psi^{(1)}_{m,L,i} - \frac{1}{2}\phi^{(1)}_{L,i}) - 4\sigma_{t,i}^2h_i^2\mu_m(\psi^{(1)}_{m,R,i} - \frac{1}{2}\phi^{(1)}_{R,i}) \\
&+\sigma_{t,i}^2h_i^3(\sigma_{t,i}\psi^{(2)}_{m,L,i} - \sigma_{t,i}\frac{1}{2}\phi^{(2)}_{L,i} + \sigma_{a,i}\frac{1}{2}\phi^{(0)}_{L,i} - \frac{1}{2}Q_{L,i}) \\
&-\sigma_{t,i}^2h_i^3(\sigma_{t,i}\psi^{(2)}_{m,R,i} - \sigma_{t,i}\frac{1}{2}\phi^{(2)}_{R,i} + \sigma_{a,i}\frac{1}{2}\phi^{(0)}_{R,i} - \frac{1}{2}Q_{R,i}) = 0 \quad \text{for } \mu_m > 0,
\end{aligned} \tag{4.73}$$

$$
\begin{aligned}
&-6\sigma_{t,i}h_i\mu_m^2(\psi_{m,R,i}^{(0)}-\psi_{m,L,i}^{(0)})\\
&-4\sigma_{t,i}^2h_i^2\mu_m(\psi_{m,L,i}^{(1)}-\frac{1}{2}\phi_{L,i}^{(1)})-2\sigma_{t,i}^2h_i^2\mu_m(\psi_{m,R,i}^{(1)}-\frac{1}{2}\phi_{R,i}^{(1)})\\
&+\sigma_{t,i}^2h_i^3(\sigma_{t,i}\psi_{m,L,i}^{(2)}-\sigma_{t,i}\frac{1}{2}\phi_{L,i}^{(2)}+\sigma_{a,i}\frac{1}{2}\phi_{L,i}^{(0)}-\frac{1}{2}Q_{L,i})\\
&-\sigma_{t,i}^2h_i^3(\sigma_{t,i}\psi_{m,R,i}^{(2)}-\sigma_{t,i}\frac{1}{2}\phi_{R,i}^{(2)}+\sigma_{a,i}\frac{1}{2}\phi_{R,i}^{(0)}-\frac{1}{2}Q_{R,i})=0 \quad \text{for } \mu_m<0.
\end{aligned}
\tag{4.74}
$$

Multiplying Eq. (4.72) by w_m and summing over $m=1,...,N$, we obtain:

$$
J_{m,i+1/2}^{(1)}-J_{m,i-1/2}^{(1)}+\sigma_{a,i}h_i\phi_i^{(0)}=h_iQ_i \tag{4.75}
$$

Multiplying Eq. (4.73) by w_m and summing over $m=N/2+1,...,N$; multiplying Eq. (4.74) by w_m and summing over $m=1,...,N/2$, and adding these two equations, we get:

$$
\begin{aligned}
&\sigma_{t,i}^2h_i^2[4J_i^{(1)}+2J_{+,R,i}^{(1)}+2J_{-,L,i}^{(1)}-\frac{1}{2}(\phi_{R,i}^{(1)}-\phi_{L,i}^{(1)})]\\
&+(4\sigma_{t,i}h_i+\sigma_{a,i}\sigma_{t,i}^2h_i^3)(\phi_{R,i}^{(0)}-\phi_{L,i}^{(0)})=\sigma_{t,i}^2h_i^3(Q_{R,i}-Q_{L,i})
\end{aligned}
\tag{4.76}
$$

We substitute from Eq. (4.71) into Eq. (4.76). After manipulation, we obtain:

$$
6\sigma_{t,i}^2h_i^2J_i^{(1)}+(4\sigma_{t,i}h_i+\sigma_{a,i}\sigma_{t,i}^2h_i^3)(\phi_{R,i}^{(0)}-\phi_{L,i}^{(0)})=\sigma_{t,i}^2h_i^3(Q_{R,i}-Q_{L,i}) \tag{4.77}
$$

Substituting Eq. (4.62) into Eq. (4.77), we obtain:

$$
-2\sigma_{t,i}h_i(\phi_{i+1/2}^{(0)}-\phi_{i-1/2}^{(0)})+(4\sigma_{t,i}h_i+\sigma_{a,i}\sigma_{t,i}^2h_i^3)(\phi_{R,i}^{(0)}-\phi_{L,i}^{(0)})=\sigma_{t,i}^2h_i^3(Q_{R,i}-Q_{L,i}) \tag{4.78}
$$

Based on Eq. (4.63), define the constant jump of scalar flux between any two adjacent spatial cells as:

$$
\Delta=\phi_{L,i+1}^{(0)}-\phi_{R,i}^{(0)}=\phi_{L,i}^{(0)}-\phi_{R,i-1}^{(0)}. \tag{4.79}
$$

The value of the boundary scalar flux for each cell is defined as:

$$
\phi_{i+1/2}^{(0)}=\frac{1}{2}(\phi_{R,i}^{(0)}+\phi_{L,i+1}^{(0)}). \tag{4.80}
$$

From Eqs. (4.79) and (4.80), we obtain:

$$\phi_{R,i}^{(0)} = \phi_{i+1/2}^{(0)} - \frac{\Delta}{2}, \tag{4.81}$$

$$\phi_{L,i}^{(0)} = \phi_{i-1/2}^{(0)} + \frac{\Delta}{2}. \tag{4.82}$$

Subtracting Eq. (4.82) from Eq. (4.81):

$$\phi_{R,i}^{(0)} - \phi_{L,i}^{(0)} = \phi_{i+1/2}^{(0)} - \phi_{i-1/2}^{(0)} - \Delta. \tag{4.83}$$

Substituting Eq. (4.83) into Eq. (4.78), we get:

$$(2\sigma_{t,i}h_i + \sigma_{a,i}\sigma_{t,i}^2 h_i^3)(\phi_{i+1/2}^{(0)} - \phi_{i-1/2}^{(0)}) - (4\sigma_{t,i}h_i + \sigma_{a,i}\sigma_{t,i}^2 h_i^3)\Delta = \sigma_{t,i}^2 h_i^3 (Q_{R,i} - Q_{L,i}), \tag{4.84}$$

Equation (4.84) is for cell *i*. If we write down Eq. (4.84) for cell *i*+1, subtract the equation for cell *i* from the equation for cell *i*+1, and algebraically manipulate the resulting equation, we obtain the following after assuming constant cross-sections and constant cell width for each spatial cell:

$$\phi_{i+3/2}^{(0)} - 2\phi_{i+1/2}^{(0)} + \phi_{i-1/2}^{(0)} = \frac{\sigma_t h^2}{2 + \sigma_a \sigma_t h^2}[Q_{R,i+1} - (Q_{L,i+1} + Q_{R,i}) + Q_{L,i}]. \tag{4.85}$$

where $i = 1,...I-1$. From Eq. (4.85), we find that the leading-order scalar flux does not satisfy a valid discretization of the diffusion equation. The LDLS scheme does not have thick diffusion limit. If we have a constant inhomogeneous source, the right side of Eq. (4.85) will be zero (0). This result is consistent with our computational results shown in the next chapter.

Summary

In this chapter, we first reviewed the asymptotic analysis for the LLDG method which gives the thick diffusion limit. We performed in detail the asymptotic analysis for the new LDLS method. The result is not so encouraging because it does not yield a diffusion equation in the thick diffusion limit. However, in the next chapter we can see that the LDLS method is more robust than the LDG method and is more accurate than the LLDG method in this 1-D slab geometry problem. Consequently, the LDLS method can be applied to advantage in the neutronics problems but not highly diffusive radiative problems.

CHAPTER V

COMPUTATIONAL RESULTS

In this chapter we present numerical results. We have implemented the different spatial discretization methods, i.e., LDG, LLDG, and LDLS, into a FORTRAN code and used the code to provide our results. We measure the L_2 errors of the methods in problems with and without scattering. Iterative convergence rates are measured for different methods and compared with the rates predicted by Fourier analysis. Thick diffusion limit calculations are performed to confirm our theoretical predictions.

L_2 measurements for pointwise and continuous errors

The purpose of this section is to provide computational evidence that the LDLS spatial discretization scheme is second-order accurate. We compare the order accuracy of the LDG, LLDG, and LDLS methods in problems with and without scattering using both continuous and discrete L_2 norms. To demonstrate the accuracy of the LDLS method, we consider the following test problem defined for Eq. (1.4): uniform mesh ($h_i = h$), $x \in [0, X]$ with $X = 1.0\,cm$, homogenous medium ($\sigma_{t,i} = \sigma_t$, $\sigma_{s,i} = \sigma_s$) with various values of σ_t and σ_s. The number of uniform spatial meshes *I* varies from 2 to 2^{10}. The discrete L_2 norm of the cell-averaged flux can be expressed as:

$$PL_2 = \sqrt{\frac{1}{I}\sum_{i=1}^{I}[\phi_i^{ave} - \phi^{S_N}(x_i)]^2}, \tag{5.1}$$

where $\phi^{S_N}(x_i)$ is the average scalar flux of the *i*th cell from the computational results, and ϕ_i^{ave} is the analytical solution for the cell-averaged scalar flux of the *i*th cell. The continuous L_2 norm error can be expressed as:

$$CL_2 = \sqrt{\sum_{i=1}^{I} \int_{x_{i-1/2}}^{x_{i+1/2}} [\phi^{exact}(x) - \phi^{S_N}(x)]^2 dx}, \tag{5.2}$$

where $\phi^{S_N}(x)$ is the S_N solution for the scalar flux as a function of *x*, and $\phi^{exact}(x)$ is the analytical solution for the scalar flux as a function of *x*. The spatial quadrature form of the continuous L_2 norm can be expressed as:

$$CL_2 = \sqrt{\sum_{i=1}^{I} \{\sum_{j=1}^{J} [\phi^{exact}(x_{i,j}) - \phi^{S_N}(x_{i,j})]^2 w_{i,j}\}}, \tag{5.3}$$

where the order of the spatial Gauss quadrature is *J*. We chose the order of the spatial Gauss qaudrature to be $J = 16$ in all the calculations.

The first set of computations is based on the S_2 equations. A vacuum boundary condition is imposed at $x = 0cm$, and an isotropic flux with a unit half-range current is incident at $x = 1.0cm$. We performed both the pure absorber problem where $\sigma_a = \sigma_t = 1.0cm^{-1}$, and the scattering problem where $\sigma_t = 1.0cm^{-1}$ with the scattering ratio $c = 0.5$. The number of uniform spatial meshes *I* varied from 2 to 2^{10}. For 1-D slab geometry, the S_2 equations are equivalent to the diffusion equation, so an analytic solution to this problem can be easily obtained. In particular, the 1-D diffusion equation is given by:

$$-D\frac{\partial^2 \phi(x)}{\partial x^2} + \sigma_a \phi(x) = 0, \tag{5.4}$$

with boundary conditions:

$$\left.\frac{\phi}{2}+\frac{3J}{2}\frac{1}{\sqrt{3}}\right|_{x=0}=0, \tag{5.5}$$

$$\left.\frac{\phi}{2}-\frac{3J}{2}\frac{1}{\sqrt{3}}\right|_{x=X}=\sqrt{3}, \tag{5.6}$$

where

$$D=\frac{1}{3\sigma_t}, \tag{5.7}$$

$$J(x)=-D\frac{\partial\phi(x)}{\partial x}. \tag{5.8}$$

Solving Eqs. (5.4)-(5.8), we obtain the analytical solution for the diffusion equation:

$$\phi(x)=\frac{2\sqrt{3}\left[\left(1+\sqrt{\frac{\sigma_a}{\sigma_t}}\right)e^{\sqrt{3\sigma_a\sigma_t}x}-\left(1-\sqrt{\frac{\sigma_a}{\sigma_t}}\right)e^{-\sqrt{3\sigma_a\sigma_t}x}\right]}{\left[\left(1+\sqrt{\frac{\sigma_a}{\sigma_t}}\right)^2 e^{\sqrt{3\sigma_a\sigma_t}X}-\left(1-\sqrt{\frac{\sigma_a}{\sigma_t}}\right)^2 e^{-\sqrt{3\sigma_a\sigma_t}X}\right]}. \tag{5.9}$$

Figs. 5.1-5.4 give the computational results for the S_2 equations from the pure absorber and scattering problems. The pointwise error for the cell-averaged flux is shown in Figs. 5.1 and 5.3. It can be observed that the LDG method is third order accurate, while both the LDLS method and LLDG method are second order accurate. However, the LDLS method is more accurate than the LLDG method.

It can be seen from the continuous L_2 error shown in Figs. 5.2 and 5.4 that all three methods yield second-order accuracy. The LDG method is the most accurate, while the LDLS method is slightly less accurate than the LDG method, and the LLDG method is the least accurate.

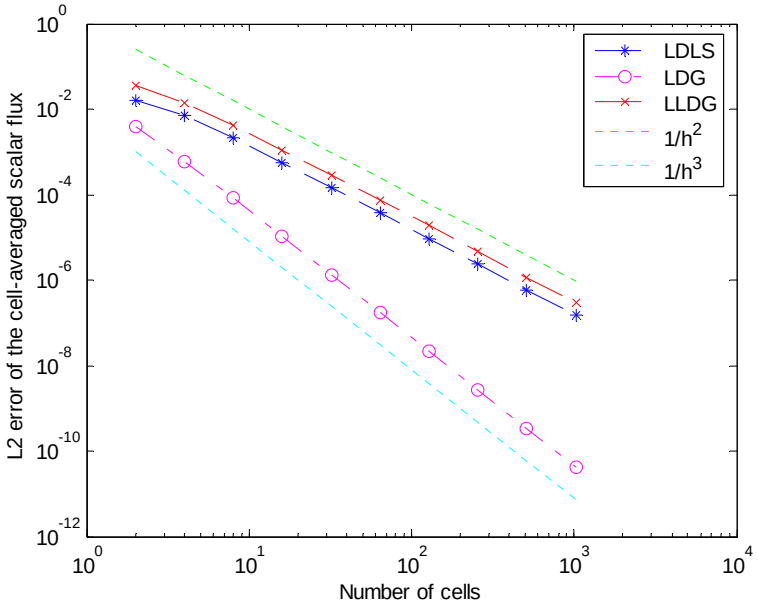

Fig. 5.1. Comparison of S_2 pointwise convergence rate of cell-averaged scalar flux with $\sigma_a = \sigma_t = 1.0 cm^{-1}$ and a unit half-range incident current.

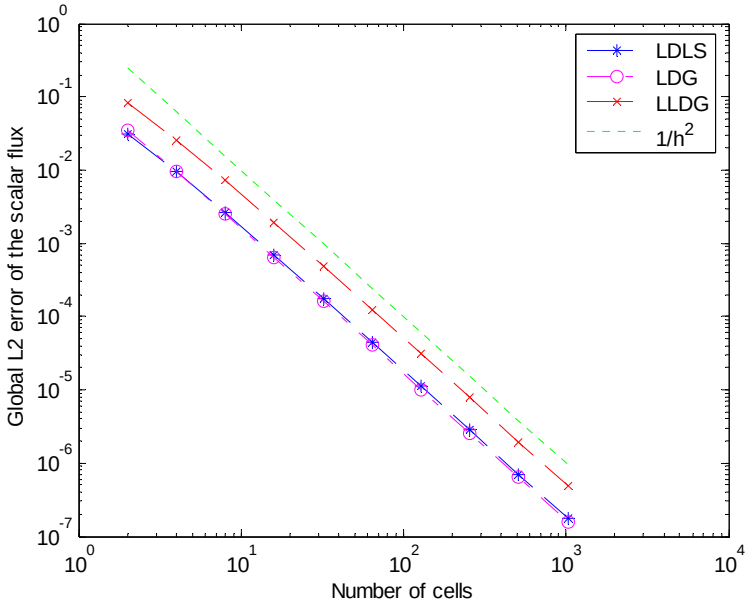

Fig. 5.2. Comparison of S_2 continuous L_2 convergence rate of scalar flux with $\sigma_a = \sigma_t = 1.0 cm^{-1}$ and a unit half-range incident current.

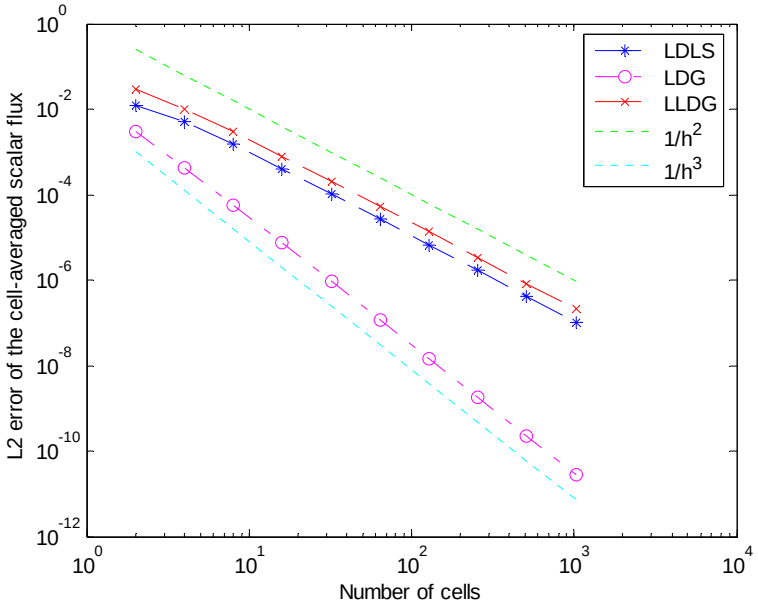

Fig. 5.3. Comparison of S_2 pointwise convergence rate of cell-averaged scalar flux with $\sigma_t = 1.0 cm^{-1}$, $c = 0.5$ and a unit half-range incident current.

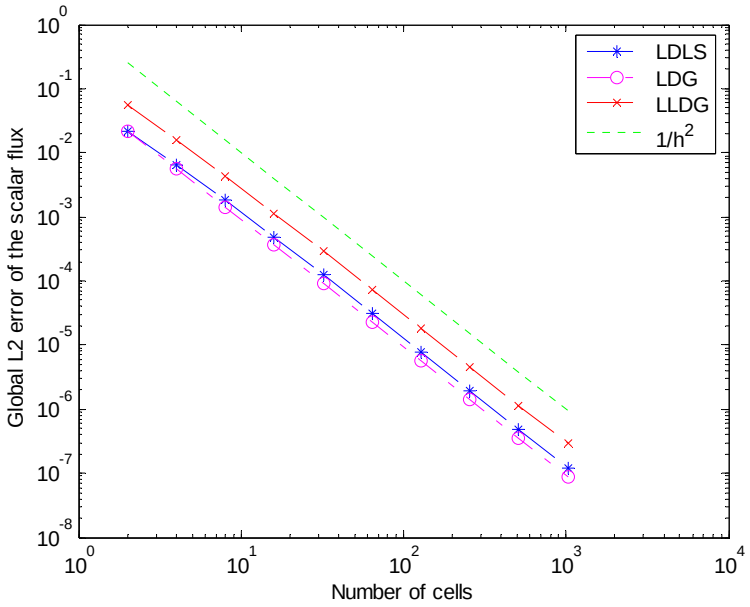

Fig. 5.4. Comparison of S_2 continuous L_2 convergence rate of scalar flux with $\sigma_t = 1.0 cm^{-1}$, $c = 0.5$ and a unit half-range incident current.

The second set of computations is based on S_N Gauss quadrature sets for the pure absorber problem ($\sigma_a = \sigma_t = 1.0\ cm^{-1}$). We performed calculations with $N = 4,8,16.$ A vacuum boundary condition was imposed at $x = 0cm$, and an isotropic flux with a unit half-range current was incident at $x = X = 1.0cm$. The number of uniform spatial meshes I varied from 2 to 2^{10}. For 1-D slab geometry, the S_N equations for the pure absorber problem have the following analytical solution:

$$\phi(x) = \frac{\sum_{m=1}^{N/2} e^{\frac{\sigma_a (X-x)}{|\mu_m|}} w_m}{-\sum_{m=1}^{N/2} \mu_m w_m}. \tag{5.10}$$

Figs. 5.5-5.10 for the S_N calculations yield the same conclusions as Figs. 5.1-5.4. In particular, for the pointwise error for the cell-averaged flux, the LDG method is third order accurate, while both the LDLS method and LLDG method are second order accurate. However, the LDLS method is more accurate than the LLDG method.

For the continuous L_2 error, all three methods yield second-order accuracy. The LDG method is the most accurate, while the LDLS method is slightly less accurate than the LDG method, and the LLDG method is the least accurate.

The third set of computations was performed to investigate the S_N equations with scattering. To obtain an analytical solution for a transport equation, we used the method of manufactured solutions. It can be described as follows. One first assumes an arbitrary angular flux solution which defines the boundary conditions. Then one substitutes that solution into the transport equation, and solves for the associated inhomogeneous source. The assumed transport solution determines the boundary conditions. We choose the

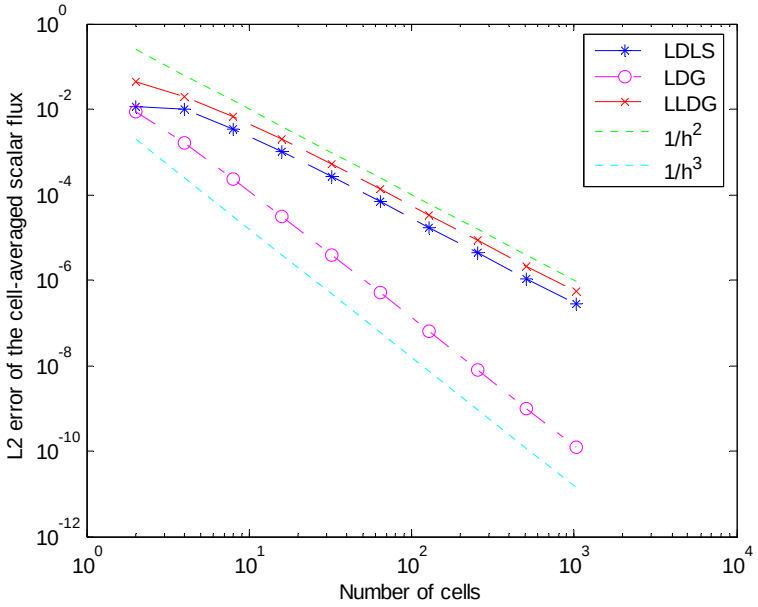

Fig. 5.5. Comparison of S_4 pointwise convergence rate of cell-averaged scalar flux with $\sigma_a = \sigma_t = 1.0 cm^{-1}$ and a unit half-range incident current.

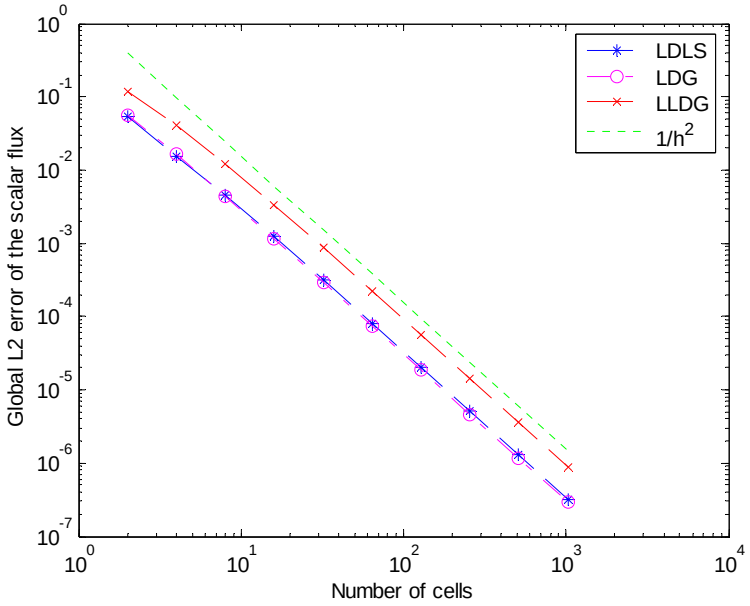

Fig. 5.6. Comparison of S_4 continuous L_2 convergence rate of scalar flux with $\sigma_a = \sigma_t = 1.0 cm^{-1}$ and a unit half-range incident current.

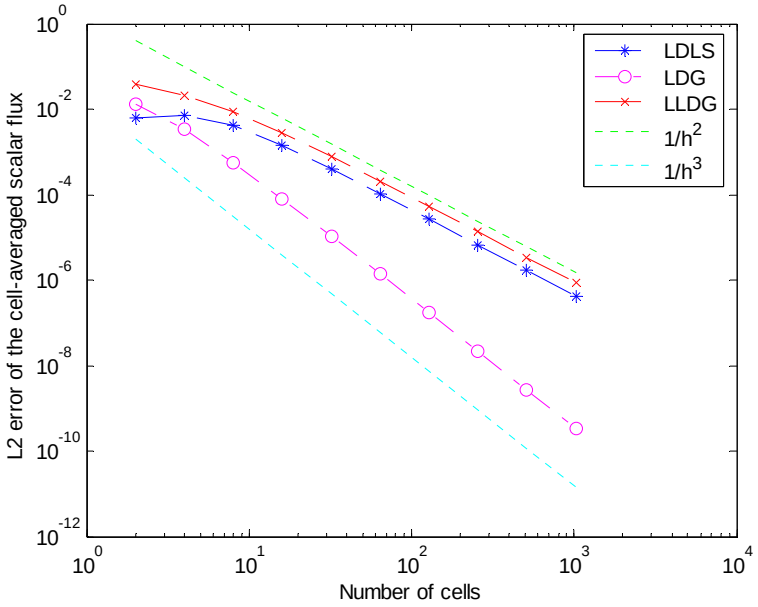

Fig. 5.7. Comparison of S_8 pointwise convergence rate of cell-averaged scalar flux with $\sigma_a = \sigma_t = 1.0 cm^{-1}$ and a unit half-range incident current.

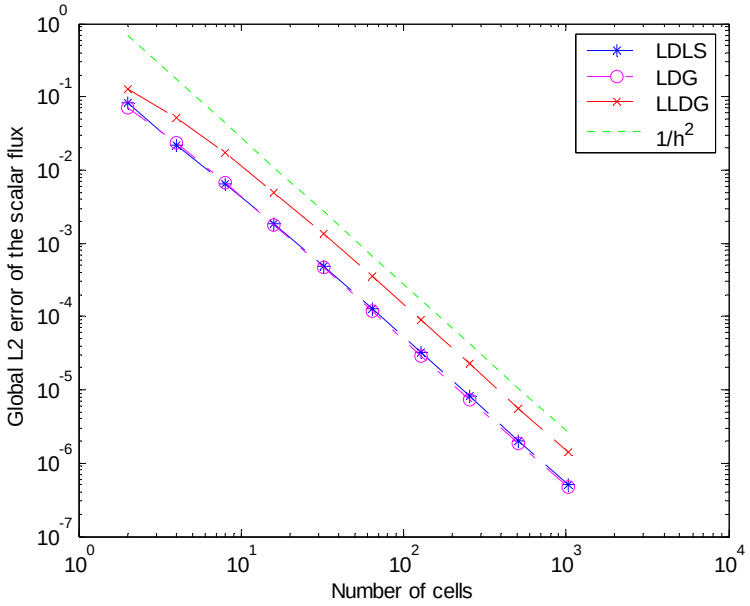

Fig. 5.8. Comparison of S_8 continuous L_2 convergence rate of scalar flux with $\sigma_a = \sigma_t = 1.0 cm^{-1}$ and a unit half-range incident current.

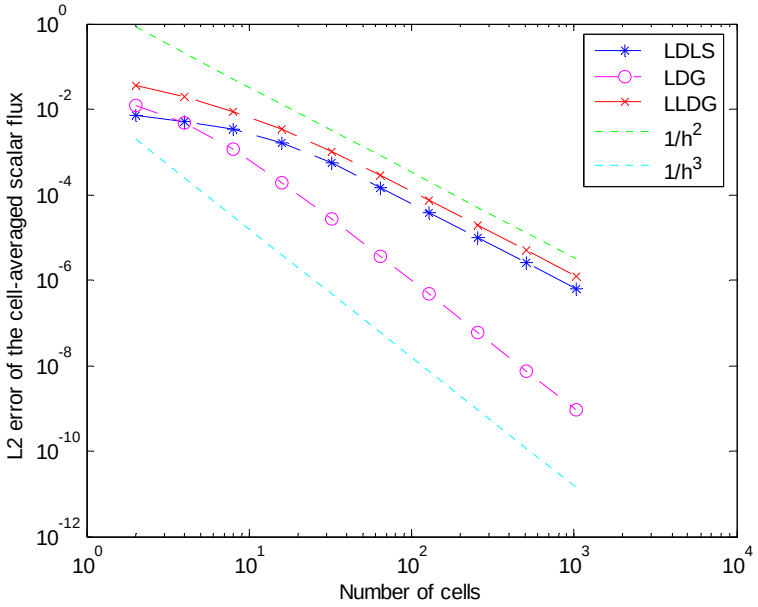

Fig. 5.9. Comparison of S_{16} pointwise convergence rate of cell-averaged scalar flux with $\sigma_a = \sigma_t = 1.0 cm^{-1}$ and a unit half-range incident current.

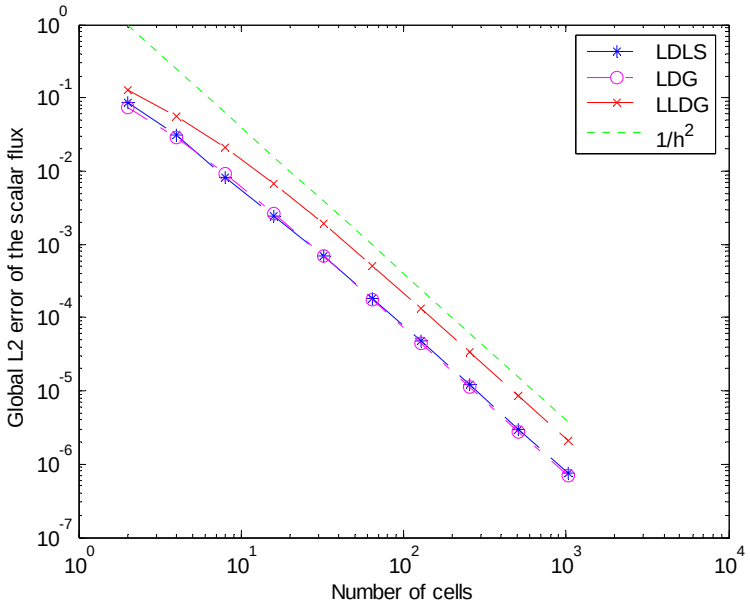

Fig. 5.10. Comparison of S_{16} continuous L_2 convergence rate of scalar flux with $\sigma_a = \sigma_t = 1.0 cm^{-1}$ and a unit half-range incident current.

following transport angular flux solution:

$$\psi_m(x) = \sin(\pi x)(1+\mu_m^2). \tag{5.11}$$

This flux solution is symmetric along the *x*-axis, and satisfies a vacuum condition at both the left and right boundaries. Substituting Eq. (5.11) into Eq. (1.4), the 1-D S_N equations, we obtain the corresponding inhomogeneous source:

$$Q_m(x) = \mu_m \frac{d\psi_m(x)}{dx} + \sigma_t \psi_m(x) - \frac{\sigma_s}{2}\sum_{m=1}^{N} w_m \psi_m(x), \tag{5.12}$$

$$Q_m(x) = \mu_m(1+\mu_m^2)\pi\cos(\pi x) + [\sigma_t(1+\mu_m^2) - \frac{4}{3}\sigma_s]\sin(\pi x). \tag{5.13}$$

We implemented Eqs. (5.11) and (5.13) into our S_N code to enable us to measure the order of accuracy of the spatial discretization schemes. We performed test transport calculations with $N = 4,8,16$. In accordance with Eq. (5.11), vacuum boundary conditions were imposed at $x = 0cm$ and $x = X = 1.0cm$, $\sigma_t = 1.0\ cm^{-1}$, and *c*=0.5. The number of uniform spatial meshes, *I*, was varied from 2 to 2^{10}.

Figs. 5.11-5.16 yield the same conclusions as the previous problems. For the pointwise error for the cell-averaged flux, the LDG method is third order accurate, while both the LDLS method and LLDG method are second order accurate. However, the LDLS method is more accurate than the LLDG method. For the continuous L_2 error, all three methods yield second-order accuracy. The LDG method is the most accurate, while the LDLS method is slightly less accurate than the LDG method, and the LLDG method is the least accurate.

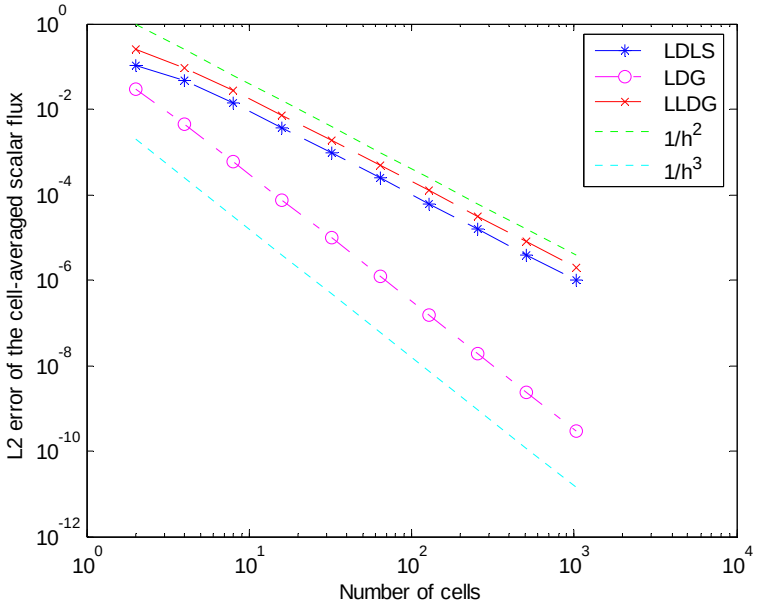

Fig. 5.11. Comparison of S_4 pointwise convergence rate of cell-averaged scalar flux with $\sigma_t = 1.0cm^{-1}$, $c = 0.5$ and the method of manufactured solutions.

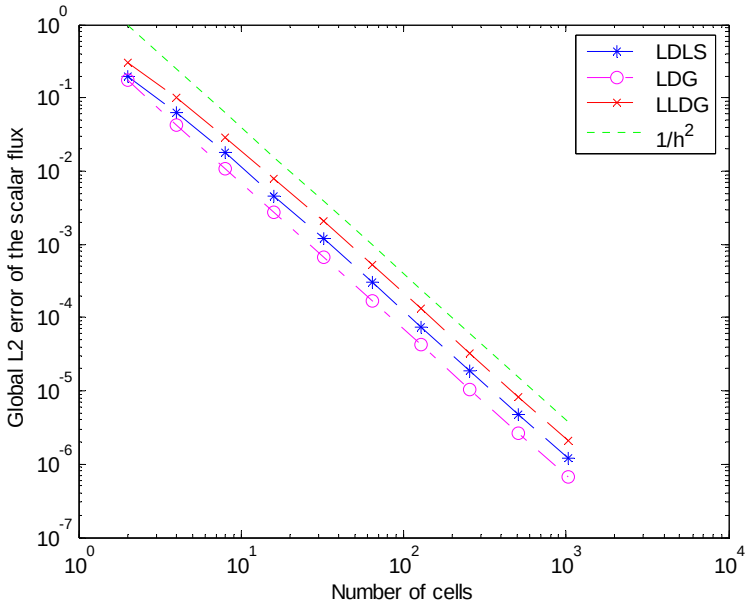

Fig. 5.12. Comparison of S_4 continuous L_2 convergence rate of scalar flux with $\sigma_t = 1.0cm^{-1}$, $c = 0.5$ and the method of manufactured solutions.

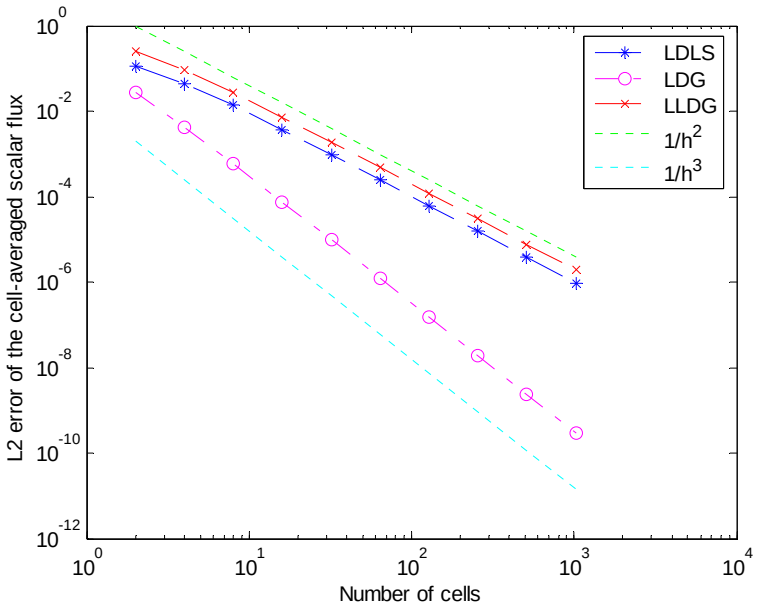

Fig. 5.13. Comparison of S_8 pointwise convergence rate of cell-averaged scalar flux with $\sigma_t = 1.0cm^{-1}$, $c = 0.5$ and the method of manufactured solutions.

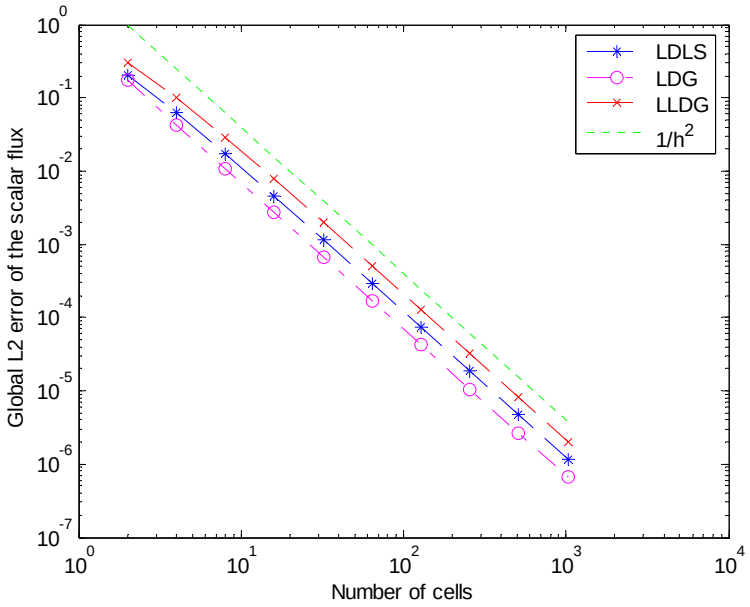

Fig. 5.14. Comparison of S_8 continuous L_2 convergence rate of scalar flux with $\sigma_t = 1.0cm^{-1}$, $c = 0.5$ and the method of manufactured solutions.

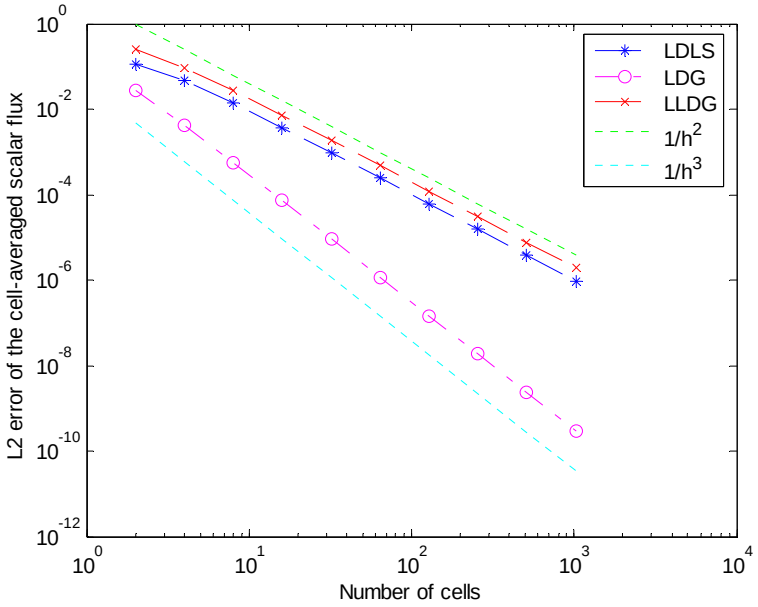

Fig. 5.15. Comparison of S_{16} pointwise convergence rate of cell-averaged scalar flux with $\sigma_t = 1.0cm^{-1}$, $c = 0.5$ and the method of manufactured solutions.

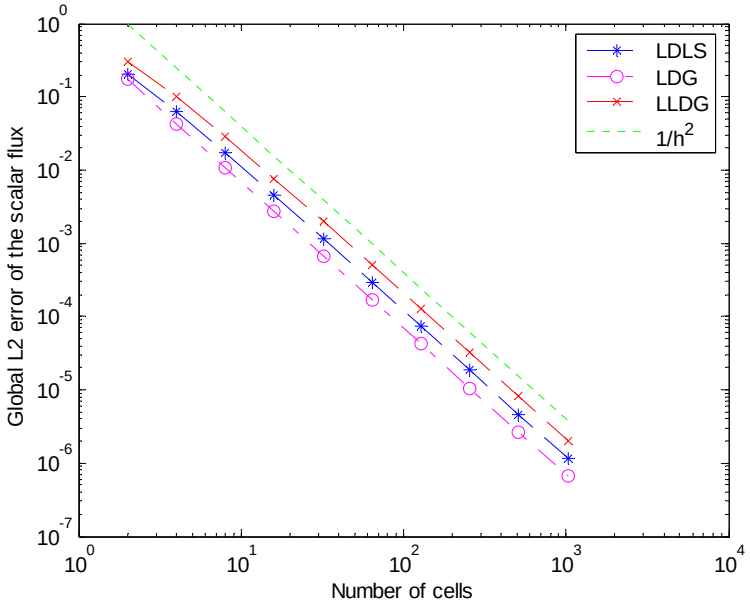

Fig. 5.16. Comparison of S_{16} continuous L_2 convergence rate of scalar flux with $\sigma_t = 1.0cm^{-1}$, $c = 0.5$ and the method of manufactured solutions.

Computational results for spectral radii and comparison with Fourier analysis

In Chapter III, we investigated the spectral radius of the LDLS method by Fourier analysis assuming an infinite homogeneous medium problem. In this section, we verify the results from the Fourier analysis by numerical calculations.

We first perform S_8 calculations for a pure scattering problem ($c = 1.0$) with $\sigma_t = 1.0$. The number of spatial meshes I and the total thickness of the X were varied in order to get different thickness for each cell width h, where $h = X / I$. In Table 5.1, spectral radii from the Fourier analysis are directly compared with computational results. We obtained these results by setting all sources to zero and assuming a random distributed scalar flux guess $\phi_i \in (0,1)$. The exact solution to this problem is the zero solution, so the solution iterate is in fact the error. This makes it very easy to compute the spectral radius ρ:

$$\rho = \frac{\left\| \phi^{l+1} \right\|_2}{\left\| \phi^{l} \right\|_2}, \tag{5.14}$$

where

$$\left\| \phi^{l} \right\|_2 = \sqrt{\frac{1}{I} \sum_{i=1}^{I} [\phi^{l}(x_i)]^2}. \tag{5.15}$$

We can observe that the computational spectral radii agree extremely well with those from Fourier analysis. We also performed calculations with $c = 0.98$. Table 5.2 gives a comparison of the spectral radii from these calculations, and the computational results are also in excellent agreement with theory.

Table 5.1

LDLS spectral radii for a pure scattering problem (S_8).

h (cm)	Total thickness (cm)	Number of cells	From Fourier analysis	From computational results
0.1	100	1000	0.2225	0.2221
0.5	100	200	0.2406	0.2404
1.0	100	100	0.25	0.2489
3.0	300	100	0.1226	0.1223
5.0	500	100	0.2146	0.2138
10.0	1000	100	0.2667	0.2658

Table 5.2

LDLS spectral radii with c=0.98 (S_8).

h (cm)	Total thickness (cm)	Number of cells	From Fourier analysis	From computational results
0.1	100	1000	0.2159	0.2154
0.5	100	200	0.2343	0.2342
1.0	100	100	0.2417	0.2407
3.0	300	100	0.1146	0.1146
5.0	500	100	0.1115	0.1112
10.0	1000	100	0.1076	0.1073

Computational results for the thick diffusion limit

This set of computations is intended to investigate the performance of the LDLS method in the thick diffusion limit. In Chapter IV, asymptotic analysis showed that the LDLS method does not preserve this limit. In this section we want to test this result computationally.

The problem we consider is characterized as follows: homogenous medium ($\sigma_{t,i} = \sigma_t, \sigma_{s,i} = \sigma_s$), $\sigma_t = 1.0$, $c = 0.5$, uniform mesh ($h_i = h$), $x \in [0, X]$ with $X = 1.0\,cm$, a unit constant distributed inhomogeneous source and a vacuum boundary condition on both boundaries.

To investigate the diffusion limit, we need to first obtain the analytical solution of the diffusion equation that the leading-order transport solution satisfies. The diffusion equation with the given boundary conditions can be expressed as:

$$-D\frac{\partial^2\phi(x)}{\partial x^2} + \sigma_a\phi(x) = Q, \tag{5.16}$$

$$\frac{\phi}{2} + \frac{3J}{2}\frac{1}{\sqrt{3}}\bigg|_{x=0} = 0, \tag{5.17}$$

$$\frac{\phi}{2} - \frac{3J}{2}\frac{1}{\sqrt{3}}\bigg|_{x=X} = 0, \tag{5.18}$$

where D and J are defined in Eqs. (5.7) and (5.8). We introduce a small parameter ε, and scale various quantities as follows:

$$\sigma_t \to \frac{\sigma_t}{\varepsilon}, \tag{5.19}$$

$$\sigma_a \to \varepsilon\sigma_a, \tag{5.20}$$

$$Q \to \varepsilon Q. \tag{5.21}$$

Substituting the above changes into Eqs. (5.16)- (5.18), we can obtain the analytical diffusion equation and boundary conditions in the limit of $\varepsilon \to 0$ as follows:

$$-\varepsilon D \frac{\partial^2 \phi(x)}{\partial x^2} + \varepsilon \sigma_a \phi(x) = \varepsilon Q, \tag{5.22}$$

$$\frac{\phi}{2} + \varepsilon \frac{3J}{2} \frac{1}{\sqrt{3}}\bigg|_{x=0} = 0, \tag{5.23}$$

$$\frac{\phi}{2} - \varepsilon \frac{3J}{2} \frac{1}{\sqrt{3}}\bigg|_{x=X} = 0, \tag{5.24}$$

Through Eqs. (5.22)-(5.24), we can solve the scalar flux $\phi(x)$. It can be observed that the diffusion equation is invariant to the scaling, and the boundary conditions become the Dirichlet boundary conditions.

For the computational results, we performed S_N calculations with $N = 2$ and $N = 8$, and choose the number of uniform spatial meshes I =16. We chose different values of $\varepsilon = 1, 10^{-1}, 10^{-2}, 10^{-3}, 10^{-4}, 10^{-5}$ to study the thick diffusion limit behavior of the LDLS method and compare it with that of the LDG and LLDG methods.

Figs. 5.17-5.22 are the computational solutions for the S_2 equations with $\varepsilon = 1, 10^{-1}, 10^{-2}, 10^{-3}, 10^{-4}, 10^{-5}$ for the three spatial discretization methods. From the figures, we can observe that when $\varepsilon = 1, 10^{-1}, 10^{-2}$, all the three methods give roughly the same result as the analytical diffusion solution. This also shows that for the 1-D problem, the S_2 equations are equivalent to the diffusion equation. For $\varepsilon = 10^{-3}$, the scalar flux from LDLS begins to be smaller than the result from other methods.

When $\varepsilon = 10^{-5}$, the scalar flux tends to go to nearly zero while the LDG and LLDG methods maintain an accurate solution. This convergence to zero was predicted theoretically in Chapter IV.

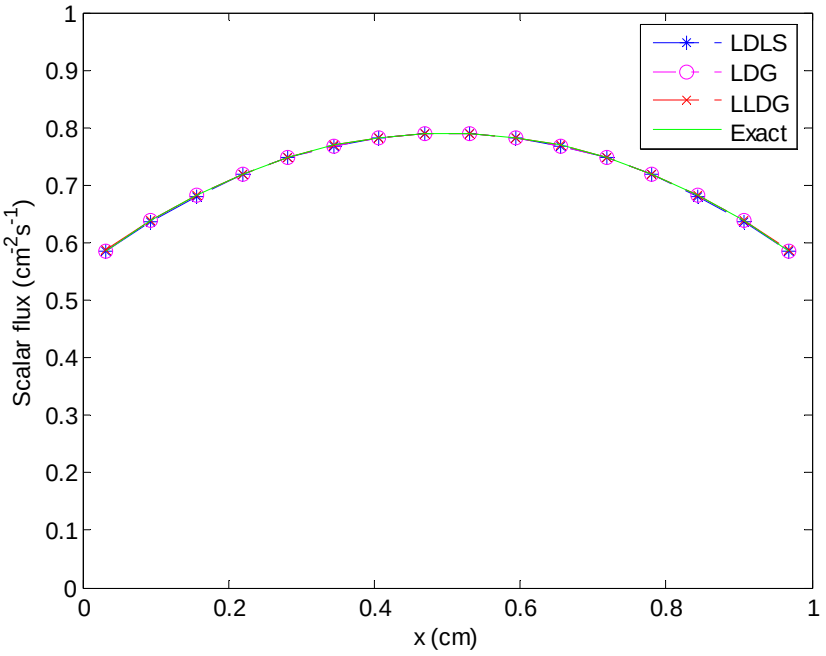

Fig. 5.17. Diffusion limit S_2 solutions with $\varepsilon = 1.0$.

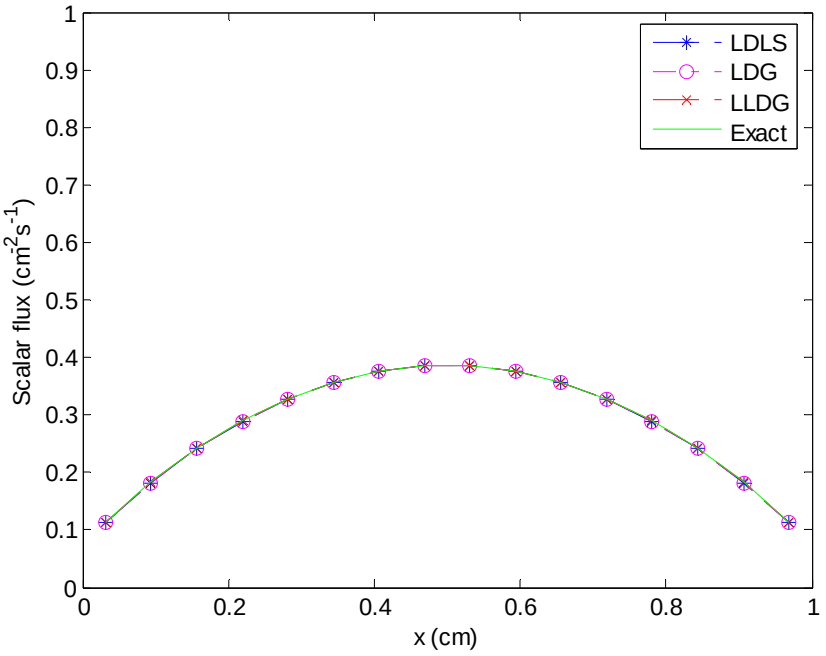

Fig. 5.18. Diffusion limit S_2 solutions with $\varepsilon = 10^{-1}$.

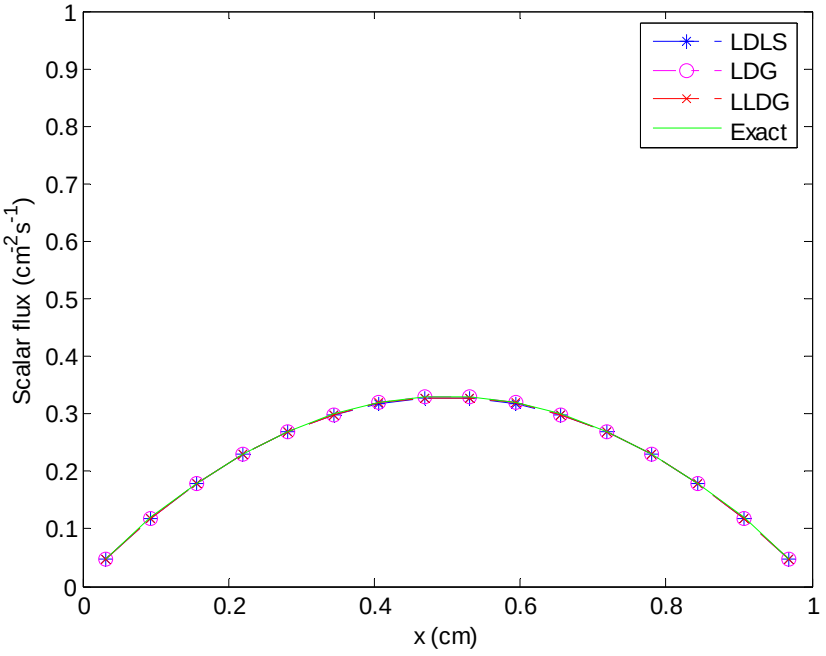

Fig. 5.19. Diffusion limit S_2 solutions with $\varepsilon = 10^{-2}$.

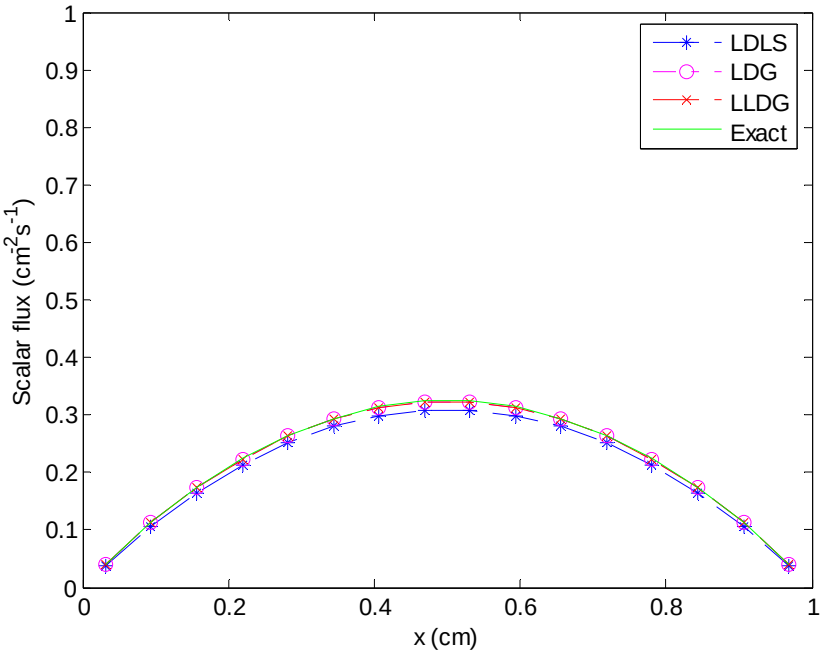

Fig. 5.20. Diffusion limit S_2 solutions with $\varepsilon = 10^{-3}$.

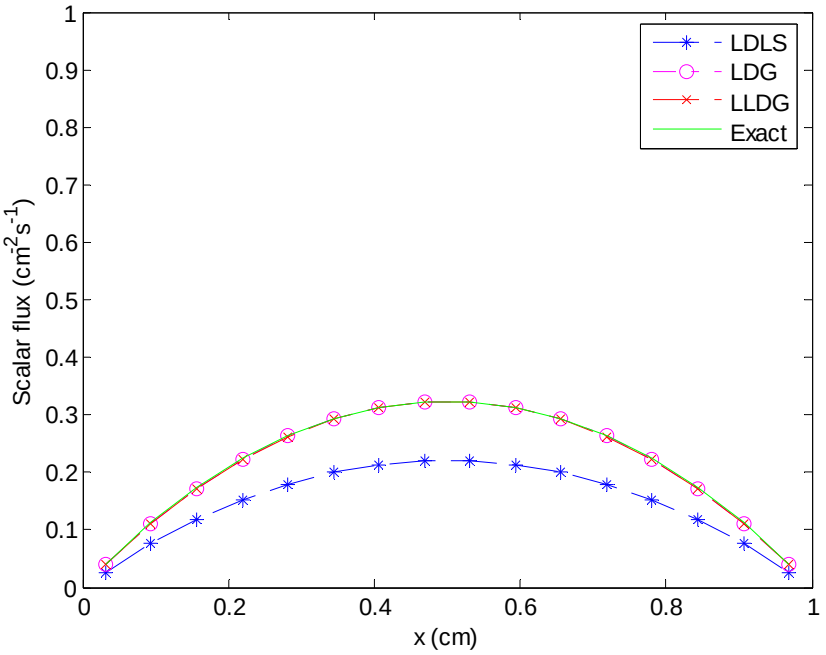

Fig. 5.21. Diffusion limit S_2 solutions with $\varepsilon = 10^{-4}$.

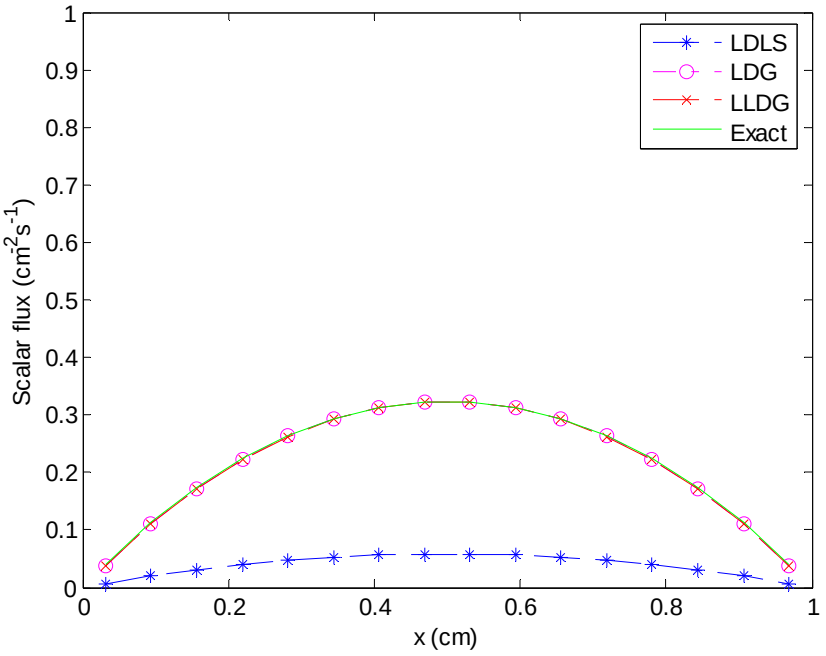

Fig. 5.22. Diffusion limit S_2 solutions with $\varepsilon = 10^{-5}$.

The computational results are given in Figs. 5.23-5.28 for S_8 quadrature with $\varepsilon = 1, 10^{-1}, 10^{-2}, 10^{-3}, 10^{-4}, 10^{-5}$ and the LDLS, LDG and LLDG methods. The results are similar to those for S_2 quadrature. We can observe that when $\varepsilon = 1, 10^{-1}, 10^{-2}$, all the three methods give roughly the same scalar flux which goes to the analytical diffusion solution with decreasing ε. For $\varepsilon = 10^{-3}$, the scalar flux solution from LDLS begins to be smaller than the solutions from the other methods. When $\varepsilon = 10^{-5}$, the scalar flux tends to go to nearly zero while the LDG and LLDG methods maintain accuracy.

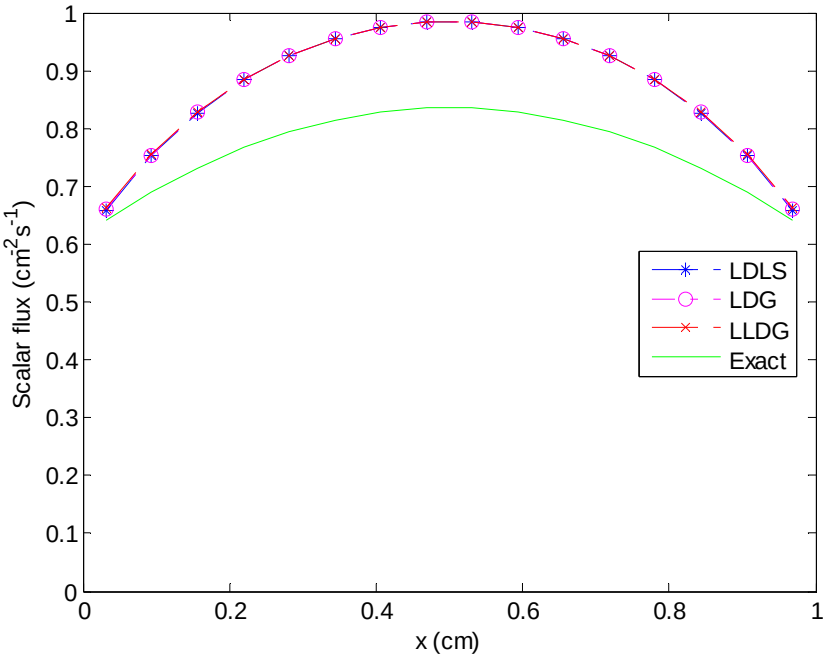

Fig. 5.23. Diffusion limit S_8 solutions with $\varepsilon = 1.0$.

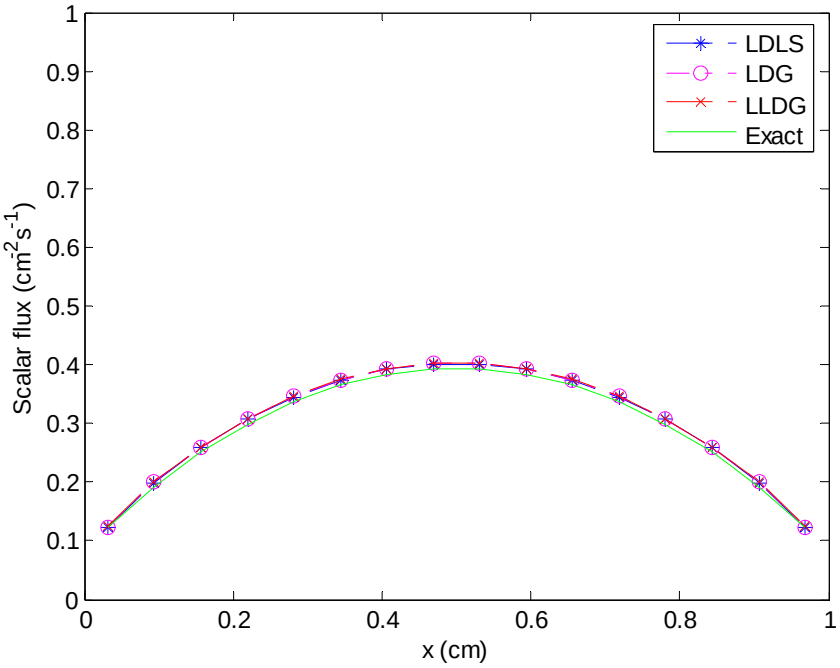

Fig. 5.24. Diffusion limit S_8 solutions with $\varepsilon = 10^{-1}$.

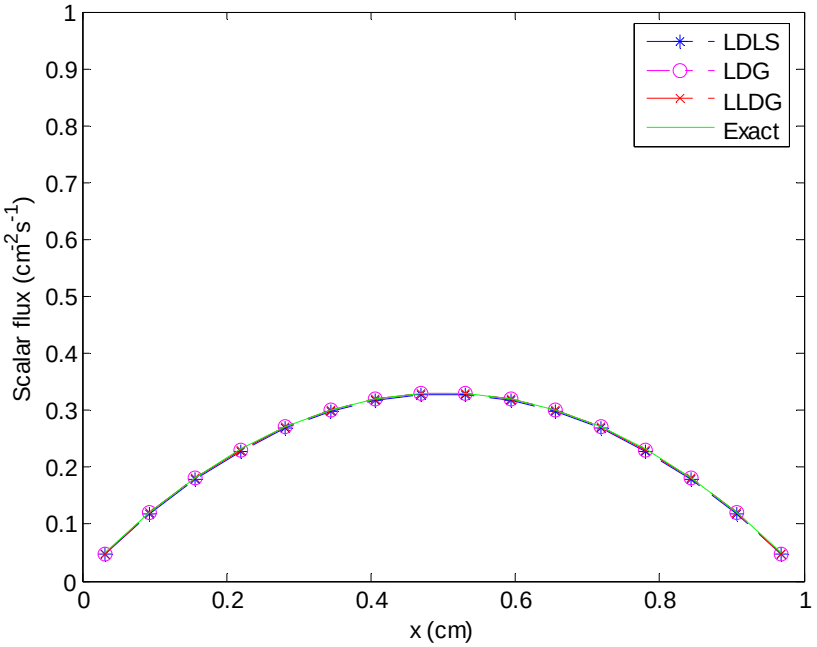

Fig. 5.25. Diffusion limit S_8 solutions with $\varepsilon = 10^{-2}$.

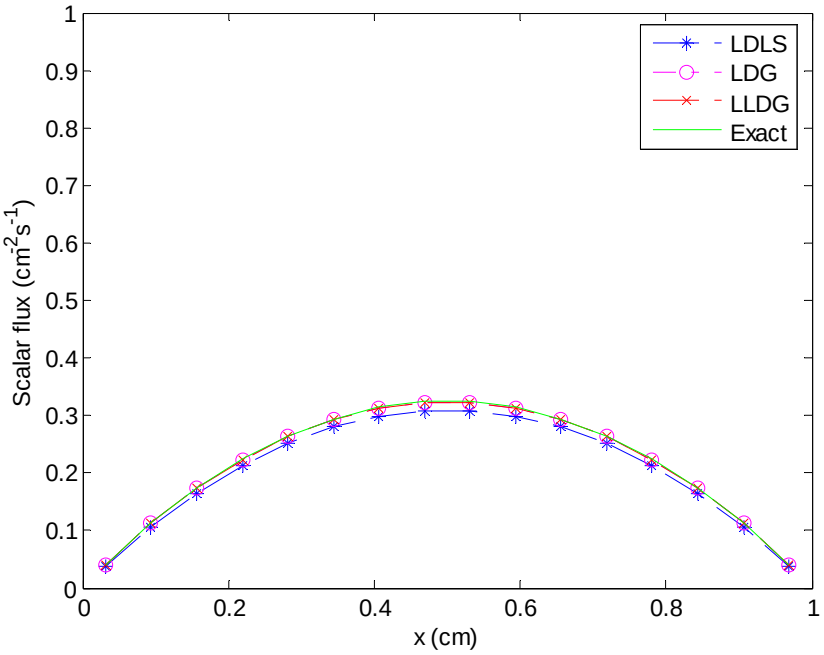

Fig. 5.26. Diffusion limit S_8 solutions with $\varepsilon = 10^{-3}$.

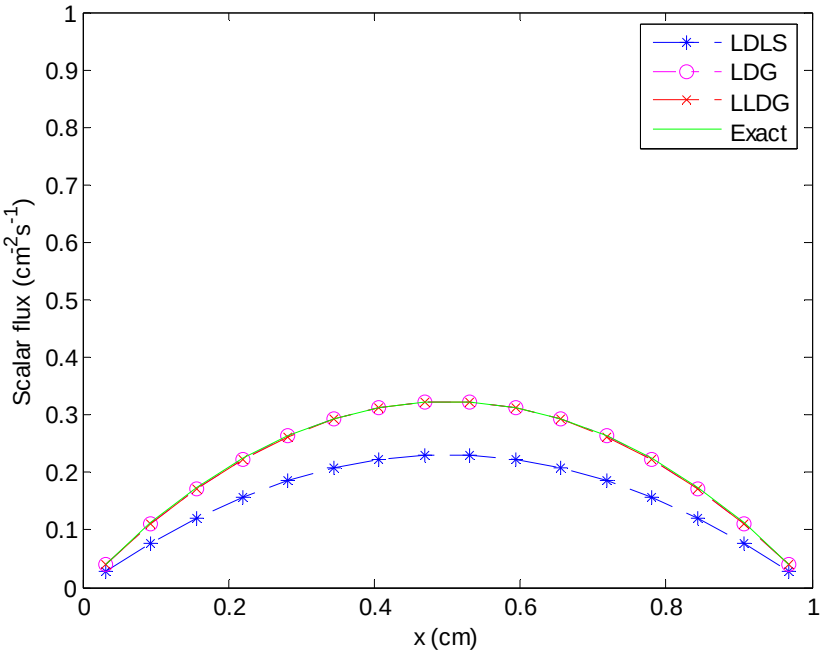

Fig. 5.27. Diffusion limit S_8 solutions with $\varepsilon = 10^{-4}$.

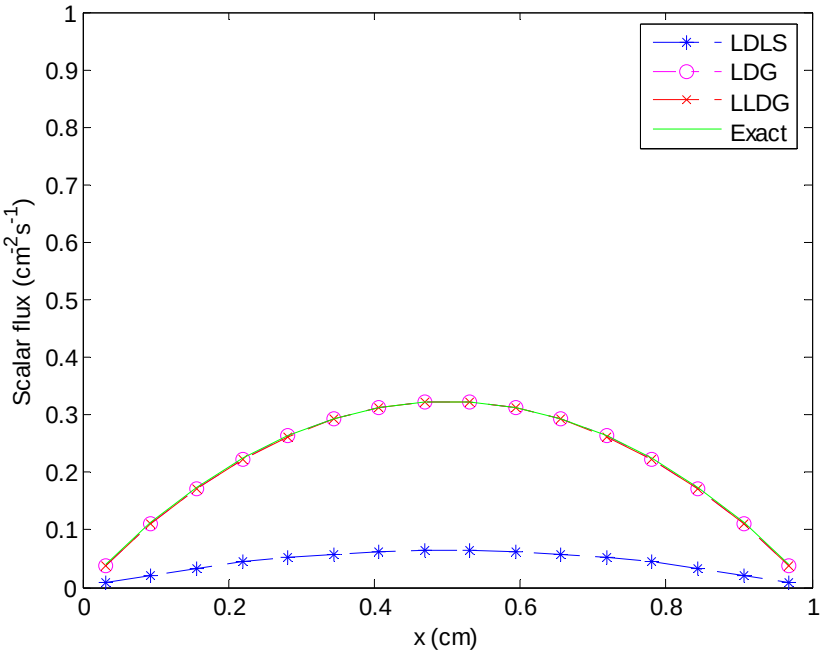

Fig. 5.28. Diffusion limit S_8 solutions with $\varepsilon = 10^{-5}$.

These results are consistent with the asymptotic analyses indicating that the LDG and the LLDG methods preserve the thick diffusion limit, while the LDLS method does not. However, the scalar flux solution from the LDLS method converges to the leading-order solution (which is zero) very slowly as $\varepsilon \to 0$. Thus, it should be quite acceptable for all but highly diffusive problems.

Summary

In this chapter, we presented a series of test problems to demonstrate various properties of the LDLS method. We first tested accuracy using both the continuous L_2 error norm and the pointwise L_2 norm for the cell-averaged scalar flux. Computational results showed that the LDLS method is second-order accurate for the continuous L_2 norm and the pointwise norm for the cell-averaged scalar flux. It is more accurate than the LLDG method, but less accurate than the LDG method. Then we studied the iterative convergence properties of the LDLS method computationally and the results were consistent with the Fourier analysis. Finally, we investigated the performance of the LDLS method in the thick diffusion limit. The results showed that it does not preserve the thick diffusion limit, which is consistent with the result from asymptotic analysis.

CHAPTER VI

SUMMARY AND FUTURE WORK

In this thesis, we developed, implemented and tested a linear-discontinuous least-squares method for spatial discretization of the 1-D discrete-ordinates equations.

The traditional least-squares method is based upon choosing the expansion coefficients to minimize an integral of the square of the residual. The derivative of a discontinuous function takes the form of a delta-function at the point of discontinuity. If the residual contains a delta-function, the integrand will contain the square of a delta-function, the integral of which is undefined.

The central theme of our approach is to first avoid the delta-function difficulty by minimizing the square of the residual over the semi-open interval, and then imparting both conservation and knowledge of the boundary value to the equations by constraining the solution to satisfy the balance equation.

We first analyzed the robustness and accuracy of the LDLS method through a simplified pure absorber transport equation, and compared the result with that from the LDG method and the LLDG method. We showed that the LDLS method yields a uniform second order global L_2 error and is more robust than the LDG method.

We derived the spatial discretization for both the source iteration and S_2 synthetic acceleration schemes, and implemented the schemes in FORTRAN. Computational results showed that the LDLS method is second-order accurate for the continuous L_2

norm and the pointwise norm for the cell-averaged scalar flux. It is more accurate than the LLDG method, but less accurate than the LDG method.

We performed a Fourier analysis to study the iterative convergence rate of the LDLS method. In the problems for an infinite, homogenous medium and uniform mesh, we found that S_2 synthetic acceleration remains effective for all cell thicknesses. The computational spectral radii agree extremely well with those from Fourier analysis.

To study the behavior in the thick diffusion limit, we performed asymptotic analysis for the LDLS method. We found that the LDLS method does not preserve the diffusion limit in thick diffusive problems, which is consistent with our computational results. Consequently, it is viable for neutronics but not for radiative transfer in the highly diffusive regime.

Although we have not previously discussed it here, we have recently developed a new form of discontinuous least-squares discretization that is both conservative and preserves the diffusion limit. We will report on this method in the future.

REFERENCES

1. W. H. REED and T. R. HILL, “Triangular mesh methods for the neutron transport equation,” *Los Alamos Nat. Lab. report*, LA-UR-73-479 (1973).

2. J. E. MOREL and J. S. WARSA, “A lumped bilinear-discontinuous S_N spatial discretization scheme for r-z quadrilateral meshes,” *Trans. Am. Nucl. Soc.*, **95**, 873 (2006).

3. M. BERNDT, T. MANTEUFFEL, and S. MCCORMICK, “Local error estimates and adaptive refinement for first-order system least squares (FOSLS),” *Elec. Trans. Numer. Anal.*, **6**, 35 (1998).

4. M. L. ADAMS and E. W. LARSEN, “Fast iterative methods for discrete-ordinates particle transport calculations,” *Prog. Nucl. Energy*, **40**, 3 (2002).

5. R. E. ALCOUFFE, “Diffusion synthetic acceleration methods for the diamond-differenced discrete-ordinates equations,” *Nucl. Sci. Eng.*, **64**, 344 (1977).

6. E. W. LARSEN and J. E. MOREL, “Asymptotic solutions of numerical transport problems in optically thick, diffusive regimes II,” *J. Comput. Phys.*, **83**, 212 (1989); see also “Corrigendum,” *J. Comput. Phys.*, **91**, 246 (1990).

VITA

Name: Lei Zhu

Address: Department of Nuclear Engineering
Texas A&M University
College Station, TX 77843-3133

Email Address: zhulei@neo.tamu.edu

Education: B.Eng., Engineering Physics, Tsinghua University, 2005
M.S., Nuclear Engineering, Texas A&M University, 2008